SUITABILITY OF ASTER AND SRTM DEMS, AND SATELLITE IMAGERY IN DETAILED GEOMORPHOLOGICAL MAPPING IN DZANANI AREA, LIMPOPO PROVINCE, REPUBLIC OF SOUTH AFRICA

By

Sylvia Motene

University of Venda

2018

SUITABILITY OF ASTER AND SRTM DEMS, AND SATELLITE IMAGERY IN DETAILED GEOMORPHOLOGICAL MAPPING IN DZANANI AREA, LIMPOPO PROVINCE, REPUBLIC OF SOUTH AFRICA

By

Sylvia Motene

15017799

Submitted to the Department of Geography and Geo-Information Science, School of Environmental Sciences, University of Venda in fulfilment of the requirement of the Degree of Environmental Sciences Masters in Geography

Supervisor: Prof B.D.O. Odhiambo

Co-supervisor: Dr N.S. Nethengwe

September 2018

DECLARATION

I, Sylvia Motene, hereby declare that this work is my own original writing. Sources referred to in the creation of this work have been appropriately acknowledged by explicit references. Other assistance received has been acknowledged. I have not knowingly copied, used words or ideas of others without acknowledgement.

Signed:_____ Date:_____

ACKNOWLEDGEMENTS

I would like to express my gratitude to my supervisors, Prof Odhiambo and Dr Nethengwe for their guidance throughout this research. Their comments and constructive criticism greatly enhanced this dissertation. I would like to acknowledge the assistance I received from the Dept. of Soil Science in the School of Agrigulture, Dept. of Mining and Environmental Geology, Dr Baanda, Given and Gift; I am grateful. This research was funded by the National Research Foundation. I would like to thank my parents for their moral support and encouragement. My dearest gratitude goes to my Lord and Saviour, Jesus Christ, for giving me comfort and strength through His Word.

ABSTRACT

Detailed geomorphological mapping is important for monitoring environmental phenomena, it is therefore crucial that the methods employed for mapping are accurate. The basis of remote sensing for geomorphological work is moving from the consideration of whether satellite data are accurate for landform mapping to how surfaces of interest can be defined from remote sensing data, since earlier approaches of mapping are deemed costly and tedious. The aim of this study is to assess the suitability of ASTER and SRTM DEMs, and satellite imagery in detailed geomorphological mapping. Field survey and aerial photo interpretation were used to prepare a reference geomorphological map for comparisons. A similar approach of demarcating landform boundaries from aerial photographs was implemented to segment the DEMs into landform classes. The software packages that were used for processing the satellite data to create detailed geomorphological maps are QGIS with GRASS and SAGA plugins, and ENVI. The resultant geomorphological units' maps from the DEMs when compared with the reference geomorphological map, show that the automated classification technique has advantages in terms of its efficiency and reproducibility. Nevertheless, distinct limitations of the technique are apparent and the technique is not suitable for detailed geomorphological mapping in the proposed study area.

Keywords: geomorphological mapping, satellite imagery, GIS, linear spectral unmixing

LIST OF FIGURES

LIST OF TABLES

LIST OF ACRONYMS

ASTER - Advanced Spaceborne Thermal Emission and Reflection Radiometer

ENVI - Environment for Visualizing Images

GEOBIA - Geographic object based image analysis

GIS – geographic information system

GRASS - Geographic Resources Analysis Support System

MRS – multiresolution segmentation

NDVI - normalized difference vegetation index

NASA - National Aeronautics and Space Administrations

QGIS – Quantum GIS

SAGA - System for Automated Geoscientific Analyses

SRTM - Shuttle Radar Topographic Mission

DEFINITION OF TERMS

Digital elevation model - a gridded representation of a landscape (Mukherjee *et al*., 2013; Rokni *et al*., 2015)

Geomorphological unit – an area containing a landform

Geomorphometry - the science of the quantification and analysis of the land surface (Bishop *et al*., 2012).

Landform - any physical feature of the earth's surface having a characteristic, recognisable shape (Hengl and Reuter, 2009).

Landform type - consists of a characteristic pattern of terrain that exhibits a defined variation in size, scale and shape of geomorphic features and occurs in a recognisable contextual position relative to adjacent geomorphic features (Hengl and Reuter, 2009). Examples of landform types include plains, hills, mountains and valleys (Hengl and Reuter, 2009).

TABLE OF CONTENTS

CHAPTER 1

INTRODUCTION

1.1. Background to the Study

Detailed geomorphological mapping plays an essential role in understanding Earth surface morphology, morphometry, processes, geochronology, natural resources, natural hazards and landscape evolution (Rao, 2002; Hayden, 2009; Bishop *et al*., 2012). Farhan *et al*. (2003) propose geomorphological mapping as a tool for recording the distribution of land surfaces and associated materials that can be used to identify past and present processes and provide environmental information for land use planners and engineers.

Geomorphological maps are a tool that may assist in monitoring landscape; therefore, they need to be true representations of landscapes without errors. Detailed geomorphological mapping may show areas where hazard zones are likely to occur (Chiliza and Richardson, 2008). The study area is located in a landslide prone area, and a detailed geomorphological map may identify areas that are susceptible to landslides to aid in settlement or development site selection (Chiliza and Richardson, 2008). Lake Fundudzi landslide is a well-known large translational rock slide or rock avalanche in the region, near where the study area located (Chiliza and Richardson, 2008).

A landslide susceptibility zone map for the Southern Africa region was produced that showed slope failures were expected in the east of South Africa (Holmes and Meadows, 2012). Other examples of slope failure included the collapse of a wall

in a hornfels quarry used for oil tank housing in Cape Town in the Western Cape Provice, failures in Bernea red sands in Durban in the Kwa-Zulu Natal province of South Africa (Holmes and Meadows, 2012). The most successful approach to geomorphological mapping is to combine field inspection with air-photo interpretation (Cooke and Doornkamp, 1990). However, this technique is deemed costly and tedious. As a result, automated mapping using digital elevation models (DEMs) is being used in geomorphology due to the availability of digital elevation data, access to fast computers and the synoptic coverage provided by DEM data.

The integrated use of DEMs and GIS enabled the establishment of automated geomorphological mapping (Wechsler and Kroll, 2006). Digital elevation models provide a base data set from which topographic parameters are digitally generated (Wechsler and Kroll, 2006). These surface derivatives provide the basics for characterization of landform and are used extensively in environmental applications, such as hydrology, geomorphology and environmental modelling (Wechsler and Kroll, 2006). However, the accuracy with which the DEMs delineate detailed geomorphological units is questionable due to the inherent errors of DEMs that constitute uncertainty (Wechsler and Kroll, 2006).

The representation of elevation in a grid framework enables neighbourhood computation of parameters, such as slope and flow direction (Wechsler and Kroll, 2006). Advanced Spaceborne Thermal Emission and Reflection Radiometer (ASTER) and Shuttle Radar Topography Mission (SRTM) DEMs are the highest resolution open source DEMs that have a near global coverage and mostly used among other DEMs for geomorphological mapping (Du *et al*., n.d.), especially in

areas where high resolution DEM data are not readily available. Remotely sensed data can enhance the rate of geomorphological mapping (Smith *et al*. 2006). In addition, remote sensing enables mapping of morphology that would otherwise be impossible from the ground and inaccessible terrain (Otto and Smith, 2013).

Digital elevation models alone are not sufficient to provide detailed geomorphological information and need to be completed by analysis of satellite imagery (Farhan *et al*., 2003; Siart *et al*., 2009; Mulder *et al*., 2011; Wei *et al*., 2017). Detailed geomorphological mapping is important for monitoring environmental phenomena, it is therefore crucial that the methods employed for mapping are accurate. Proposed solutions to environmental problems are inadequate if they lack a geomorphological component (Cooke and Doornkamp, 1990).

1.2. Problem Statement

Different studies have been conducted to assess the accuracy of automated geomorphological mapping from the global DEMs. However, few studies have been conducted in terms of detailed geomorphological mapping and the accuracy of the DEMs is such mapping has not been adequately assessed (Chiliza and Richardson, 2008; Diko *et al*., 2014). Automated mapping is usually done without assessing the extent to which the methods of mapping are accurate (Kaya, 2000; Sa˘vulescu and Mihai, 2011). Digital Elevation Model data are often accepted as true representation of the Earth's surface and not as models (Wechsler and Kroll, 2006). Consequently the DEMs are used without quantifying the effects of DEM error (Wechsler and Kroll, 2006).

The problem here is that the basis of remote sensing for geomorphological work is moving from consideration as to whether the satellite data are accurate for surface mapping to how surface of interest can be defined from the abundant remote sensing data (Evans, 2012). The accuracy with which the DEMs can delineate geomorphological units has not been adequately documented. The purpose of this study is therefore, to assess the suitability of ASTER and SRTM DEMs, and satellite imagery in detailed geomorphological mapping in the Dzanani area.

1.3. The General Objective

The general objective is to assess the suitability of SRTM and ASTER DEMs used in combination with satellite imagery for detailed geomorphological mapping.

1.4. Specific Objectives

The specific objectives of the study are to:

- produce a reference geomorphological map from photo interpretation and field survey;
- generate detailed geomorphological maps from the DEMs and satellite imagery;
- assess DEMs quality in terms of elevation and slope accuracies; and
- evaluate the suitability of the geomorphological maps generated from ASTER and SRTM DEMs, and satellite imagery by comparing them with the reference geomorphological map.

1.5. Research Questions

This study was conducted to answer:

- How accurately can ASTER and SRTM generated DEMs and satellite imagery perform in detailed geomorphological mapping when compared with aerial photograph interpretation and field survey?
- Does DEM quality influence the accuracy of geomorphological units derived from DEMs?

1.6. Scope of the Study

This study sought to generate detailed geomorphological maps. As a result, the elements of a detailed geomorphological map (surface form, materials, and processes) were assessed. Various algorithms exist for calculating topographic parameters from DEMs, and each method can produce different results (Wechsler and Kroll, 2006).

The accuracy of DEMs and satellite imagery are evaluated in this study; therefore, the algorithms that were deemed suitable for geomorphological mapping from the reviewed literature were used (Berhanu, 2005; Drăguţ and Eisank, 2012; Vidhya et al., 2015). However, the different algorithms and their performance are not presented in this study. Similarly various GIS software packages are used for geomorphological mapping. The suitable software and algorithms that were used in this study were instructed by reviewed literature and their performance (Berhanu, 2005; Mergili et al., 2014; Wei et al., 2017). Thus, the performance of

different software is not reported in this study, although different GIS packages were used.

1.7. Description of the Study Area

The study area (Figure 1.1) is located within the Local Municipality of Makhado, in the Limpopo Province, South Africa. The study area is approximately 43 Km^2 and is found between latitudes 22°51'22" S and 22°54'25" S, and longitudes; 30°6'46" E and 30°11'9" E, with elevations ranging from 750 up to 1100m. The area is characterised by a humid climate and has a wet summer followed by a dry winter. Mean annual rainfall ranges from 755 mm to 798 mm (Chiliza and Richardson, 2008). The mean maximum daily temperature over the area ranges between 30℃ and 34℃ in summer, and between 22℃ and 26℃ in winter (Chiliza and Richardson, 2008).

The geology of the area comprises of sandstone, quartzite, red shaly sandstone, basalts and alluvium (Laurenta *et al*., 2013). These represent the Soutpansberg Group. The Soutpansberg Group is underlain mainly by north dipping quartzite (Laurenta *et al*., 2013) and has highly block-faulted formations that consist of a volcano-sedimentary sequence of mainly basaltic lavas (Chiliza and Richardson, 2008).

The topography varies from relatively flat areas to mountainous relief (Chiliza and Richardson, 2008). The present geomorphologic configuration of the area is the result of several processes such as denudation, deposition and tectonics.

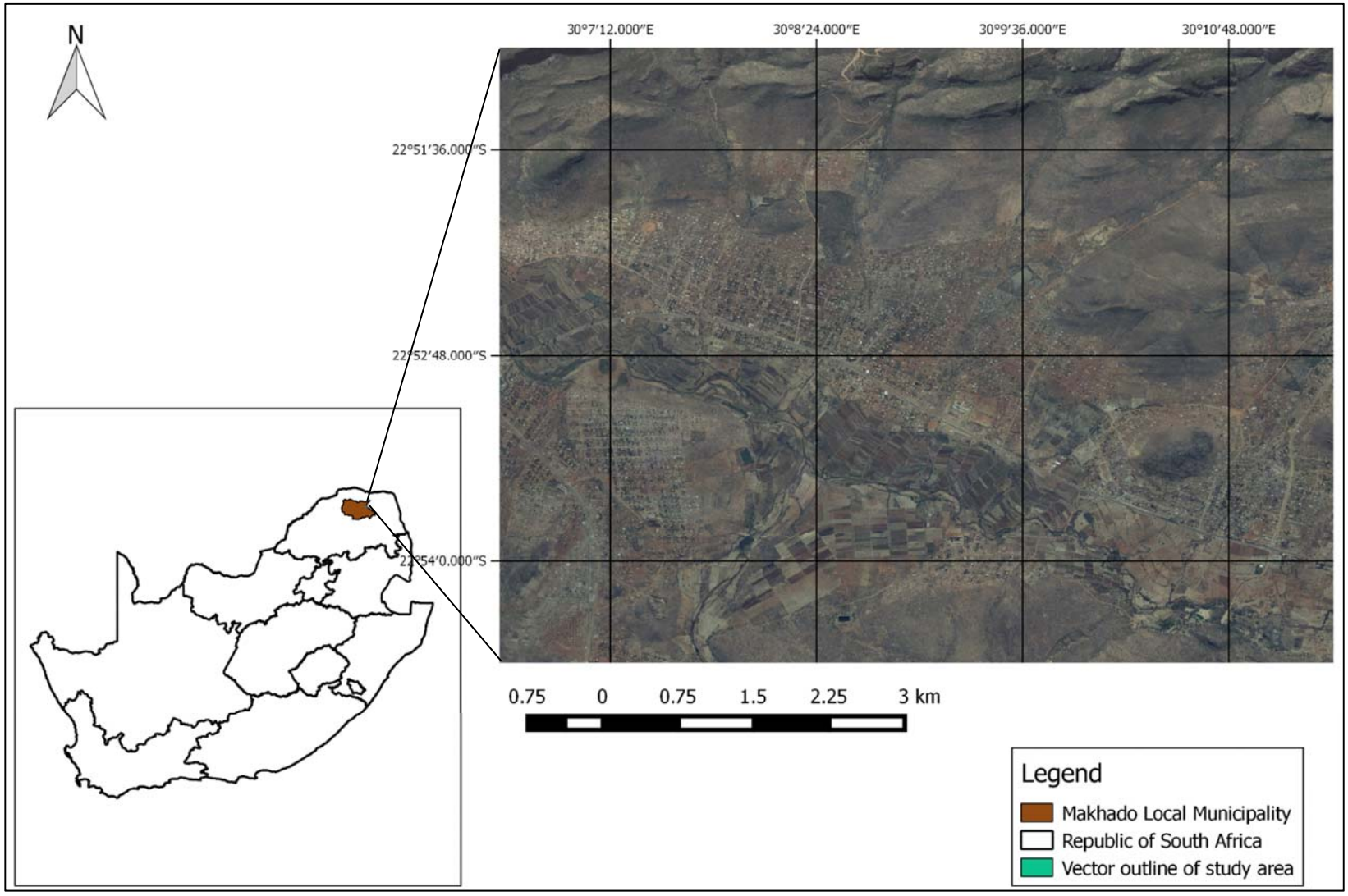

Figure 1.1: Location map of study area

The land use practice in the study area is mixed, mainly agriculture along the river system. The settlement area is located between the river system and the upper part of the study area. The area is sparsely vegetated.

1.8. Justification of the Study

The 30m resolution global DEMs (ASTER and SRTM) are freely available high resolution products which cover the most part of the earth (Du *et al*., n.d.). The DEMs can be used for geomorphological mapping in areas where there is little, no recorded DEM data or data costs are high. This study was conducted to determine whether the commonly used global DEMs (ASTER and SRTM) are suitable for detailed geomorphological mapping.

The results obtained from the study would ascertain whether the use of the global DEMs is suitable for detailed geomorphological mapping to offer frequent updates for land management or not. Geomorphological mapping can provide environmental information for land use planners and engineers (Farhan *et al*., 2003). This is particularly important in Dzanani since the study area is located in a landslide prone area.

The increase in human settlement has encroached onto slopes that are prone to landslides. A detailed geomorphological map can identify such areas and aid in policy making and land management. Should the DEMs be found accurate, the monitoring of the terrain in the study area could be done frequently and applied in similar areas as well.

1.9. Structure of the dissertation

This dissertation has been developed as a series of chapters which are connected to each other. Chapter 2 explores the different detailed geomorphological mapping techniques: manual mapping from field survey and aerial photo interpretation; and automated mapping from DEMs and satellite imagery. Chapter 3 outlines the research design that was adopted in this study, types of data used, methods of data collection and analysis. Chapter 4 presents the results that were obtained from each geomorphological mapping technique and the analysis, as well as the discussions. Chapter 5 draws conclusions from the results of the study and gives recommendations for further research.

CHAPTER 2

LITERATURE REVIEW

2.1. Introduction

This chapter outlines the literature that was reviewed in this study. Referenced sources included software manuals. This chapter first looks into detailed geomorphological mapping and the applications thereof, then the different techniques of producing a detailed geomorphological map. A summary is provided at the end of the chapter.

2.2. Detailed Geomorphological Mapping

There are two forms of terrain mapping that are valuable in environmental management, namely, land systems and geomorphological mapping (Cooke and Doornkamp, 1990). Land systems mapping divides an area into morphological regions rather than individual landforms (Cooke and Doornkamp, 1990). Geomorphological mapping (which is the focus of this study) entails the detailed mapping of landforms, materials and specific processes, in some cases, the age of the landforms and is essential for many projects (Cooke and Doornkamp, 1990; Walstra *et al*., 2011).

Geomorphological mapping provides information about landform distribution, soils and rock materials, features created by surface processes that can be used by land use planners and engineers for policy making, monitoring development impacts on the environment, resource management, engineering and land management projects (Cooke and Doornkamp, 1990; Farhan *et al*., 2003; Kamal and Midorikawa, 2004; Mulder *et al*., 2011; Smith and Griffiths, 2017). Sketches

and maps of landscapes and landforms have been vital tools for analysing and visualising earth surface features (Castiglion *et al*., 1999) ever since early geomorphological research (Otto and Smith, 2013) began.

Geomorphological maps are categorised into either basic maps (representing observed features of a landscape either in part or entirety) or derived maps (focusing on a specific theme, e.g. risk causing phenomena) (Otto and Smith, 2013). These map categories are similar to general and specific geomorphometry termed by Evans (1972) (cited in Hengl and Reuter, 2009). Specific geomorphometry applies to and describes discrete landforms such as eskers, drumlins, sand dunes or volcanoes, whereas general geomorphometry applies to and describes the continuous land surface (Hengl and Reuter, 2009). Compared to the extraction of specific landforms, the classification of a whole land surface is considered difficult (Evans, 2012).

Geomorphological maps aid in the implementation of hazard mitigation policies (Mili and Acharjee, 2014). For example, areas prone to flood risk, bank erosion can be visualised on maps, and thus minimising the risk of the region by providing information to control land use in floodplain areas (Otto and Smith, 2013). Maps at scales of between 1:10000 and 1:50000, occasionally up to 1:100,000 can be used for various applications, such as hazard maps, planning and nature conservation and engineering geomorphology purposes (Gustavsson *et al*., 2006). Prior development, geomorphological maps may be a preliminary tool for land management; policies for mitigating geomorphological and geological risks (Mili

and Acharjee, 2014); and provide baseline data for landscape ecology, forestry or soil science (Otto and Smith, 2013).

Cooke and Doornkamp (1990) demonstrate the importance of adequately assessing a geomorphological system affected by engineering projects prior to development. Geomorphology can contribute towards the solution of many environmental problems and the proposed solutions for such problems are inadequate if they lack a geomorphological component (Cooke and Doornkamp, 1990).

2.3. Constructing a Detailed Geomorphological Map

A detailed geomorphological map conveys terrain that is segmented into conceptual entities based on morphology, morphometry, morphogenesis, morphochronology, and morphodynamics (Giles, 1998; Bishop *et al*., 2012).

Originally, before the use of remote sensing, landforms were mapped directly in the field (Smith and Clark, 2005). Contemporary remote sensing technologies are satellite imagery and aerial photography that have been used to map landforms (Smith and Clark, 2005). The basis of remote sensing for geomorphological work is moving on from consideration of whether data are accurate for surface mapping to how surface of interest can be defined from the abundant remote sensing data (Evans, 2012).

Landform elements differ from one another in terms of characteristics such as shape, size, orientation, relief and contextual position, as well as the processes that were involved in their formation (Hengl and Reuter, 2009). Size and shape of

landforms have been used to deduce hillslope forming processes such as erosion and denudation, deposition and accumulation (Hengl and Reuter, 2009). The vertical and horizontal resolution of DEMs influences on the level of detail of surface features, the accuracy with which they are portrayed and the values of land surface parameters (Hengl and Reuter, 2009). No single resolution is capable of computing local land surface parameters to depict and classify terrain, therefore, the resolution used, need to be suitable for delineating and describing surface features of interest for a particular application (Hengl and Reuter, 2009).

The classification of landform elements involves segmentation of individual hillslopes into more or less homogenous classes or facets along a category sequence from ridge crest to valley bottom (Hengl and Reuter, 2009). Giles and Franklin (1998) described procedure for partitioning two-dimensional slope profiles into geomorphological objects, which they called slope units. Slope units are defined as a section of a two-dimensional downslope profile having relatively homogenous form, process, and lithology with upper and lower boundaries located at breaks of slope (Hengl and Reuter, 2009).

Morphological mapping is based on recording the nature and position of slope junctions of different steepness, cliff forms, as well as amount and direction of slope (Cooke and Doornkamp, 1990). Straumann (2010) defines landform which is synonymous with landform unit, relief unit, landform component, to name a few, as a physical feature of the Earth's surface such as a hill, alluvial fan, or plain; these are in turn responsible for soil formation. Landform elements are zones of a hillslope with a defined range of surface morphological attributes (Straumann,

2010). They are defined by similar ranges of various terrain parameters such as gradient, aspect, plan and profile curvature (Straumann, 2010).

Van Zuidam and van Zuidam-Cancelado (1989) proposed slope steepness and their description (Table 2.1). A slope unit is a section of a cross-sectional downslope profile with upper and lower boundaries located at successive breaks of slope (Giles, 1998). The use of breaks of slope to mark the boundaries of slope unit objects is supported by the commonly used techniques in geomorphological mapping (Giles, 1998). Breaks of slope are often identified as significant topographic features, indicating the boundaries between adjacent geomorphological units on a map (Giles, 1998).

Arrows are included to show direction of slope and numerical values of shading show slope steepness (Cooke and Doornkamp, 1990). Surface materials occur either as a solid rock or superficial deposits (soils) (Cooke and Doornkamp, 1990). Methods of surveying slopes include the use of tape and abney, pantometer, levelling, total station with prism (Clowes and Comfort, 1987). Slope influences the velocity of surface and subsurface flow, soil water content, erosion potential, and several other surface processes and is therefore an important component in various environmental applications such as land compatibility classification, vegetation mapping, and hazard zonation (Lobin, 2015).

Table 2.1: Slope steepness as proposed by van Zuidam and van Zuidam-Cancelado (1989)

Proposed slope steepness (%)	**Description**	**Other classification**	
		US soil survey	**Universal soil**
0-2	Flat or almost flat	0-2	1-2
3-7	Gently sloping	2-6	2-7
8-13	Sloping	6-13	7-12
14-20	Moderately steep	13-35	12-18
21-55	Steep	25-55	18-24
56-140	Very steep	>55	>24
>140	Extremely steep	N/A	N/A

Surface processes are recorded as an interpretation of forms and surface materials that associate with a specific process. Landslide for example, indicates the process and the extent of the area potentially susceptible to this risk (Cooke and Doornkamp, 1990). Mwaniki *et al*. (2015) explained that the methods of landslide mapping require the identification of land degradation or disturbed vegetation, which are related to the incidents of landslide. Land degradation is assessed through land use land cover change (Mwaniki, 2015). A landslide scar indicates the incident of mass movement processes, and can be classified as recent of relict (Townsend and Rosser, 2012). With recent landslide scars, the headscarp and debris areas can be distinguished; whereas relict landslide scars include potentially older deposits where there is reason to suspect a landslide (Townsend and Rosser, 2012). Relict landslide scars cannot be associated with a

particular source area as the scarp may have been degraded (Townsend and Rosser, 2012).

The different aspects of a detailed geomorphological map can be represented in a map by coloured area symbols, patterns and line symbols (Walstra *et al*., 2011). Colours, including hue and intensity, and symbols, lineation, shading, stipples or hatching, letters and numbers can be used alone or in combination to present data for geomorphological maps (Gustavsson *et al*., 2006). A standardised geomorphological mapping legend is yet to be developed (Otto and Smith, 2013). Therefore, a legend system or mapping symbols are determined by the purpose the map is to serve (Otto and Smith, 2013). The methods (manual and automated) of delineating landforms are discussed in detail in the following sections.

Compared to the traditional methods of geomorphological mapping, aerial photographs may reduce costs involved in mapping, inventorying and planning (Morgan *et al*., 2010). Although traditional methods of analysing aerial photographs may be time consuming and subjective; manual interpretation of aerial photographs by highly trained individuals remains one of the most effective and commonly used approaches for interpreting of aerial photographs (Morgan *et al*., 2010). Manual interpretation of aerial photographs relies greatly on the personal experience, knowledge, and expectations of the interpreter for a given location. Well trained aerial photo interpreters are currently in short supply (Morgan *et al*., 2010). Therefore, training should be provided for interpreters (Morgan *et al*., 2010).

Emphasis of university curricula and the training of spatial analysts has shifted from aerial photographs to digital platforms due to the proliferation of satellite

imagery that resulted from the advent wide range of digital image analysis techniques (Morgan *et al*., 2010).The same image analysis techniques are now available for aerial photographs (Morgan *et al*., 2010). Satellite imagery has broad spatial coverage and regular re-visitation frequency, and has provided researchers and cost-effective alternative compared to aerial photography (Morgan *et al*., 2010).

A lack of long-term satellite imagery (prior to the 1970s) limits the use of satellite data in change detection analyses to the past three decades (Morgan *et al*., 2010). In addition, the spatial resolution of the most widely available and free satellite imagery is generally coarser than that of aerial photographs (Morgan *et al*., 2010). There is no recorded data about when the landslides might have occurred in the past in Dzanani.

2.3.1. Manual Mapping

Field inspection and aerial photo interpretation have been viewed as the most successful approach to geomorphological mapping (Cooke and Doornkamp, 1990; Morgan and Gergel, 2013). According to Karmal and Midorikawa (2004), stereoscopic geomorphological mapping involves the delineation and classification of polygons (boundaries of homogenous area) based on landscape characteristics such as tone, shape, texture, size, pattern, site, situation, local topography and narrow waterways as line features (Walstra *et al*., 2011; Morgan and Gergel, 2013). Aerial photographs are suitable for detecting smaller landforms (Siart *et al.,* 2009).

Aerial photo interpretation can be performed using stereoscopes or heads-up on-screen digitization (Morgan and Gergel, 2013). Van Zuidam and van Zuidam-Cancelado (1989) and Hayden (2009) give a detailed guideline on how to interpret aerial photographs for geomorphological mapping. Morgan and Gergel (2013) conducted a study to automatically classify landform objects from aerial photographs by automatic segmentation. The results were compared with manually delineated landform objects from aerial photographs which showed that automatic classification had relatively low accuracies. To manually produce a detailed geomorphological map; firstly, slope units are delineated and thereafter, additional details as perceived from the aerial photographs are delineated (Hayden, 2009).

Breaks of slope indicate where process and slope form change between adjacent units (Hayden, 2009). The interpretations are manually digitised directly from the photographs and georeferenced for rectification through ground control points (Bocco *et al*., 2001). Detailed geomorphological mapping is deemed a time consuming and costly activity (Otto and Smith, 2013), produces inconsistent results as they are difficult to replicate (Morgan and Gergel, 2013). Therefore, the activities focusing on such mapping as a scientific discipline have been declining, leading to the focus of the discipline being on themes and applications rather than the holistic scientific maps (Gustavsson *et al*., 2006).

2.3.2. Automated Mapping of Landforms

In automatic mapping of landforms, individual measurements are grouped and each group is labelled as a class based on similarity so that terrain units with the

same landform type have maximum similarity and minimum differences in their morphological characteristics Wei *et al*. (2017). DEMs can be used to derive land surface parameters (Smith and Pain, 2009; Pipaud *et al*., 2015).

Pixel-based methods of classification, such as maximum likelihood classifier were criticised and a new paradigm, object based image analysis (OBIA) was developed, later renamed geographic object based image analysis (GEOBIA) to distinguish from medical science (Blaschke *et al*., 2014). GEOBA can be used to delineate and classify detailed landforms from DEMs and land cover from satellite imagery without the shortcomings of pixel-based classification approaches that give a salt and pepper effect when applied to high resolution DEMs (Verhagen and Dragut, 2012).

Satellite imagery represents landscape as pixels (Blaschke *et al.*, 2014). GEOBIA involves pixels first being grouped into objects based on either spectral similarity or an external variable such as ownership, soil or geological unit (Blaschke *et al.*, 2014). In general, GEOBIA provides increased accuracy and detail for classification purposes (Blaschke *et al.*, 2014). Pixel based image analysis has been a typical method for classification of remote sensing data, whereby pixels are used as numerical basis for categorisation (Chigbu *et al.,* 2015). Pixel based includes supervised classification (maximum likelihood classifier) and unsupervised classification (K-means and ISODATA) (Chigbu *et al*., 2015).

Per pixel classification generates square classified pixels, whereas GEOBIA generates objects of different shape and scale (Chigbu *et al.,* 2015). This approach is called multi-resolution segmentation (Chigbu *et al*., 2015). Van Niekerk (2010)

(cited in Mashimbye *et al*., 2014) performed MRS for landform classification and found MRS to perform better compared to other segmentation algorithms and more sensitive to morphological discontinuities compared to automated land component mapper and iterative self-organising data analysis technique algorithm (ISODATA). Pixel classification of landforms is not desirable since it causes scattered classes due to overlap between the classes (Gerçek, 2017). Conversely, GEOBIA techniques represent the landscape as formed by homogenous objects rather than individual pixels (Gerçek, 2017).

Topographic position index (TPI) is another technique that many be used to classify landforms from DEMs, whereby the landscape is classified into slope position (ridge tops, upper, middle, flat and lower slopes, and valley bottoms) and landform category (steep narrow canyons, gentle valleys, plains, open slopes) (Seif, 2014). The use of high resolution satellite images and DEMs has become popular due to their ability to provide high level of detail, multispectral properties and global coverage (Siart *et al*., 2009) and has proved to be a vital tool in morphometric analysis, especially where field data is impractical (Otto and Smith, 2013). Remote sensing data are repetitive and therefore can be used to monitor landscapes (Mili and Acharjee, 2014). For example, effective erosion control plans can be formulated through the use of remote sensing to identify erosion prone areas (Mili and Acharjee, 2014).

Pike 1988 (cited in Giles, 1998) combined the use of DEMs with satellite imagery to describe the morphometric characteristics of a landscape using variables derived from the DEMs to overcome the problem of classification from satellite

imagery. McDermid and Fanklin (1995) (cited in Giles, 1998) extended the work of Pike 1988 (cited in Giles, 1998) by using slope profile for landscape classification and found that the profile variables had the highest overall classification accuracy compared to the spectral and texture variables of satellite image which are not scale dependent.

A DEM facilitates automated landform mapping based on geomorphometric parameters (Bishop *et al*., 2012) model pathways of mass and energy transport through the landscape by hillslope and fluvial processes (Pelletier, 2008). Sharma and Kujur (2012) suggested that DEM and satellite data can be used for visualization and interpretation of an area in terms of geology and geomorphology. Although DEMs provide better functionalities, they need to be used in combination with spectral data to improve landform classification (Farhan *et al*., 2003; Siart *et al*., 2009; Mulder *et al*., 2011; Wei *et al*., 2017). GIS and DEMs enable morphometric parameters to be calculated with speed, precision and reproducibility (Grohmann *et al*., 2007).

Studies conducted for geomorphological mapping from DEMs have used geomorphometric parameters such as elevation, slope, aspect, plan and profile curvature, surface roughness and flow accumulation (Bolch *et al*., 2005; Wechsler and Kroll, 2006; Grohmann *et al*., 2007; Mulder *et al*., 2011; Wei et al., 2017). The geomorphometric parameters are extracted using standard software tools (Bolch *et al*., 2005).

Sa˘vulescu and Mihai (2011) performed geomorphometric analyses stating that elevation, aspect, slope angle (to identify geomorphic forms), vertical curvature,

and tangential curvature are useful in identifying and describing geomorphological forms and processes. The parameters may be calculated through pixel or object based classification (Mulder *et al*., 2011). Kaya (2000) used a slope map to characterise landforms, by categorising slope angles that define each landform to distinguish flat terrain formed by erosion (terraces) in the Isiklar Mountain. Siart *et al*. (2009) examined the applicability of SRTM and ASTER DEMs to detect karst features, by deriving geomorphometric parameters.

Forkuor and Maathius (2012) suggested that landslides can be depicted directly from a DEM. However, this approach depends on the time period between the occurrence of the landslide and the time of data acquisition, as shown in Townsend and Rosser (2012) that the evidence of incidences like landslide occurrence may disappear over time.

Photogrammetry and field survey are time consuming and labour intensive, as a result, the use of DEMs has become popular for the extraction of topographic information (Gonga-Saholiariliva *et al*., 2011). The availability of remotely sensed data (aerial and satellite imagery and DEMs) led to the advancement of mapping (Otto and Smith, 2013; Mashimbye *et al*., 2014). Remotely sensed data provide information that is not readily obtained by other means (Cooke and Doornkamp, 1990).

Geographical Information Systems (GIS) enables spatial data handling and analysis within a single framework (Evans, 1972) where landform mapping can be done digitally with speed and accuracy (Bolch *et al*., 2005; Grohmann *et al*., 2007; Mulder *et al*., 2011) where several algorithms are used to compute terrain

derivatives from elevation data. The results obtained from DEM and GIS are reproducible (Bolch *et al*., 2005; Grohmann *et al*., 2007). SRTM and ASTER DEMs are the most comprehensive space borne survey of the Earth that has been undertaken (Cooke and Doornkamp, 1990; Bishop *et al*., 2012; Du *et al*, n.d.). The DEMs are used for a variety of applications, such as the analysis of terrain characteristics (Ehsani and Quiel, 2008; Forkuor and Maathius, 2012).

Procedures for automatically extracting and classifying landform types and landform elements vary in terms of the kinds of classification methods applied to extract entities (Hengl and Reuter, 2009). The classification of landform elements has been achieved using a wide variety of classification methods including knowledge-based heuristic approaches, supervised classification, and unsupervised classification (Hengl and Reuter, 2009). Automated approaches have the advantage of being consistent, repeatable, updatable, and quantifiable. GIS packages process geographically referenced data and all have some functionality in common (e.g. they can import, display and process digital elevation models) (Hengl and Reuter, 2009). They vary in the emphasis placed upon generic GIS tasks, geomorphometric and hydrological analysis (Hengl and Reuter, 2009). While there are considerable advantages in using established GIS, they do not necessarily provide sufficient functionality for all geomorphometric tasks (Hengl and Reuter, 2009). Functionality is not the only criterion for choosing a software package; price, availability and existing expertise play a part (Hengl and Reuter, 2009).

Geologic and geomorphological processes that act on the Earth's surface give rise to landform structures (Gerçek *et al*., 2011). Local geometry, synonymous with form or morphometry is represented by slope and curvature of surface (Gerçek *et al*., 2011). Terrain can be categorised into landform classes from DEMs by making use of slope and profile, plan, maximum and minimum curvature parameters (Gerçek *et al.*, 2011). Geographic object based image analysis (GEOBIA) can be performed in eCognition software and other GIS platforms such as QGIS with GRASS and SAGA plugins can be used to obtain objects from slope and the four curvature parameters (Gerçek *et al*., 2011).

Landforms have specific organization, where, for instance, peaks and ridges are at the crests of hills and mountains; hence, they are positioned at highest points and/or correspond to the divides (Gerçek *et al*., 2011). Ridges on a vertical plane are followed by shoulders and side slopes (Gerçek *et al*., 2011). The footslope constitutes the lower parts of a sloping terrain and it is adjacent to channels or plains. Slopes on the horizontal plane have hollows and spurs in sequential order (Gerçek *et al*., 2011). Relative position across the landscape is incorporated to construct this organization (Gerçek *et al*., 2011). Contextual information that reveals the relative position of features across the landscape is gathered from a local elevation-based model terrain position index categorized into three as upper, mid, and low. GEOBIA proved to be an efficient tool in obtaining representative terrain objects rather than scattered pixels (Gerçek *et al*., 2011).

Guth (2010) stated that slope and shaded reflectance maps derived from DEMs are able to convey DEM quality precisely compared to elevation alone. However,

this method does not explicitly show the extent of accuracy. The method may be used to compare the accuracy of different elevation models. Using Lidar data, the results were found to be accurate. Lidar data is not available globally; therefore, the results cannot be comparable to other areas. Wei et al. (2017) found that automated classification of landforms from DEMs was capable of accurately reconstructing a detailed geomorphological map. Their study had a classification accuracy of 72.9% and kappa coefficient of 0.66. They concluded that automated classification of landforms is accurate and efficient if the appropriate terrain data resolution is used and could be applied in geomorphological mapping and landform characterization studies in the future.

Contrary to Wei *et al*. (2017), Mulder *et al*. (2011) recognised that the use of most automated landform classification has several general problems. Geomorphologic elements that can be recognised depend on scale (Mulder *et al*., 2011). If the element to be mapped is minute on the map scale used, it might be lost (Guzzetti *et al*., 2012). Landslide inventories are commonly compiled from using stereo-aerial photographs aided with field investigation. However, this exercise is not efficient, it is time consuming and costly (Gustavsson *et al*., 2006). Lidar derived DEMs provide adequate landslide factor maps to identify the landslide occurred areas, which could be used for further landslide assessment and site planning (Guzzetti *et al*., 2012). The suitability of the use of GRASS GIS For geomorphological mapping is documented in Mergili *et al.* (2014).

2.4. Surface Material and Methods of Analysis

Soil texture refers to the relative proportion of sand, silt and clay in the fine earth fraction (Schaetzl and Anderson, 2005). Soil is composed of mineral particles, namely, sand, silt and clay, each referred to as soil separates (Schaetzl and Anderson, 2005). Soil texture can be quantitatively determined in a laboratory using either spectrometry, remotely sensed data, the sieve method, pipette or hydrometer method by dispersing soil samples collected in the field so that sand, silt and clay act as independent units (Schaetzl and Anderson, 2005). The data on the soil contents are plotted on a textural triangle to place the soil samples in a specific soil class (Schaetzl and Anderson, 2005).

Universal soil grain sizes are as follows: soil particles between 0.02 and 2.0 mm in diameter are sand; between 0.002 and 0.05 mm are silt; and soil particles less than 0.002 mm is clay (Jensen, 2007). Soil texture provides information about the soil characteristics such as soil moisture retention, nutrient holding capacity and susceptibility to erosion (Vidhya *et al*., 2015). Remote and soil sensing provide new dimensions to predict soil properties and processes (Vidhya *et al*., 2015). In a satellite image, coarse sandy soils are identifiable by a relatively high reflectance as they are well drained and have low moisture content while poorly drained fine texture soils have a low reflectance (Vidhya *et al*., 2015).

Shabou *et al*. (2015) noted that existing soil maps often describe soil types rather than soil texture and point measurements through soil analysis are expensive and dense sampling is required which makes it difficult to quantitatively evaluate soils at a broad scale (Shabou *et al*., 2015). Remote sensing data offers surface

reflectance related to soil properties, thereby reducing costly field surveys and providing maps that can be updated frequently (Shabou *et al*., 2015). A flood can change some soil horizon leaving existing maps out-dated (Shabou *et al.,* 2015).

It was demonstrated that many soil attributes can be measured by spectral analysis of soil samples under laboratory conditions (Aksoy *et al*., 2009; Mulder *et al*., 2011). Examples include sand, silt and clay, soil organic matter, soil moisture, salt and carbonates. Accurate estimation of soil attributes is hampered if the pixels have a vegetation cover over 20% (Mulder *et al*., 2011). Although variables measured using remote sensing do not entirely cover the area to be mapped, Mulder *et al*. (2011) used univariate kriging to map continuous soil properties and classes. Ordinary kriging was preferred compared to simple kriging which is not suitable for heterogeneous areas (Mulder *et al*., 2011). Ordinary kriging is a typical geostatistical approach that relies on the observed soil textures and their corresponding spatial positions to predict the soil textures at un-sampled locations (Liao *et al*., 2013).

Soil can be analysed for texture, soil organic matter and moisture, salt and carbonates (Mulder *et al*., 2011). Information derived from a DEM, i.e. surface elevation, slope% and slope direction, could be used with the satellite images to increase their capabilities for soil mapping (Guzzetti *et al*., 2012). A geomorphic unit has a specific set of characteristics, for example, texture, tone, and reflectance that determines its image signature (Novak and Soulakellis, 2000). Commonly used supervised classification methods such as maximum likelihood classifiers are not appropriate for a detailed differentiation of certain soil classes. Therefore, linear

spectral unmixing was selected for classification. Understanding the spatial distribution and variability of soil texture is essential for land use planning and other activities related to agricultural management and environmental protection (Liao *et al*., 2013).

Vidhya *et al*. (2015) used spectral unmixing to retrieve soil properties (soil texture and moisture content) from Landsat ETM+ and Ikonos. Vidhya *et al*. (2015) found that remote sensing and digital image processing show potential when compared to results obtained from laboratory tests to generate digital soil maps. Ali and Moghanm (2013) used DEM and Landsat ETM+ image to map landforms, with field work conducted to assess the accuracy of the mapping. They linked laboratory soil analyses with their geographical locations to produce thematic soil properties.

2.5. Accuracy assessment

Although field work provides the basis of detailed geomorphological mapping, technical possibilities offered by the use of computers offer added flexibility in data collection, data handling and presentation (Gustavsson *et al*., 2006; Bishop *et al*., 2012). However, the uncertainty remains about the reliability of the generated maps from remote sensing and GIS. Sefercik *et al*. (2007), DEM quality is represented by the accuracy and morphologic details from the DEM.

Similar to manual methods of geomorphological mapping, DEM data also have limitations. DEMs constitute uncertainty as they contain inherent errors due to the methodology followed to generate DEMs or post-processing steps (Forkuor and Maathius, 2012) and are often used without quantifying the effects of these errors

(Wechsler and Kroll, 2006). Milledge *et al*. (2009) raise issues of data quality that DEM error affects individual point elevations as well as the geomorphological parameters determined from them.

Van Den Eeckhaut *et al*. (2004) (cited in Gustavsson *et al*., 2008) illustrate the advantages of field investigations over the interpretation of aerial photographs and shaded DEMs for interpretation of geomorphological features in densely vegetated areas. Despite the advances made in the interpretation of satellite data and high resolution DEMs, a detailed assessment of landform genesis and material distribution remains complex (Gustavsson *et al*., 2008). Hence, field check remains necessary for landform interpretation and classification validation. DEM error is the difference between the model's elevation value and true elevation value (Fisher and Tate, 2006).

Schirrmeister *et al*. (2005) evaluated the performance of CARONA images to classify periglacial compared to aerial photographs. CARONA images were found to perform better; however, the approach used other remotely sensed data that are also subject to error. Contrary to the study by Siart *et al*. (2009) that DEMs have had heights of vegetation, buildings, and other cultural features digitally removed; Grohmann *et al*. (2007) found that SRTM DEM over an area covered by dense vegetation tends to account for elevation variations thereby increasing DEM height and hiding minor areas.

Vertical and horizontal accuracies vary for the different data sets (Mulder *et al*., 2011). 3- arc SRTM has an absolute elevation accuracy of $\pm$ 16m (Du *et al*., n.d.); 1-arc ASTER DEM has a vertical accuracy of $\pm$ 20m (Du et al, n.d.; Pipaud *et al*.,

2015), and 1-arc SRTM an absolute vertical accuracy of 20m (Mulder *et al*., 2011). DEM elevation can be used to evaluate the accuracy of a DEM (Jobin and Prasannakumar, 2015; Salleh *et al*., 2015). To assess DEM accuracy, DEM elevation is compared with the elevation of reference points (Rokni *et al*., 2015). The minimum amount of reference point for comparison is 28 (Jobin and Prasannakumar, 2015).

Jobin and Prasannakumar (2015) used RMSE to measure the estimation of error amongst other statistics such as ME, MAE. RMSE accounts for random and systematic errors introduced during the data generation process. DEM resolution plays a role in the computation of slope since the slope of a pixel is calculated as a change in elevation with respect to surrounding pixels (Jobin and Prasannakumar, 2015). Warren *et al*. (2004), erroneous slope estimates may result in varying estimates of environmental phenomenon such as soil erosion.

Guth (2010) compared the performance of SRTM and ASTER DEM to determine which DEM better depicts topography looking beyond elevation distributions. The study compared derived parameters (slope and shaded reflectance) to indicate DEM quality. This approach relies on visual judgement and does not quantify the extent to which each DEM is accurate. The method of DEM to DEM can only get the relative DEM accuracy (Du *et al*., n.d.). The study by Guth (2010) shows that SRTM overestimated slopes in gentle topography, and underestimated in slopes in steep terrain). Mashimbye *et al*. (2014) delineated test morphological discontinuities from digital aerial images to serve as backdrops when assessing the accuracy of DEM delineated land components.

Rusli *et al.* (2014) compared SRTM and ASTER DEMs and found that 1-arc ASTER presents smoother DEM compared SRTM; the ridge lines could be clearly seen ridge lines can be seen clearly. GEOBIA classification was found to be successful in depicting well individualised areas that are bound by major discontinuities and less successful in highly heterogeneous areas (Drăguţ and Eisank, 2012). Pipaud *et al.* (2015) used shape of landforms to assess the performance of different DEMs delineated by computing hillshade, slope and curvature raster datasets. The results were evaluated by Landsat ETM.

When using DEMs for geomorphological mapping an accuracy assessment is required (Guth, 2010). Field checking is required for accuracy assessment (Guth, 2010). GPS measurement data verification is one of the most common methods to verify DEM accuracy which can obtain ground control points with higher accuracy. However, field cost a large deal of work and time consuming, so that it is difficult to get a large number and area of measurement points (Du *et al*., n.d.). A global assessment of DEM data has been performed, however, it is impossible to apply the general conclusion to all the regions (Du *et al*, nd). Variations in the computation of slope from digital elevation data can result in significantly different slope values and can, in turn, lead to widely varying estimates of environmental phenomenon such as soil erosion that are highly dependent on slope.

To assess the performance of an image classification, the results are validated with ground truth data Berhanu (2005). An error matrix is commonly used to assess the accuracy of a classification. Producer's, user's and overall accuracies as well as kappa coefficient can be derived from the error matrix. Producer's accuracy is

the number of correctly classified pixels in each class divided by the number of pixels used for that class. The user accuracy is calculated by dividing the number of correctly classified pixels in each class by the total number of pixels that were classified as that class. The overall accuracy is the number of correctly classified pixels divided by total number of pixels checked. The overall accuracy strongly overestimates the accuracy.

Kappa coefficient is defined as an estimate of a measure of overall agreement between image data and reference data. This is a widely used technique and it considers within class correlation as well as overall image correlation. Kappa value of less than 0.40 shows poor agreement; 0.40 – 0.59, fair agreement; 0.60 – 0.74, good agreement; and of greater than 0.74, excellent agreement (Berhanu, 2005). K value of 1 implies perfect agreement since K is always less than or equal to 1 (Berhanu, 2005).

2.6. Chapter Summary

From the literature reviewed in this chapter, the provided concepts were found to be relevant for this study. Guidelines of generating a detailed geomorphological map using automated methods were governed by the reviewed literature. The shortcomings of each method in mapping and how to overcome them; identification of landforms were also applied. The following chapter outlines the methods of data collection and analysis.

CHAPTER 3

METHODOLOGY

3.1. Introduction

This chapter outlines the methods that were utilised to evaluate the suitability of ASTER and SRTM DEMs, and Landsat 8 image in detailed geomorphological mapping. The quality of the DEMs that were assessed determined whether these data sets are suitable for delineating geomorphological units similar to the geomorphological units generated from stereoscopic analysis of aerial photographs and field survey. The data used and methods of data collection, as well as analyses are outlined in the following sections.

3.2. Research Design

The main objective of this study is to determine whether ASTER and SRTM DEMs and satellite imagery are suitable for detailed geomorphological mapping. To achieve this objective, a detailed geomorphological map was generated from stereoscopic analysis of aerial photographs which served as a reference map for comparison with the maps generated from the DEMs and satellite imagery.

The DEMs were assessed mainly for accurate derivation of drainage channels, slope (for landform delineation) and elevation accuracy, while Landsat 8 imagery was used to extract soil texture to give terrain characteristics, since soil texture and land cover cannot be obtained from DEMs. The steps followed are presented in Figure 3.1.

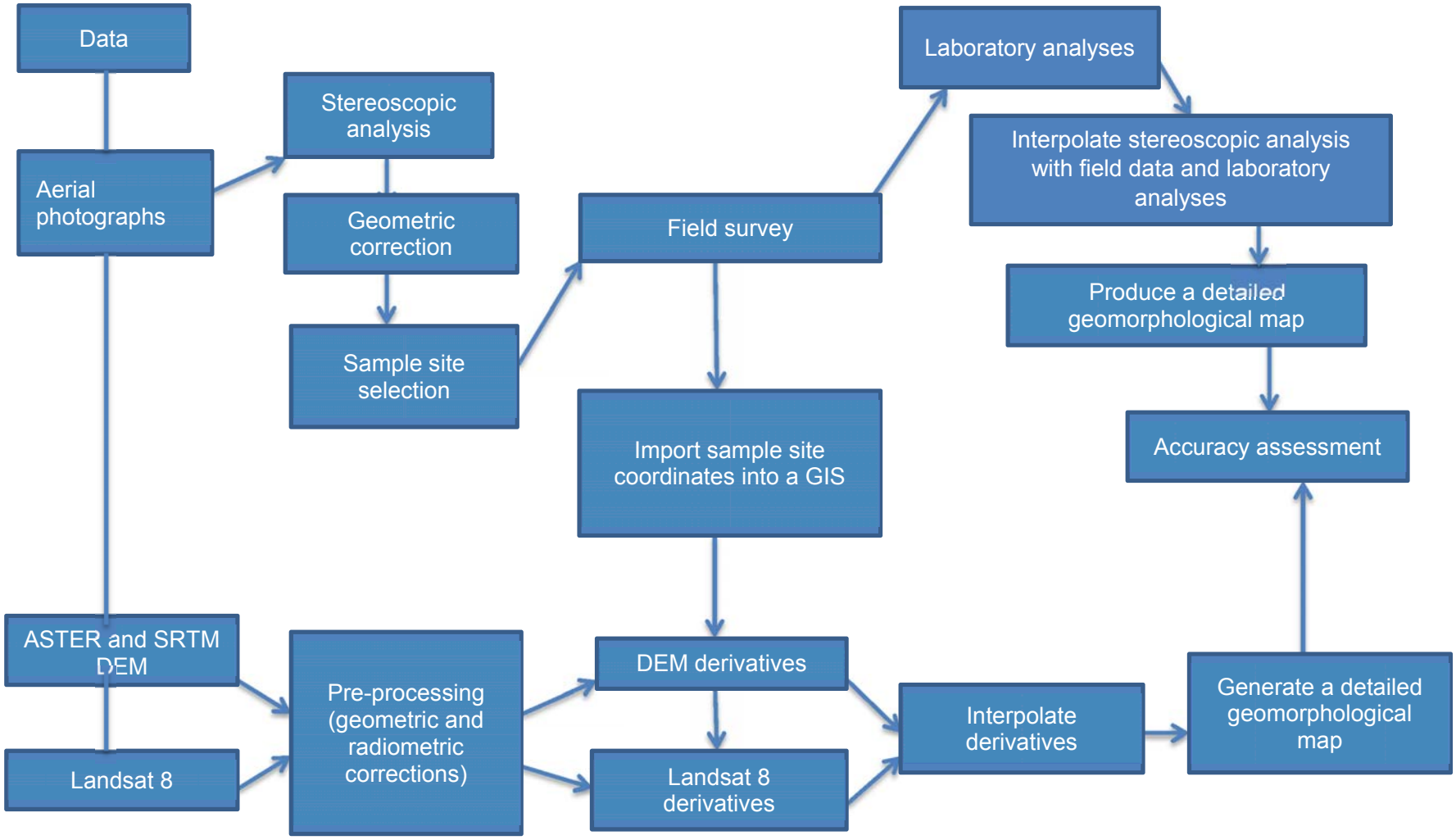

Figure 3.1: Flow chart of the methodological steps followed in this study

The research design adopted in this study is descriptive survey. Aggarwal (2008) (cited in Neeru, 2012) describes a descriptive research design as an approach that involves the collection of data about current conditions for the purpose of analyses, description, interpretation, comparisons and identification of relationships. The survey may be qualitative or quantitative, employing scientific methods of analysing and interpreting data. Qualitative methods for landscape characterisation rely on expert evaluations and opinions to make estimates from variables based on the assumption of the relationships between them, while quantitative methods include statistical methods (He and Beighley, 2008).

3.3. Types of Data Used

The data needed for analyses and interpretations include field survey and secondary data sources. Both primary and secondary data were used in this study. The primary data were collected during a field survey and included slope and elevation measurements, soil samples, and the geographical coordinates of the samples. The secondary data consisted of aerial photographs (Appendix A), resized ASTER and SRTM DEMs (Appendix B), and Landsat 8 image (Appendix C) for the mapping of geomorphological units. The dates on which secondary data were acquired and sources from which they were acquired are given in Table 3.1

Table 3.1: Secondary data used in this study

Data	Scale/ spatial resolution	Date acquired	Source of data
ASTER	30m	2011	Downloaded from USGS website United States Geological Survey (USGS) website.
SRTM	30m and 90m	2011	Downloaded from USGS
Aerial photographs	0.5m 1:30000	2004	Department of rural development and land reform, National Geo-spatial Information (NGI) branch
Landsat 8 imagery	30m	2017	Downloaded from USGS website

3.4. Reference Geomorphological Map

In order to assess the accuracy of the DEMs, a reference geomorphological map is required for comparison. For the purpose of this study, the interpretations from aerial photos and field survey were used to generate a reference geomorphological map.

3.4.1. Stereoscopic Analyses of Aerial Photographs

Before the field survey was conducted, aerial photo interpretation was performed in order to inform sample site selection. The photo interpretation was performed using two aerial photograph series (sheets 0465 and 0466 at the scale of 1:30 000) acquired in September 2004 (Appendix A). The photographs were used to create a preliminary geomorphological map to support field survey (Fonseca, 2011), as well as to serve as reference map (Mashimbye *et al*., 2014; Odhiambo, per. comm, 2017). The assumption is that there are no significant changes in the landforms between the dates (Jones *et al*., 2007) when the aerial photographs were acquired

(2004) and when the field survey was done (April 2017). This was verified and confirmed through visual inspection during the field survey.

Stereoscopic analysis and interpretation of aerial photographs were used to identify geomorphological units that were transferred onto a tracing paper (Appendix D.1). The stereoscopic photo interpretation enables identification of photo characteristics (such as tone, pattern, texture, mottling, shape, size, shadow, site and situation) that are used to depict the geomorphological terrain units (Evelpidou *et al.,* n.d.; Odhiambo, per. comm, 2017).

The geomorphological map was then scanned at 300dpi resolution and then transferred into a QGIS/GRASS environment. The map was georeferenced to rectify the map for radial distortions using 20 ground control points (GCPs) with the Georeferencer tool in QGIS. Georeferencing also enabled the geomorphological map to be overlaid onto the corresponding maps generated from DEMs and Landsat 8 imagery; and the selection of sample sites using correct geographic coordinates. Simple line geometry was used initially for digitizing slope units. This was subsequently followed by detailed break of slope mapping, outlining individual landforms with polygons (Appendix D.2). Figure 3.2 shows the photomap of the study area and the location of the sampled sites. The final detailed geomorphological map was produced at the scale of 1:20 000 (Figure 4.1).

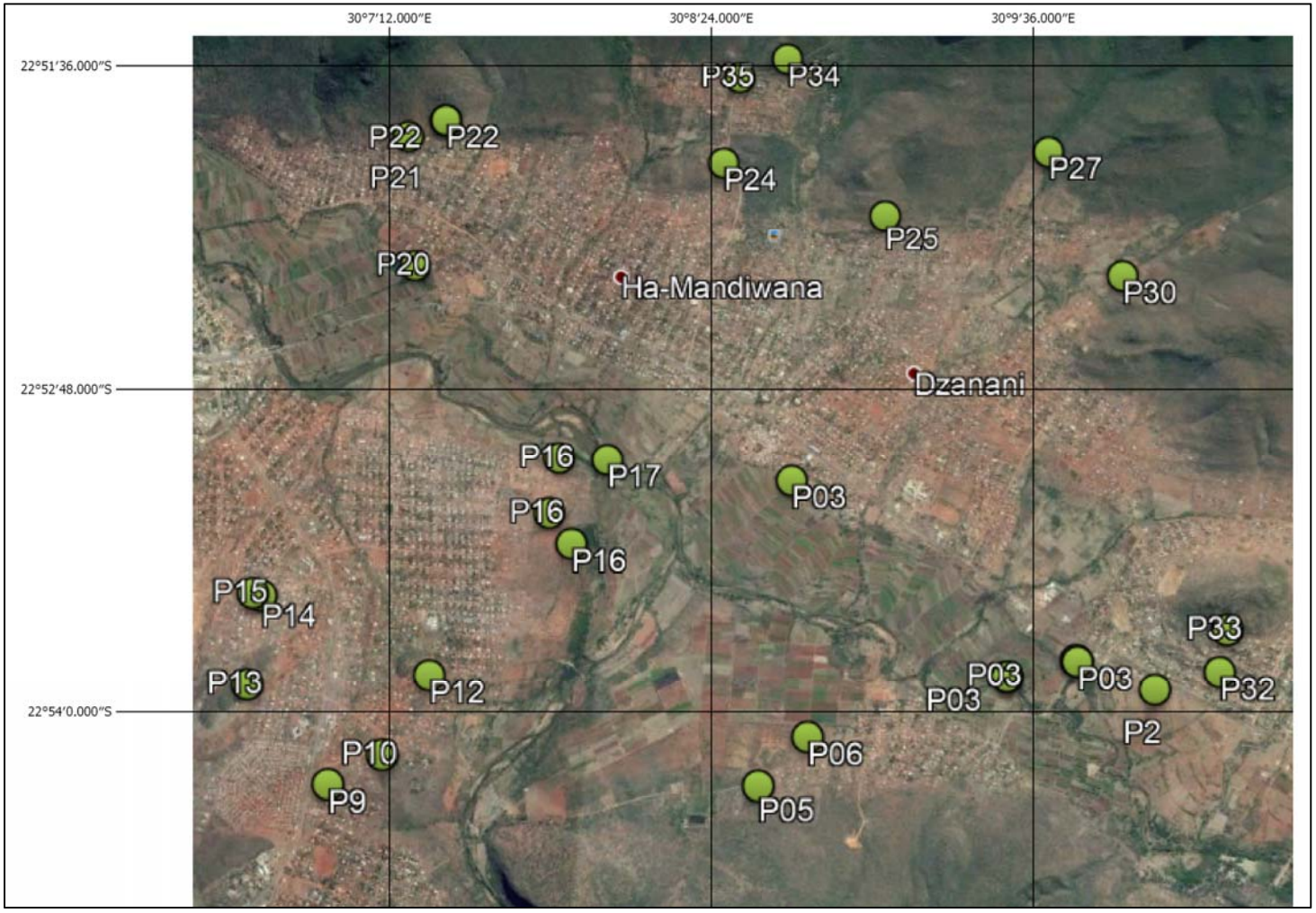

Figure 3.2: Location of sample sites for field data collection

3.4.2. Sampling Methods, Size and Unit of Analysis

The aerial photo interpretation aided the selection of the sampling points for the field survey. The field survey provides complementary data to the aerial photo interpretation to produce a detailed geomorphological map. The sampling methods that were adopted in this study are a combination of stratified sampling and purposive sampling. The stratified sampling approach subdivided the study area into strata (according to image characteristics), and enabled both accuracy and statistical validity to be done (Dogan and Kılıç, 2013).

The study area was stratified into slope units. Slope units were selected as the unit of analysis from the geomorphological units generated from stereoscopic analysis of aerial photographs. Landforms that appearred similar in morphology and the processes involved in their formation were classified as a similar unit; as a result, not every slope unit needed to be sampled. A total of 30 sample sites were randomly distributed within the sampled strata. Accessibility sampling was used in cases where a sample site was found to be on inaccessible terrain (Rhoads and Thorn, 1996).

At each sample site, data were collected for slope angle in percentage, elevation in meters and soil samples, then geographic coordinates of the locations where the data were collected was determined, as well as description of geomorphological units. The geographic coordinates allowed for the sampled locations in the field to be imported into a GIS environment for comparisons with

the DEMs and Landsat 8 derivatives. Slope angles were measured using a Total Station with prism (Figure 3.3).

Figure 3.3: Using the Total Station in the field

Elevation data were collected with a handheld GPS to serve as ground truth when assessing DEM quality. The geographic coordinates of the sample sites were recorded, saved as CSV (comma delimited) format along with the attribute data (slope angle and elevation) and imported into a GIS for comparison with map outputs from DEMs and Landsat 8 imagery. Surface soils samples (extracted using a soil sampling auger to the depth of tillage) were taken in order to determine the texture of the soil (in terms of its clay, silt and sand fractions; see also Figure 3.4) found in each geomorphological unit.

During the field survey, some of the sample sites fell on scree slopes with poorly developed soils. As a result, soil samples could not be collected for analysis in such polygons and a total of 19 soil samples were collected out of the 30 sampled sites. The surface material on the scree slopes was larger than the 2mm soil particle for textural classification; therefore soil samples could not be collected. However, data were collected for slope angle and elevation and the samples' geographic coordinates. The geomorphological units were then described accordingly. The collected soil samples were put into plastic sample bags and labelled for laboratory analysis. The data collected for slope and elevation are presented in Appendix E, and were compared with slope and elevation data derived from DEMs.

3.4.3. Analyses of Soil Samples

The soil samples collected in the field were analysed for soil texture, moisture content, and pH to describe the terrain characteristics. The procedures carried out for the soil analyses are presented in Appendix F following the similar approach by Dogan and Kılıç (2013) and Vidhya et al., (2015). Soil texture was determined by plotting soil fractions in a soil textural triangle (Figure 3.4). The results from the soil analyses are presented in Appendix G.1 to G.3, and they were used to describe the surface materials of the geomorphological units interpreted from the aerial photographs presented in Table 4.1.

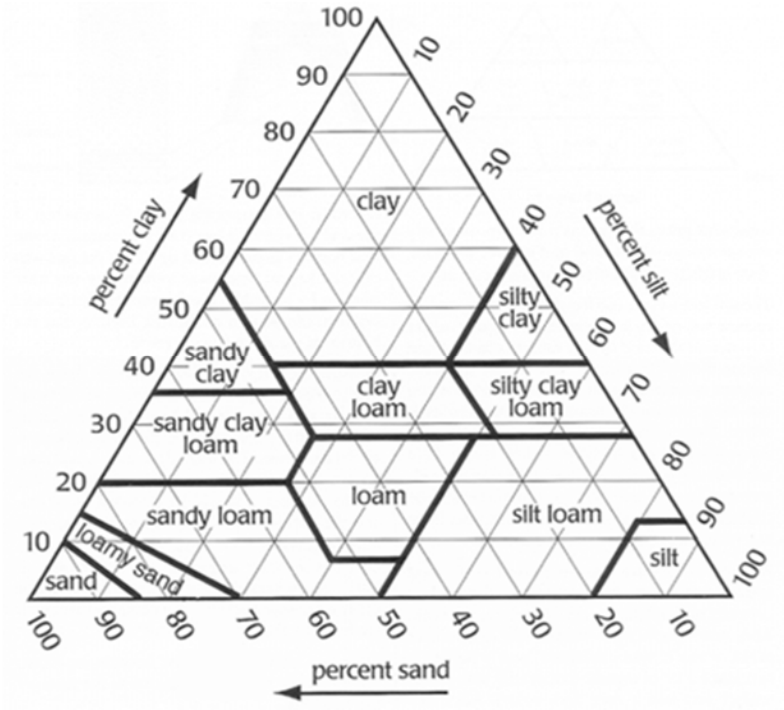

Figure 3.4: A soil textural triangle used to determine soil textural class from the percentages of sand, silt, and clay in the soil (van Zuidam and van Zuidam-Cancelado, 1989)

The data from field survey and laboratory soil analyses were incorporated onto the aerial photo interpretations to produce a detailed geomorphological map that served as a reference geomorphological map. The reference geomorphological map was then used to assess the suitability of DEMs and Landsat 8 imagery in detailed geomorphological mapping. The final detailed geomorphological map was produced at the scale of 1:20 000 (Figure 4.1).

3.5. Geomorphological Map from ASTER and SRTM DEMs

Geomorphological maps were generated from the DEMs. Although 3-arc SRTM DEM has a coarse resolution compared to the 1-arc DEMs, the 3-arc DEM was used to assess the influence of DEM resolution on its accuracy in terms of landform

characterisation. To generate the geomorphological maps, the DEMs coordinates were first adjusted to comply with the UTM WGS 84 (Zone 32 south) coordinate system, which then makes it possible for other datasets to be overlaid (Berhanu, 2005; Maselli *et al*., 2008).

The GIS that was used for the processing of DEMs for the production of geomorphological maps is the QGIS 2.14.22 Essen with GRASS 6.4.3 and SAGA plugins. To create geomorphological maps from DEMs, slope maps were first generated from the DEMs. The slope maps were used to delineate landforms. The *r.slope.aspect* module in GRASS GIS was used to generate slope classes from each DEM. Landforms are classified by slope position (Seif, 2014). Slope classes were reclassified to generate geomorphic units (polygons of similar slope classes). The *r.reclassify* module was used to reclassify the slope classes into a relevant general class of landform (Gerçek, 2017).

Slope units have distinct characteristics that can be summarized from a digital data set and used to generate a geomorphological map (Giles, 1998). Slope maps were reclassified into five categories and described as proposed by van Zuidam and van Zuidam-Cancelado (1989) as follows: 0-2% (flat or almost flat); 2-7% (gently sloping); 7-13% (sloping); 13-20% (moderately steep) and 20-55% (steep). The reclassified slope maps from each DEM were loaded into ArcMap 10.3 for post classification generalization to eliminate edges on slope boundaries and to remove pixels that are too small to fit geomorphological symbols (van Zuidam and van Zuidam-Cancelado, 1989). For this purpose the majority filter and boundary clean tools in ArcMap were used.

Similar to multiresolution segmentation, the *r.slope.aspect* generates raster maps of slope, aspect, curvatures and first and second order partial derivatives from a raster map of true elevation values (Horn, 1981; Mitasova, 1985; Hengl and Reuter, 2009). However, the *r.slope.aspect* module does not offer the user the ability to specify the scale of segmentation. The reclassified maps were used to derive landforms.

The accuracy of the DEM derived slope angles was evaluated by comparison with the field data. The coordinates of each of the sample sites were imported into GRASS GIS as a delimited text layer from Microsoft Office Excel 2007 so that the sampled sites could be identified from the DEM generated maps. Once the sampled sites were imported, the slope classes in which they belonged were compared with the slope angles measured from the field to determine whether the DEMs assigned similar slope angles.

The downside of DEM usage is that the researcher has to be knowledgeable about the area under study to know what kind of geomorphological units exist in the area. The reason for this is that multiple DEM computations are needed to come up with the different derivatives that a DEM can provide. A DEM from a single computation of derivatives has a limited ability to show landform types (Smith et al., 2006).

To generate a detailed geomorphological map, more geomorphological units had to be derived from the DEMs. Terrain units can be classified into slope position (ridge tops, upper, middle, flat and lower slopes, and valley bottoms) and landform category (steep narrow canyons, gentle valleys, plains, open slopes) using Topographic Position Index (TPI) values (Figure 3.5) (Seif, 2014). The TPI was

computed in SAGA GIS. The Topographic Position Index (TPI) compares the elevation of each pixel in a DEM to the mean elevation of a specified neighbourhood around that cell. Positive TPI values represent locations that are higher than the average of their surroundings, as defined by the neighbourhoods (ridges); while negative TPI values represent locations that are lower than their surroundings (valleys). TPI values near zero are either flat areas (where the slope is near zero) or areas of constant slope (where the slope of that point is significantly greater than zero.

The TPI landform classification that was used in this study is presented in Figure 3.5, which describes the scenery of the study area. The TPI was reclassified into three classes highlighting valleys, flat areas and ridges. The drainage channel was delineated in QGIS for each DEM using the D∞ flow accumulation algorithm.

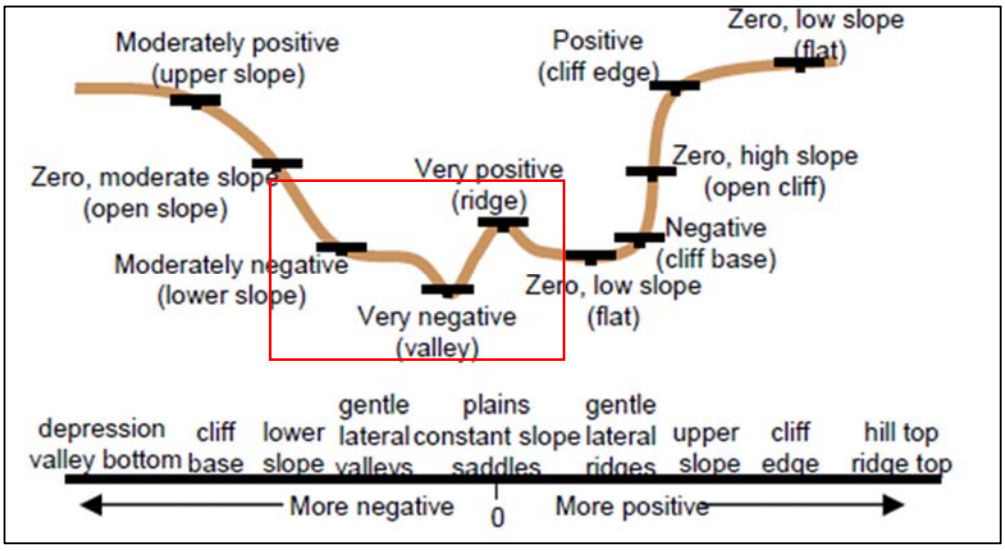

Figure 3.5: TPI and slope position (Seif, 2014)

3.6. Geomorphological Map from Landsat 8 imagery

Soil reflectance can be obtained in the field using a field spectrometer or from satellite imagery (Berhanu, 2005). Surface material and land cover cannot be extracted from DEMs; and therefore Landsat 8 imagery was used for this purpose. The areas of agricultural practice and settlement are described in the geomorphological units as seen in Appendix C. The aerial photographs and the Landsat 8 image show similar land use land cover types. For this reason, automated classifications of land use land cover of the study area from Landsat 8 image was not performed, nor were they included on the reference geomorphological map.

3.6.1. Image Preparation

Remote sensing information is collected on a per pixel basis and therefore geometric corrections need to be made to the data to ensure that each pixel can be referenced to a real world coordinate system and then can be used with other spatial datasets. The Landsat 8 imagery was corrected for geometric and radiometric distortions before processing.

The geometric corrections were done to set the image geographic coordinate system as the sample site (UTM WGS 84 (Zone 32 south) coordinate system), which then makes it possible for other datasets to be overlaid (Berhanu, 2005; Maselli *et al*., 2008). The radiometric correction is necessitated by the factors which influence the radiance as measured by a system over an object and was done to convert the digital numbers of the image to top of atmosphere reflectance (ToA) using band math (Liao et al., 2013; Shabou et al., 2015).

3.6.2. Linear spectral unmixing

Mapping soil texture attributes was carried out using reflectance data from different spectral bands (Bands 3, 4 and 5) of Landsat 8 imagery. To determine soil texture, a Landsat 8 image was used and the ENVI version 4.4 was used for processing. Linear spectral unmixing in ENVI software was used to classify soil textures based on reflectance. This method can be used in digital soil mapping. Figure 3.6 shows the steps followed to determine texture from satellite imagery.

The mapping of soil texture was carried out using spectral reflectance in different bands (Bands 3, 4 and 5) of Landsat 8 image. The bands were loaded into ENVI 4.4 software. The RGB band composite of Landsat was stacked using the layer stack tool. The layer stack was resized to the size of the study area and the GPS coordinates of the sampled sites were imported into the image to enable the selection of regions of interest (ROI) based on sample sites.

In every remotely sensed image, a large number of mixed pixels are usually present (Berhanu, 2005). A mixed pixel is a picture element representing an area occupied by more than one ground cover type (Berhanu, 2005). Linear spectral unmixing (LSU) was performed in order to separate the mixed spectra from the image pixels for each generated endmember. The linear spectral unmixing outputs were rescaled from spectra to bit by converting the min-max of negative and positive to 0-255 min-max.

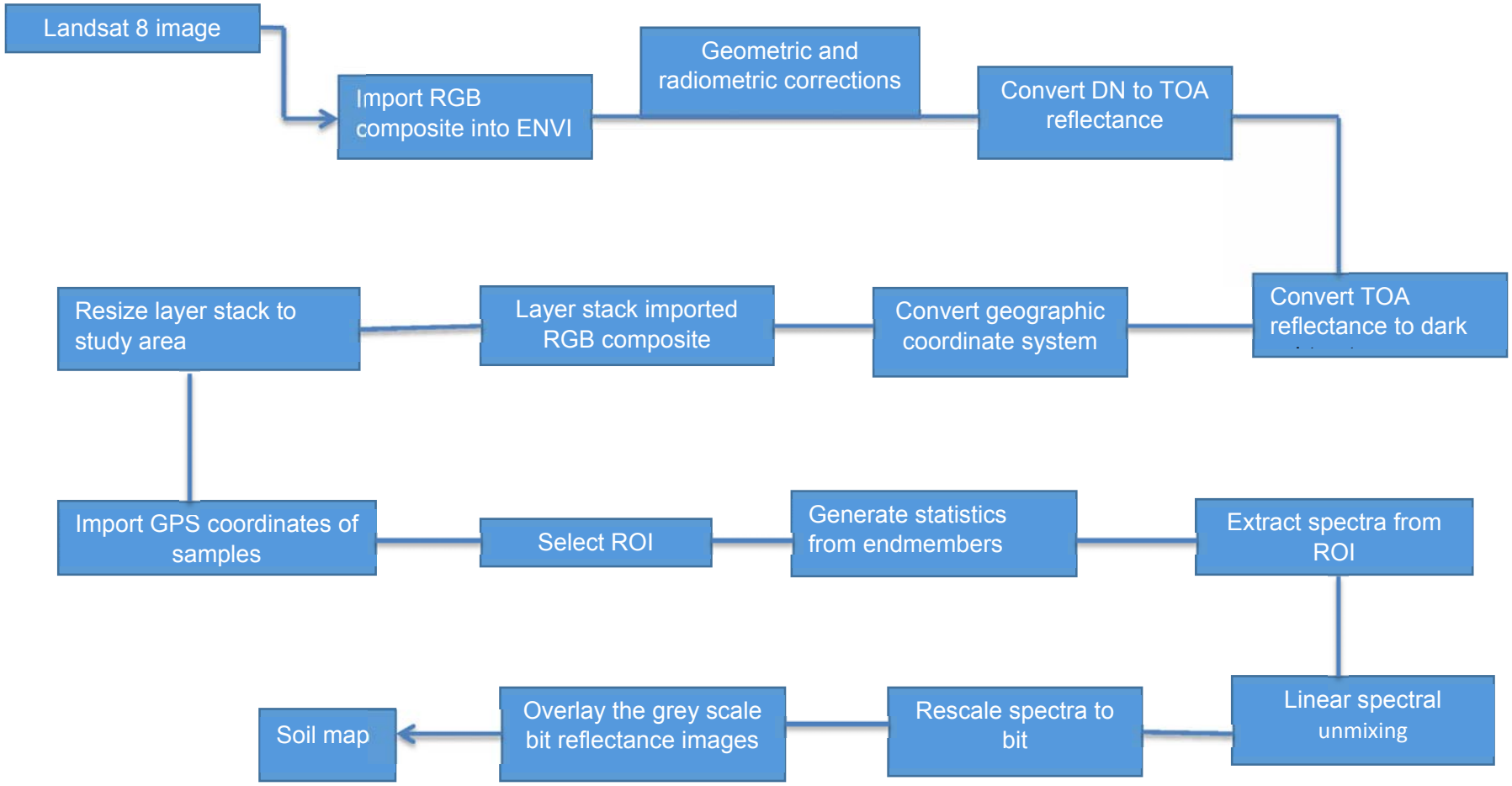

Figure 3.6: Flowchart of the steps followed to determine soil texture from Landsat 8

The density slice was used to set the anomaly area by making use of the mean and standard deviation of the endmember using the equaions:

$$\text{Anomaly area}_{(1\text{st range})} = \text{mean} + 2 \text{ standard deviations} \quad (1)$$

$$\text{Anomaly area}_{(2\text{nd range})} = \text{mean} + \text{standard deviations} \quad (2)$$

The start range was then changed from 0 to the value obtained from the anomaly area calculation, and the end range remained as 255. This gave an output of 0-1 min-max so that the desired endmember spectra were reflected as 1 and undesired spectra as 0 on the unmixed pixel image. The 0 shows no reflectance for the generated endmember and 1 shows reflectance for the generated endmember.

The output images were then overlaid to show the reflectance of each endmember, thereby showing the areas that had similar soil reflectance as the generated endmembers. Landsat 8 imagery was used in combination with the DEMs to produce a detailed geomorphological map. Thereafter, the map produced is compared with geomorphological map produced from aerial photo interpretation and field data for accuracy assessment. Density slicing was calculated to separate the rescaled map to show the regions of interest as well as the areas which have the same reflectance as the ROI (Figure 3.7).

The study area had sparse to no vegetation where the soil samples were collected. An NDVI image was prepared to identify vegetated and bare soil areas (Mulder et al., 2011) and the map shows areas with a NDVI value of 0.2.

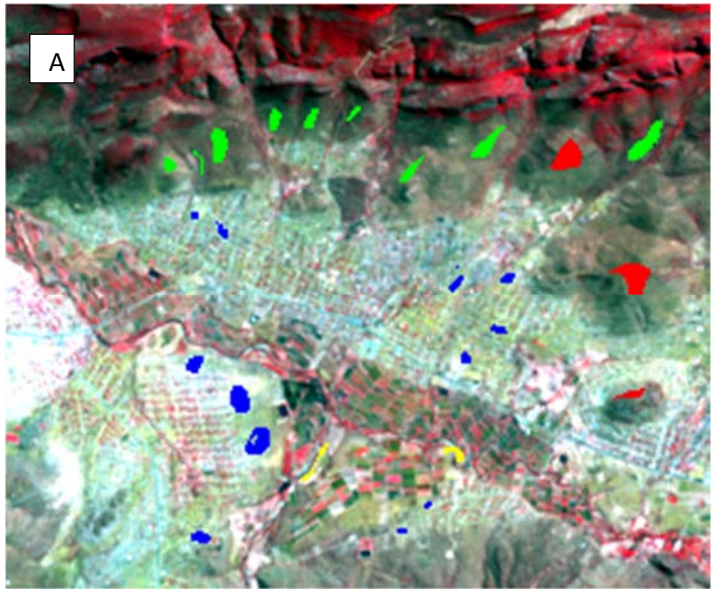

B

ROI Name	Color	Pixels	Polygons
A	Red	261	3/261
B	Green	378	9/378
C	Blue	342	12/342

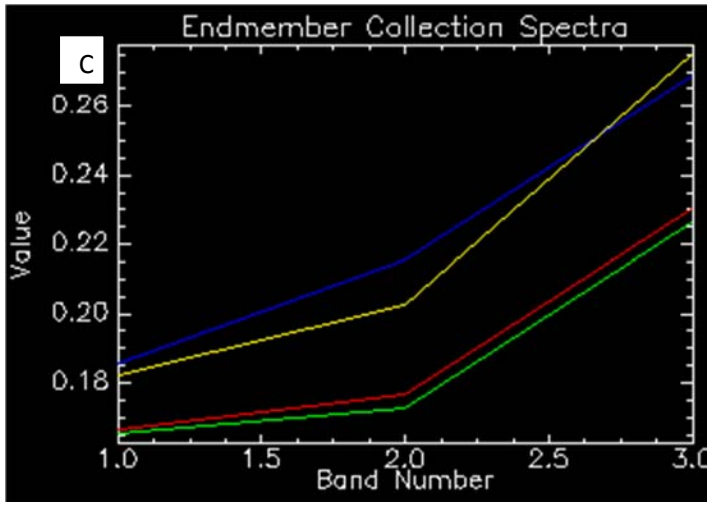

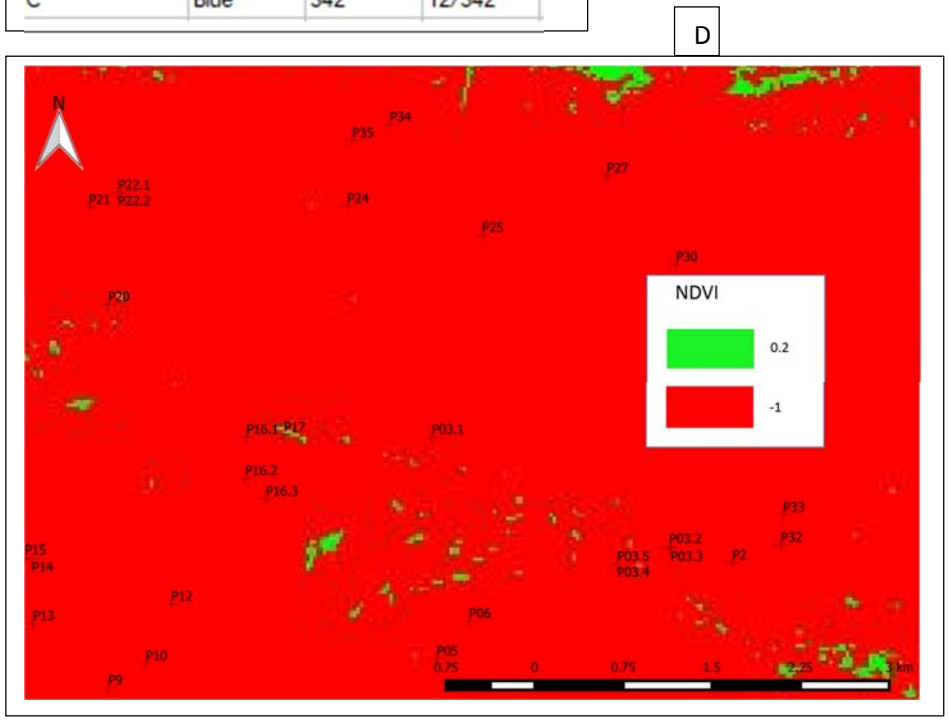

Figure 3.7: A – ROI, B – soil classes, C – spectra reflectance from ROI, and D – NDVI image

The green in the NDVI image shows sparse vegetation and the red shown areas with no vegetation -1. Using density slicing, a map of continuous soil classes was generated based on endmember spectra created from the regions of interest. Linear spectral unmixing method was applied for mapping soil reflectance. The geomorphological maps from DEMs and satellite imagery generate a detailed geomorphological map which was compared with the reference geomorphological map for accuracy assessment.

3.7. Accuracy Assessment of Automated Mapping

An assessment of how accurate the DEMs and Landsat 8 imagery are in terms of producing a detailed geomorphological map was performed by comparing the map outputs from the DEMs and Landsat 8 image with the reference geomorphological map.

3.7.1. DEM Quality Assessment

The quality of the DEM was assessed by determining the accuracies of the DEM elevation and slope angles. DEM quality affects the morphologic detail derivatives (Sefercik *et al*., 2007). Accuracy assessment was carried out by comparing the elevation values obtained from the DEMs with the field collected elevation data. A total of 30 elevation points were extracted. The assessment of the elevation accuracy was done using RMSE and correlation coefficient. The RMSE and correlation coefficient were computed to determine how far off the DEM elevations are from ground truth.

Vertical and horizontal accuracies vary for the different data sets (Mulder et al., 2011). 3-arc SRTM has an absolute elevation accuracy of ± 16m; 1-arc ASTER DEM has a vertical accuracy of ± 20m, and 1-arc SRTM an absolute vertical accuracy of 20m (Pipaud *et al*., 2015).

An error matrix was tabulated for slope to assess the slope accuracies from which producers, user and overall accuracies (Berhanu, 2005) were computed, as well as the kappa coefficient (computed as shown in equation 3). The error matrix compares the performance of an automated classification to a reliable classification method. The slope data collected from the field survey were used as ground truth reference data for accuracy assessment.

Kappa coefficient (k) is calculated by dividing the difference between the product of the total sample points and sum of correctly classified samples, and the product of the sum of all the row and column totals with difference between the total number of samples squared and the sum of all the row and column totals (Equation 3). The results of this computation are presented in Table 4.4 through to 4.6.

$$K = \frac{\text{Total} * \text{sum of correct} - \text{sum of all the(row total} * \text{column total)}}{\text{Total squared} - \text{sum of all the (row total} * \text{column total)}} \quad (3)$$

3.7.2. Accuracy of Geomorphological Units

To determine whether the DEM geomorphological maps delineated similar geomorphological units (GUs) as the reference geomorphological map, qualitative and statistical analyses were performed. The qualitative analysis involved a visual comparison, whereby the GU map from DEMs were overlaid onto the reference geomorphological units map produced from photo interpretation and field data. A

shaded relief map calculated from each DEM, and Landsat 8 image were separately used at 80% transparency overlay for the geomorphological units derived from the DEMs to enhance the visualisation of the geomorphological units (Grosse *et al*., 2005).

The statistical analysis was performed to determine the similarity index of the geomorphological units from DEMs with geomorphological units from the reference geomorphological map. For this purpose the Kappa coefficient was computed to determine the level of accuracy of the correctly classified pixels from the DEMs (Berhanu, 2005).

3.8. Chapter Summary

The research design adopted as well as the methods of data collection and analysis have been outlined to achieve the objectives of this study. The methods involved stereoscopic aerial photo interpretation and field survey, and automated methods for mapping geomorphological units. The automated output maps are assessed for accuracy by comparing them with the reference geomorphological map. The following Chapter 4 presents and discusses the results obtained.

CHAPTER 4

RESULTS AND DISCUSSION

4.1. Introduction

This chapter presents the results obtained using the methods described in Chapter 3, so as to achieve the main objective of the study. The suitability of DEMs and Landsat 8 imagery in detailed geomorphological mapping is assessed by evaluating the performance of the aforementioned datasets compared to the reference geomorphological map using qualitative and statistical tools.

4.2. Reference Geomorphological Map

From the aerial photo interpretation and field data, a detailed geomorphological map was produced presented in Figure 4.1 and complementary legend in Figure 4.2, which serves as a reference geomorphological map. The map shows the landform types, processes, materials and land use practice present in the study area. The data collected from the field survey (including elevation, slope angles, soil samples and the sample sites' geographic coordinates) are represented in Table 4.1 to help describe the characteristics of the geomorphological units.

The soil samples were analysed for soil texture, pH and moisture content, and the results from the laboratory analyses are also presented in Table 4.1. The reference geomorphological map was produced at the scale of 1:20 000 and exported at the resolution of 300 dpi. The geomorphological units are described in terms of geomorphic processes, rock/soil type and other geological and pedological characteristics (soil moisture content and pH).

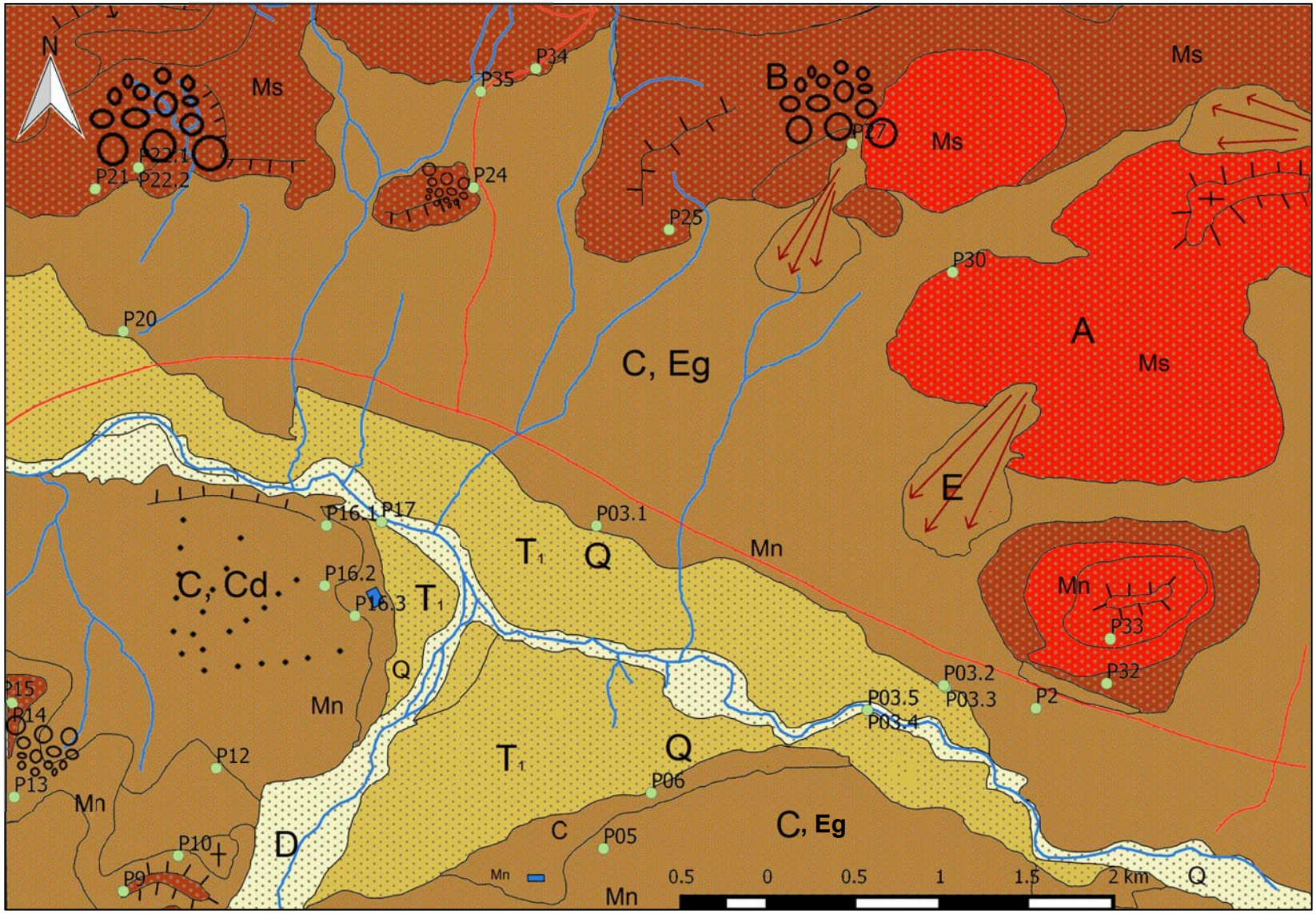

Figure 4.1: 1:20 000 detailed geomorphological map of Dzanani

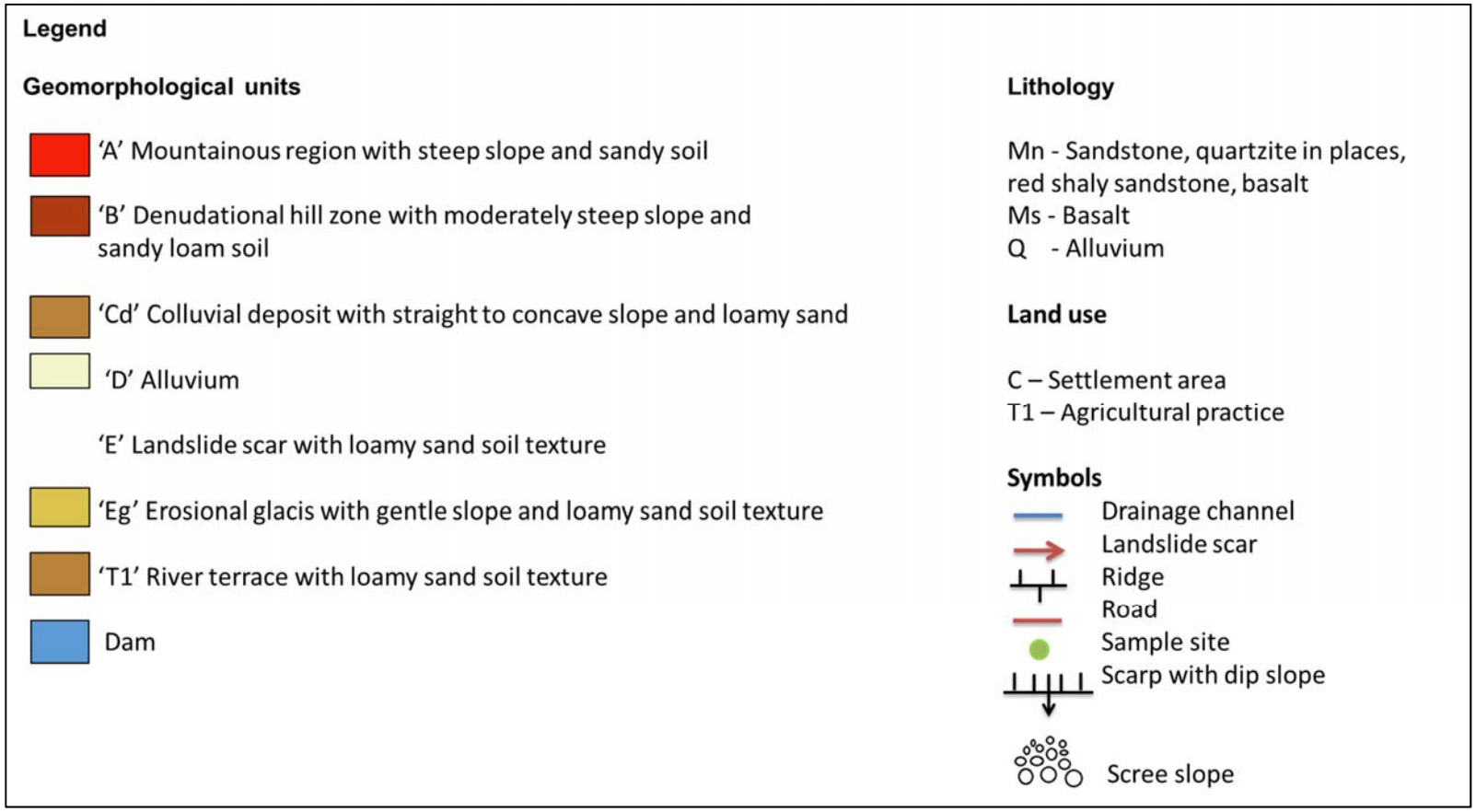

Figure 4.2: Legend of the reference geomorphological map

The map gives a detailed picture of morphology of the terrain with breaks of slope. The polygons are the different landforms that characterize the geomorphological units. In Figure 4.1, 'P' represents the sample site location; however, the slope angles and elevation are presented in Table 4.1. The soil texture on the map is symbolised by colours. Landforms A and B have a similar soil texture which is sandy loam. The lithology of the study area represents the Soutpansberg Group lithology: Ms (basalt), Q (alluvium), and Mn (sandstone, quartzite in places, red shaly sandstone, basalt).

Mountainous regions (A) with steep slopes were formed by slow denudational processes. The selected sample sites where data were collected in the 'A' unit are P30 and P32. The lithology of the unit is Ms with neutral sandy loam soils. Denudational hill zone (B) with moderately steep slopes were formed by weathering, rain-wash erosion and mass movement. The lithology of the unit is Ms with pH neutral loamy sand soils. The sample sites selected in (B) include P21, P22.1, P22.2, P34, P25, P27, and P32. P9, P15, and P14 are denudational hill zones formed by weathering and rain-wash erosion; with Mn lithology and loamy sand soils

The settlement area is concentrated in the geomorphological unit (C) which represents two types of landforms formed by two different processes with the same lithology, which is Mn and alkaline loamy sand soils. The flat plains (C;Eg) were formed by erosional glacis. The sample sites that were selected in (C,Eg) are P20, P35, P24, P2, P03.1, P03.2, P03.3, P5 and P6. The polygon 'C,Cd' is a moderately sloping geomorphological unit with straight to concave slope formed by debris

accumulation of colluvial deposits. The selected sample sites include P13, P12, P10, P16, P16, and P16.

The Nzhelele River runs through the geomorphological unit 'D'. The geomorphological unit is characterised mainly by alkaline sandy soil. The selected sample sites in the unit are P03.4, P03.5, and P17. The river runs through 'D' forming (T_1), where agricultural practices occur. Geomorphological unit 'E' are areas where landslides have occurred in the past. Ridges and scarps are present on some of the hill or mountain tops. Soil samples could not be collected from certain sample sites due to a lack of developed soils, for example, P21, P22, P27 and P2, and others, therefore, were not analysed for soil characteristics as shown in Table 4.1. In terms of pH, the soils are predominantly basic (alkaline).

Three main soil textures were analysed, namely; loamy sand, sandy loam and sand. A colluvial deposit in the form of a fan (at Sample site P16) is composed of poorly sorted material; from fine to rounded huge cobblestones of different sizes and composition (e.g. dolerite, granitic gneisses, and quartzite). Upslope are similar boulders by the roadside, possibly moved during road construction. On the footslope of denudational hills ('B' at sample sites P21 and P22) is debris flow composed of assorted of sorted angular rocks including indurated sandstones. At sample sites P25 and 34 are soils that are derived from basaltic rocks that are spheroidally weathered. On the mountainous region of complex geology are steep slopes with high relief (at sample site P33) prone to landslides.

Table 4.1: Description of terrain units, characteristics and land qualities

Terrain units	Terrain characteristics and land qualities							
	Geomorphological units	**Main Geomorphic Processes**	**Sample site**	**Slope angle (%)**	**Rock type**	**Soil moisture content**	**Soil type**	**Soil pH**
A	Mountainous region	Active tectonic; faulted; with steep slopes, landslides, scree slopes	P30	28.32	Ms	2.0	Sandy loam	7.88
			P33	32.15	Mn	8.0	Sandy loam	7.17
B	Denudational zone	Weathering, rain-wash erosion and mass movement	P9	1.44	Mn	3.1	Loamy sand	7.94
			P21	39.42	Ms	-	-	-
			P22.1	19.84	Ms	-	-	-
			P22.2	23.01	Ms	-	-	-
			P34	24.59	Ms	11.2	Sandy loam	8.41
			P25	9.41	Ms	2.9	Loamy sand	6.62
			P27	3.63	Ms	-	-	-
			P32	12.03	Mn	7.2	Loamy sand	8.35
			P14	8.75	Mn	-	-	-
			P15	5.95	Mn	-	-	-
C, Cd	Moderately sloping	Colluvial deposit	P13	27.77	Mn	-	-	-
			P12	3.85	Mn	3.9	Sandy loam	8.12
			P10	9.34	Mn	-	-	-
			P16.3	4.95	Mn	1.7	Loamy sand	8.05
			P16.1	3.77	Mn	4.8	Loamy sand	7.996
			P16.2	3.77	Mn	-	-	-
			P35	8.75	Ms	2.3	Loamy sand	8.14
			P24	4.42	Ms	-	-	-
C, Eg	Flat plain	Erosional glacis	P2	1.68	Mn	-	-	-
			P03.5	1.85	Q	3.9	Loamy sand	8.70
			P03.4	2.58	Q	10.1	Loamy sand	7.60
			P03.1	0.03	Mn	8.0	Loamy sand	8.50
			P05	9.19	Mn	5.0	Loamy sand	7.78
			P06	7.28	Mn	4.7	Loamy sand	7.74
			P20	5.86	Mn	7.3	Loamy sand	8.33
D	Valley	Water activity	P17	2.11	Q	8.5	Loamy sand	8.39
			P03.2	6.43	Q	0.4	Sand	7.37
			P03.3	1.53	Q	3.1	Sand	8.38

From the aforementioned terrain characteristics in combination with other criteria such as groundwater prospects, land suitability can be evaluated for land management. Soil moisture content can be determined from satellite imagery; however, they were not assessed for accuracy due to the differences in acquisition dates of the suitable satellite image and field data collection.

4.3. Geomorphological Maps Generated from DEMs

Using the methods described in Section 3.5, the results of the slope classes generated from the 1-arc ASTER, 1_1arc SRTM and 3-arc SRTM DEMs are presented in Figures 4.3 through to 4.5, respectively. The slope classes were automatically assigned by the software, hence the variation in slope ranges. The assigned slope angles range from 0 to 90%, with 0% being the lowest slope angle and 90% being the highest slope angle. The slopes shown as white/yellow represent the lowest slope angles and are thus flat areas. The red/black coloured slopes represent the highest slope angles which are hilly and mountainous areas.

The slope values of each sample location were determined so that they could be compared with slopes measured in the field to assess how the DEMs perform in assigning slopes. Since the slope classes overlap making it difficult to determine the slope angle from the classification, the identify tool was used to locate each sample site in order to determine their true slope value. The comparisons of the field measured slopes and slopes from the DEMs are presented in Table 4.2.

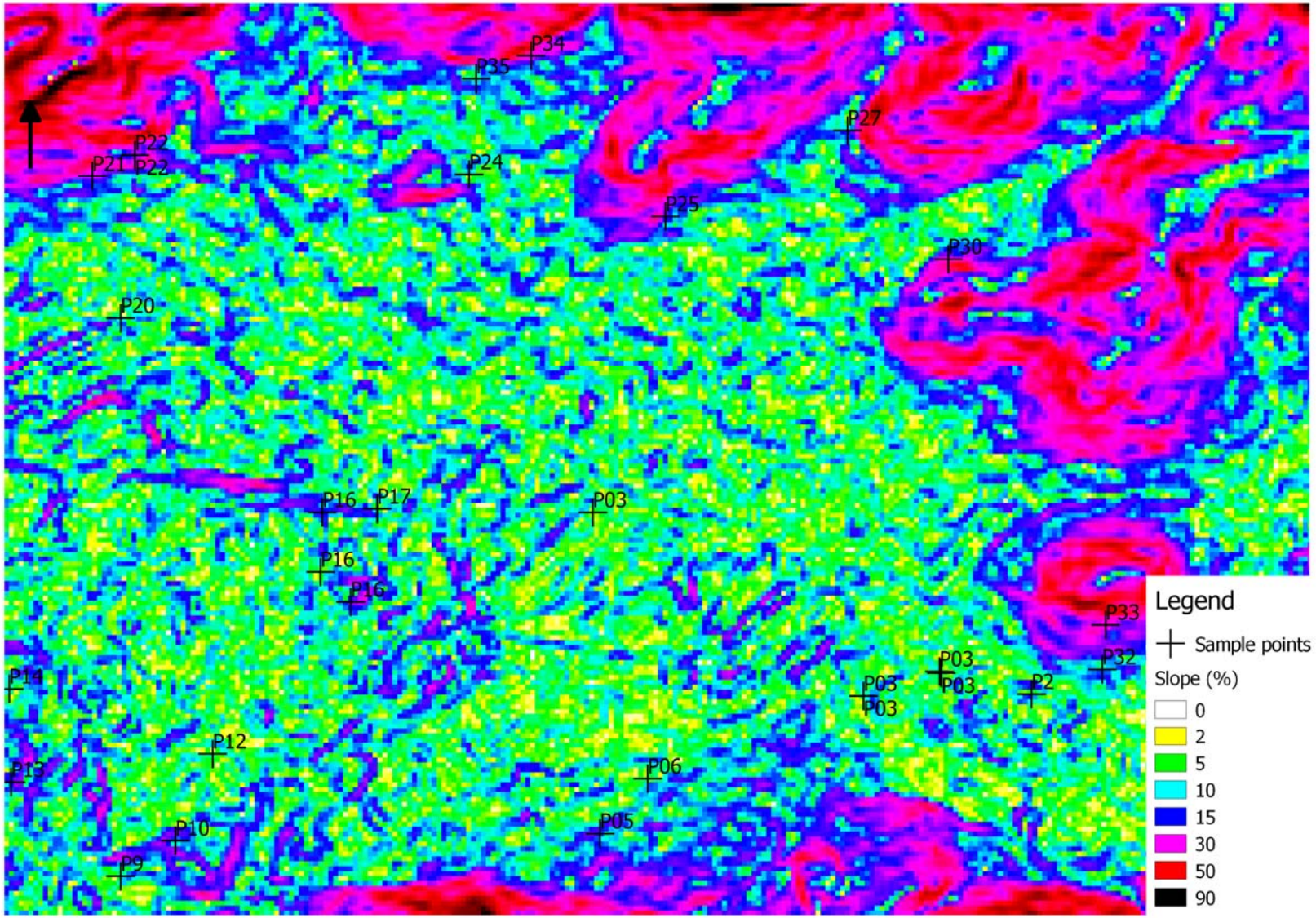

Figure 4.3: Slope map derived from 1-arc ASTER DEM

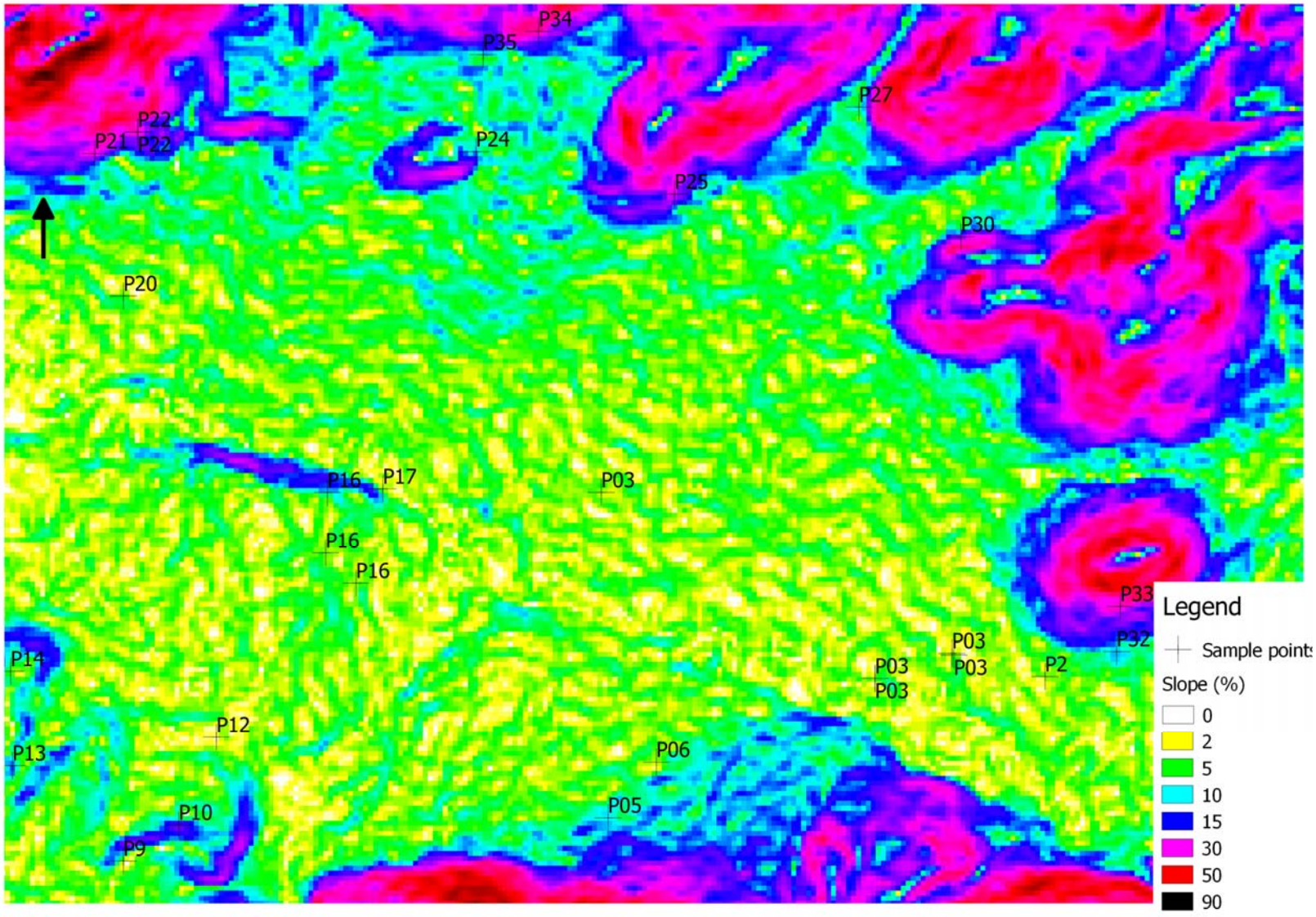

Figure 4.4: Slope map derived from 1-arc SRTM DEM

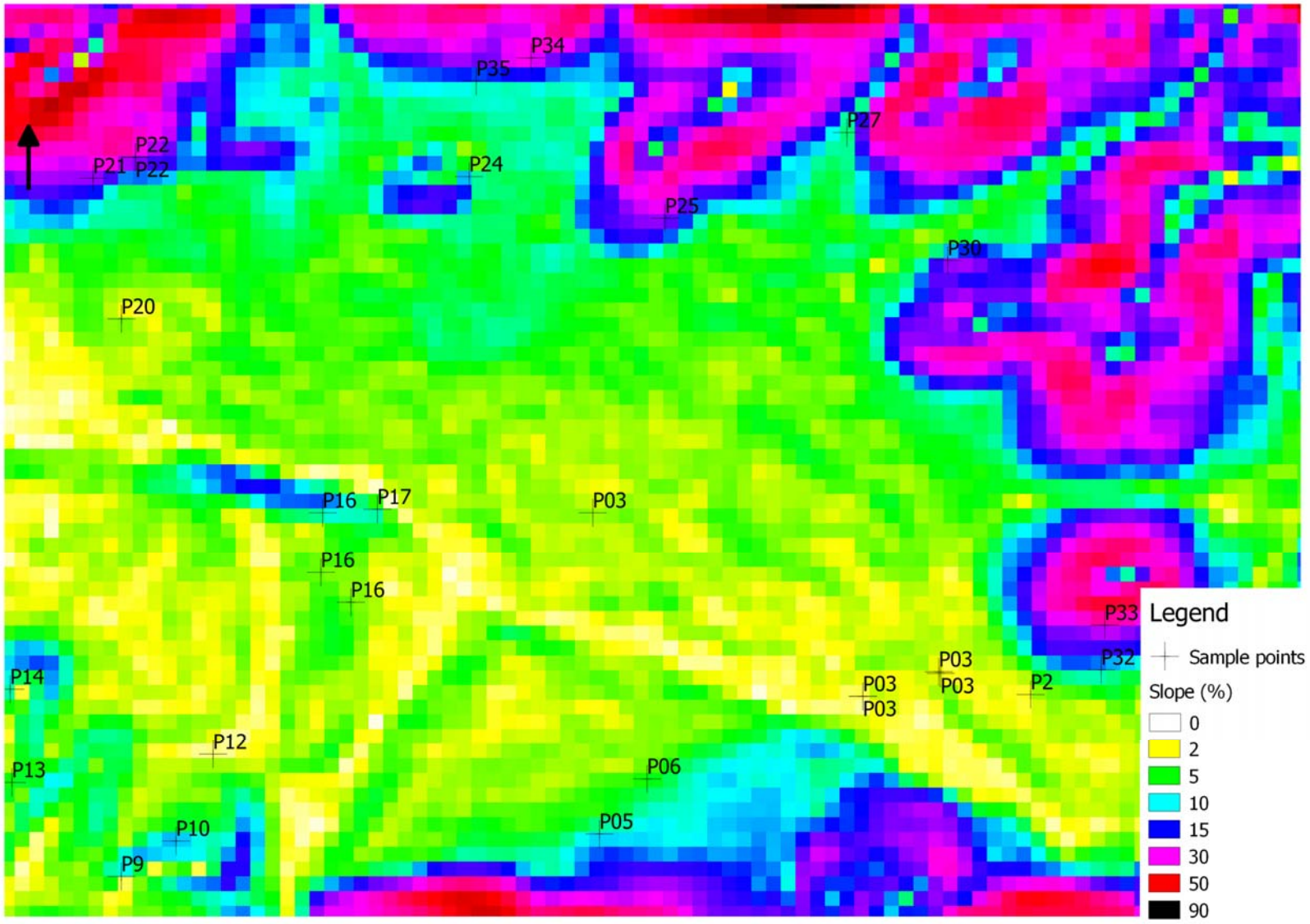

Figure 4.5: Slope map derived from 3-arc SRTM DEM

Table 4.2: Slope comparisons of field data with DEM derived slopes

Sample	1-arc SRTM DEM	1-arc ASTER DEM	3-arc SRTM DEM	Field measured slope (%)
P13	12.64	16.45	4.84	27.77
P9	2.59	5.95	1.38	1.44
P12	0.60	8.42	1.38	3.85
P10	17.74	14.39	11.30	9.34
P15	13.80	11.65	10.28	5.95
P14	3.96	8.29	8.26	8.75
P16.3	3.30	20.74	4.03	4.95
P16.2	3.68	5.44	3.83	3.77
P16.1	11.98	16.84	7.77	3.77
P17	6.27	10.90	8.18	2.11
P21	30.60	28.07	23.81	39.42
P22.1	32.66	21.01	22.80	19.84
P22.2	32.66	21.01	22.80	23.01
P20	5.0	10.14	3.56	5.86
P34	32.94	26.05	28.00	24.59
P35	11.52	7.74	13.76	8.75
P24	12.72	1.79	11.27	4.42
P25	28.57	23.06	25.83	9.41
P27	8.81	17.05	7.44	3.63
P30	21.44	31.39	23.93	28.32
P33	33.32	30.58	37.58	32.15
P32	10.84	8.98	12.78	12.03
P2	3.88	4.77	1.74	1.68
P03.2	3.67	6.34	1.39	6.43
P03.3	3.67	6.34	1.39	1.53
P03.5	3.86	6.60	2.39	1.85
P03.4	3.86	6.60	2.39	2.58
P03.1	3.69	3.09	3.20	0.03
P05	10.10	13.47	10.72	9.19
P06	2.44	6.68	4.79	7.28

The slope comparisons show that the DEMs tended to either overestimate or underestimate slope values, perhaps because of the pixel resolution of the DEMs. A DEM computes slope values for each pixel and may be affected by neighbouring cells (Sefercik *et al*., 2007). The DEM generated slopes were inconsistent with field slopes. The pixel cover a bigger area and slope values are an average of the slope

values within that pixel compared to the sample sites being measured. Such inconsistency is shown for instance at sample site P13 among others. The field measured slope for P13 is 27.77%; but 1-Arc SRTM, 1-Arc SRTM and 3-Arc SRTM assigned P13 slope values of 12.64%, 16.45% and 4.84%, respectively.

As shown in the DEM generated slope maps (Figures 4.3 to 4.5), there are no distinct slope classes from which geomorphological units can be delineated, especially in the low lying areas. The classes seem to be fuzzy and there are no clear boundaries to distinguish between the slope units and were then reclassified (Gerçek, 2017). As a result, the slope maps were reclassified into categories using reclassification rules as shown in Table 4.3, adapted from van Zuidam and van Zuidam-Cancelado (1989). The *r.reclass* command in GRASS GIS was used to reclassify the slope classes and create landform boundaries.

Table 4.3: Format of reclassification rules as used in GRASS GIS

0 thru 2	=1
2 thru 7	=2
7 thru 13	=3
13 thru 20	=4
20 thru 55	=5

The reclassified maps were assigned colours to show the slope class of each polygon. The reclassified slope maps do not represent the slope angles of the classified slopes; instead, they represent the slope categories of the reclassified slope angles. It is from these reclassified slope maps that slope polygons were generated. The results of the reclassified maps are presented in Appendix H.1 to H.3 for 1-arc ASTER, 1-arc SRTM and 3-arc SRTM DEMS, respectively. The

comparison of the field slope categories with slope categories from reclassified slopes of DEMs is presented in Appendix I.

The slopes were reclassified into five slope categories. The first category, category 1 has a slope range of 0-2%, which represents a flat or almost flat area; category 2 has a slope range of 2-7%, gently sloping areas; category 3 has a slope range of 7-13%, sloping areas; category 4 has a slope range of 13-20%, moderately steep areas and category 5 has a slope range of 20-55%, steep areas

The reclassification still maintained inconsistencies in terms of slope classification. For example, after reclassification, P13 among others is still misclassified. The slope category of P13 is 5; however, 1-Arc SRTM, 1-Arc ASTER and 3-Arc SRTM DEM slope categories are 3, 4 and 2, respectively. The misclassification is reported in an error matrix (Table 4.4 to 4.6) to show how each of the DEM classifies slope in comparison with the slope ranges of field measured slope as shown in Appendix I.

Post classification of the DEMs included the use of majority filter and boundary clean tools in ArcMap to generalize the delineated geomorphological units in a raster (Siart *et al*., 2009). Thereafter, the raster maps were imported into QGIS. The white marks on the reclassified slope maps represent the very steep slopes in the study area and/or inaccessible terrain with slope values greater than the slope values of the sampled points which were not considered in the classification rules. The reclassification assigned these areas a colour that did not include the sampled slope categories. The classification rules of the slopes were categorized based on

the slope values sampled during the field survey and according to the classification system provided by (van Zuidam and van Zuidam-Cancelado, 1989).

The DEMs from a single computation of derivatives have limited ability to show slope position. Therefore, the Topographic Position Index (TPI) computed to define the position of slope on the landform. The TPI map classification generated three classes (Appendix K.1 to K.3). The red class represents the highest areas; yellow, represents flat and low slope areas and blue represents the lowest areas in comparison to the neighbourhood cells.

4.4. Analysis of Geomorphological Maps

Both qualitative and statistical analyses were undertaken for the geomorphological units to determine whether the DEMs generated similar geomorphological units as the reference geomorphological map. Further statistical analyses were performed to evaluate how well the DEMs can produce a detailed geomorphological map compared to the reference map. Slope and elevation accuracy were performed to assess the DEM quality and the results are presented below.

4.4.1. Analyses of Geomorphological Units

The geomorphological units from DEMs were visually compared with the geomorphological units from the reference geomorphological map to assess their accuracy (Figure 4.6 to 4.8). Generally, the DEMs delineated geomorphological units similar to the geomorphological units delineated from the reference map.

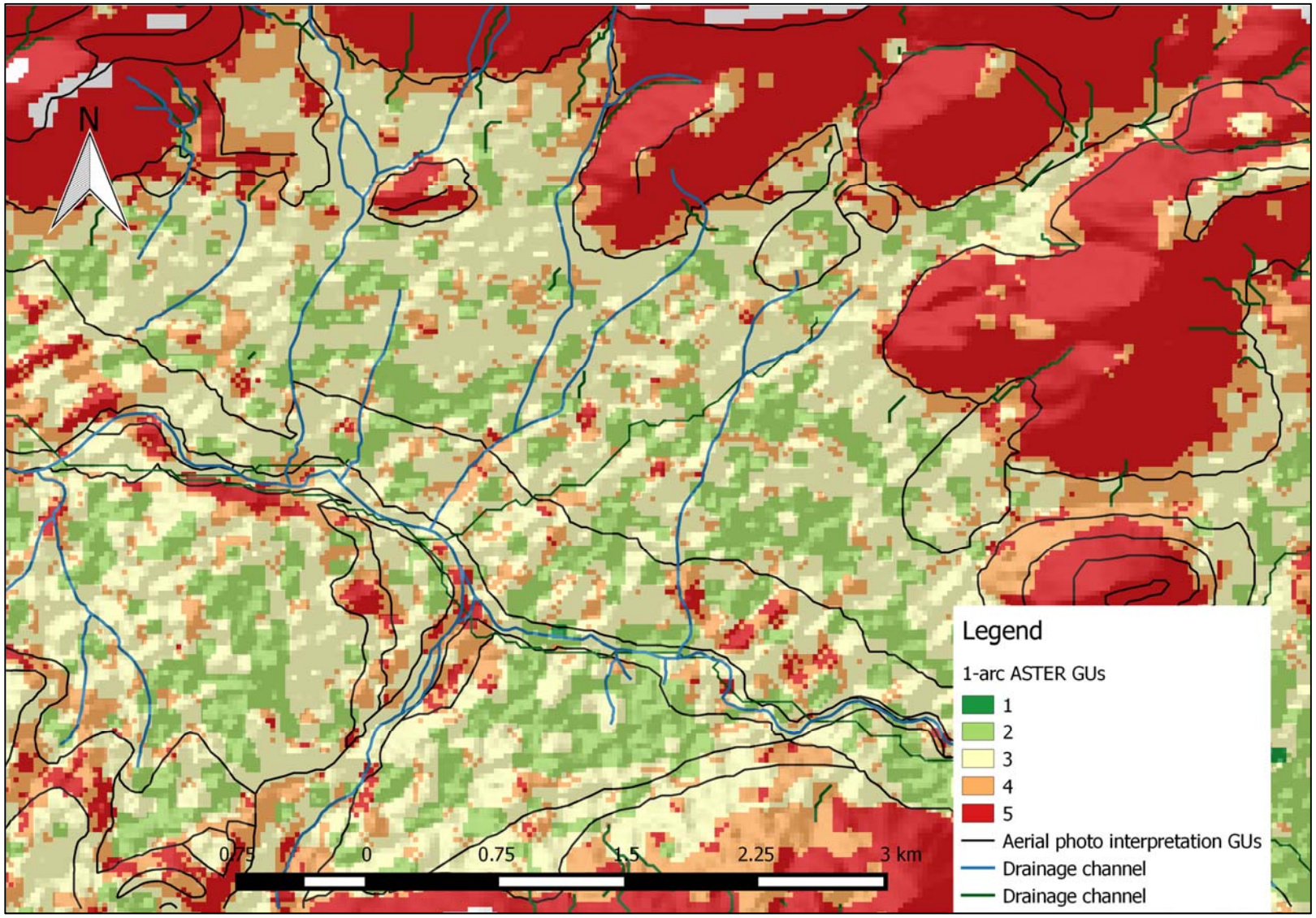

Figure 4.6: Comparison between aerial photo interpreted and 1-arc ASTER DEM delineated polygons

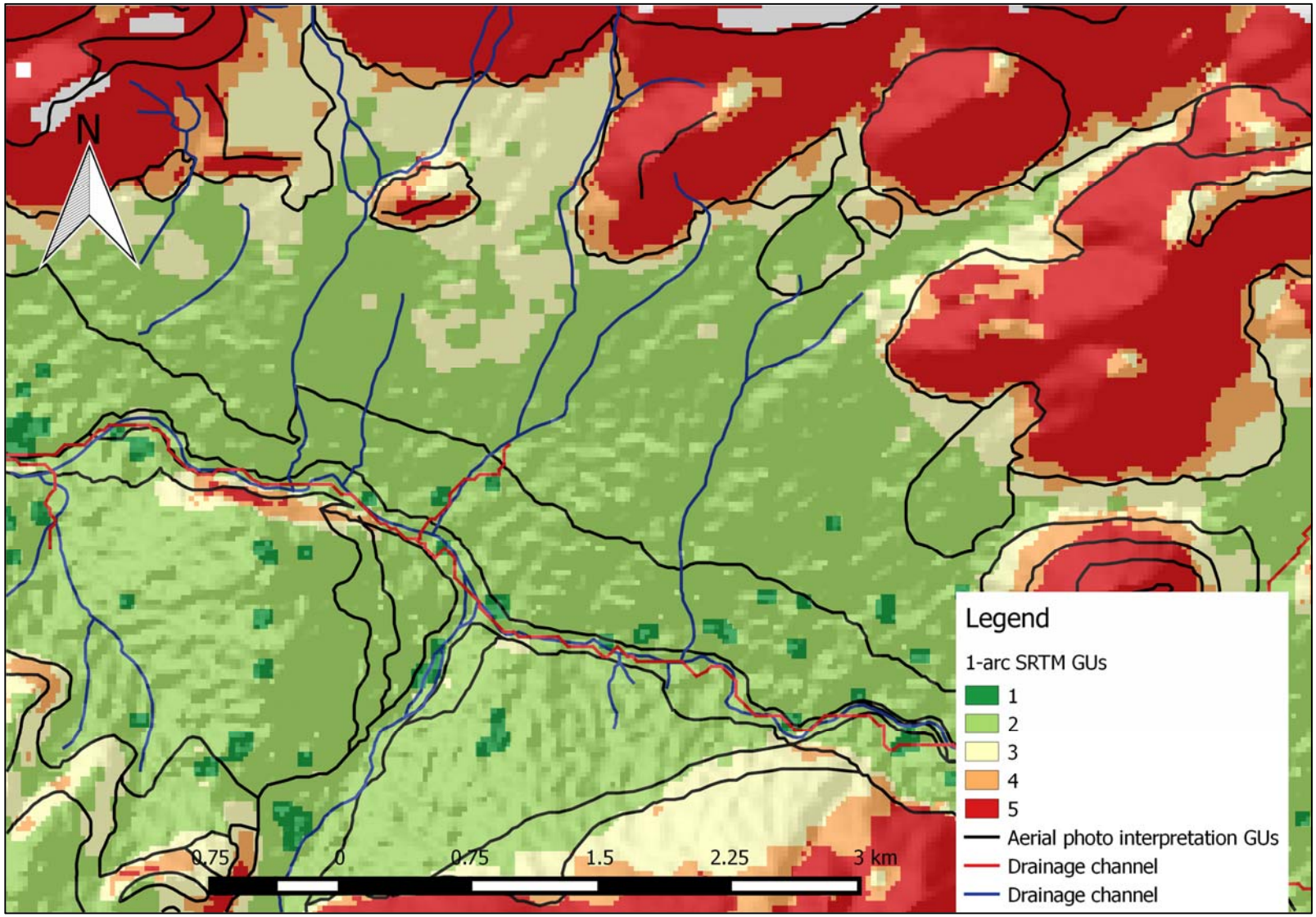

Figure 4.7 Comparison between aerial photo interpreted and 1-arc SRTM DEM delineated polygons

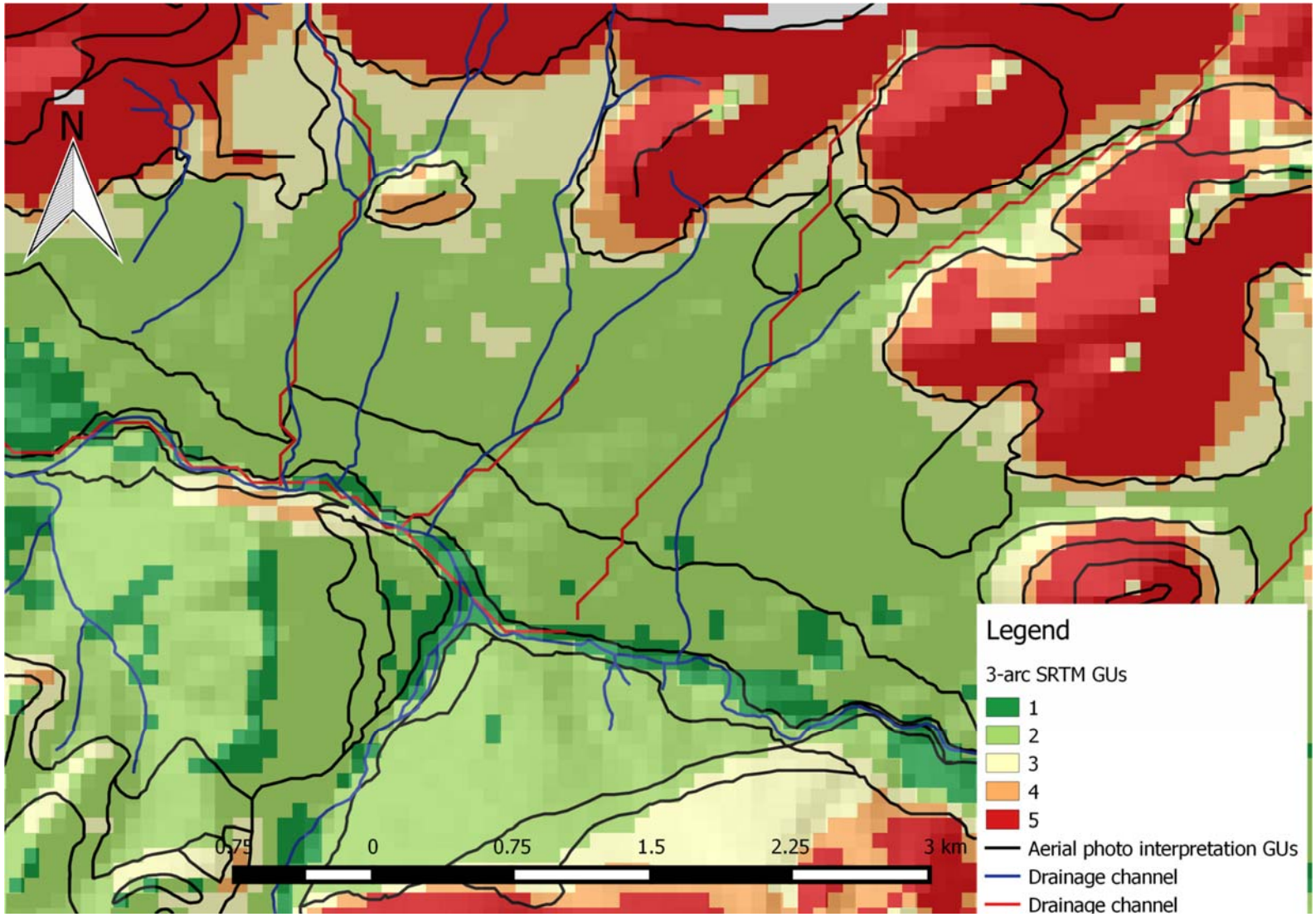

Figure 4.8: Comparison between aerial photo interpreted and 3-arc SRTM DEM delineated polygons

The black lines are the slope polygons from aerial photo interpretation which were overlaid on the DEM generated geomorphological units to determine whether the model would delineate the same polygons.

Evidently, the 1-arc ASTER map (Figure 4.6) classifies the slope categories poorly, especially the categories within low slope classes. The first terrace level is not clearly depicted in the 1-arc ASTER map. The river valley and the first level of terrace should show a break of slope between the adjacent slope units; however, this distinction is not apparent in the DEM results. Drainage systems normally have low slope values similar to valleys; however, the model generated slopes of different categories within the system including higher slope values. The 1-arc ASTER DEM seems to be consistent in classifying landforms of higher slopes.

Slope category 5 is the only category that was accurately delineated among the other slope categories, and the position of ridges is distinctly shown.

The 1-arc SRTM DEM (Figure 4.7) performed like the ASTER DEM, except that the flat area is more defined showing a single slope class with a few patches of a second slope class. The model classified category 5 slopes distinctively and the position of ridges. The low areas were treated as a single slope polygon. Figure 4.8, the 3-Arc SRTM DEM also seems to accurately delineate the slope categories. The drainage system and ridges stand out clearly in the map, unlike in the previous two maps.

In the low lying areas which are predominantly flat, the reference geomorphological map shows the river valley, first terrace level, moderately sloping and flat plain landforms. However, the DEMs poorly classify the landforms into different slope

categories. This can be attributed to the technique of aerial photo interpretation, where boundaries between features are delineated based image characteristics such as tone, texture and pattern. These attributes are not depicted on the DEMs and could be the reason why there is no clear boundary between the slope classes in the low lying areas. The DEMs were able to delineate slope polygons where there was an apparent change between two slope classes.

Sharp breaks in slope are clearly identifiable in the high lying areas on all the DEM geomorphological maps, and automated detailed mapping can be performed. However, comparison with the reference map shows significant differences. Smith et al., 2006 found that automated landform mapping could only be satisfactorily performed where breaks in slope are clearly identifiable. Similar to what was found by Drăguţ and Eisank (2012); GEOBIA was successful in depicting well individualised areas that are bound by major discontinuities.

The drainage channel delineated from aerial photo interpretation is not apparent in 1-arc ASTER and 1-arc SRTM DEM maps. The landforms are treated as homogenous with the neighbouring landforms without showing the breaks of slope as in the photo interpretation. Figure 4.3 shows relict landslide scars that were not depicted in either of the DEMs. Mwaniki *et al*. (2015) conducted a study to delineate relict landslide scars from Landsat images using image segmentation for change detection. These methods could not be applied in this study. The DEMs used in this study were probably acquired long after the landslide incidences had occurred. The study area has settlement houses built on the landslide scars; therefore, image segmentation would not be able to detect areas of landslide which

uses reflectance among others as parameter for segmentation (Mwaniki *et al*., 2015).

The results contradict what was found by Bolch *et al*'s. (2005) findings, that SRTM DEMs offer more precise elevations, and ASTER DEMs offer more precise geomorphological detail. From the three DEMs used in this study, the ASTER DEM was found to have low accuracy for generating geomorphological units compared to the other two DEMs and also producing poor slope correlation with reference data (section 4.3.2). The elevation accuracy for all the DEMs was high (section 4.3.3). Rusli *et al*. (2014) compared SRTM and ASTER DEMs and found that 1-arc ASTER presents smoother DEMs compared SRTM. The results show that the 1-arc SRTM DEMS performed poorly overall in delineating geomorphological units.

Statistical analysis was performed for each DEM generated map in order to evaluate the accuracy of the classification by comparing the number of correctly classified pixels in the DEM generated landforms with the reference geomorphological map. The geomorphological units derived from 1-arc ASTER, 1-arc SRTM and 3-arc SRTM DEMs had accuracies with k value of 0.01, 0.21, and 0.39, respectively. The results obtained from the classification had relatively low accuracies compared to the study by Wei et al. (2017) had relatively high classification accuracies. Wei *et al*. (2017) found that the landform types determined using automatic classification were highly consistent with the actual landform types with average classification of 72.9% and a k value of 0.66.

Mashimbye *et al*. (2014) also did a visual comparison to determine whether the DEM generated landform components that are similar in shape compared to 0.5m ortho-rectified aerial photographs. In their study, Mashimbye *et al*. (2014) found that the 90m DEM was less sensitive to morphological discontinuities compared to the high resolution DEMs used, although similar land components (similar in shape) were delineated, they attributed this to the low resolution nature of the DEM. Although resolution is said to play a part in DEM accuracy, the 1-arc SRTM and the 3-arc SRTM DEMs appeared to be more suitable for land component mapping than the 1-arc ASTER DEM.

A similarity index was performed whereby a Kappa coefficient was computed for the geomorphological units to determine how well the DEMs performed mapping was compared to reference geomorphological map. The results obtained show that DEMs performed with relatively low accuracies. The k values obtained for 1-arc ASTER, 1-acr SRTM and 1-arc SRTM were 0.01, 0.21 and 0.39 respectively. These results disagree with the results obtained by Jobin and Prasannakumar (2015) and Warren *et al*. (2004) who obtained relatively high accuracies. This could be attributed to the resolution of the DEM as proposed by Sefercik *et al*. (2007) that, as slope is calculated per pixel, therefore, pixel resolution will impact on the quality of the DEM derivatives. DEM quality also affects the morphologic detail derivatives (Milledge *et al.,* 2009).

4.4.2. Analysis of Surface Materials

Spectral libraries are not a reliable source of soil mapping due to the differences in soil from place to place, the spectral reflectance of the soils generated from

regions of interest (ROI) were used (Berhanu, 2005). ROI were generated from the geographic coordinates of the sampled points. The reflectance for the soil sample and other areas with similar reflectance generated the soil reflectance map.

The map was then compared to the soil map generated from soil samples collected in the field. The soil reflectance map was overlaid with the soil map generated from field collected soil samples (Figure 4.9). The Landsat image was able to produce a similar soil reflectance map as in Figure 4.1. A soil reflectance map was generated from Landsat 8 using linear spectral unmixing in ENVI software. Endmember collection spectra were extracted to show the reflectance of the regions of interest (ROI) (Figure 3.7). The ROI were labelled according to the polygons in which each field sample was found.

Most values of the normalized difference vegetation index (NDVI) are smaller than 0.2 in the study area. This indicated that the agricultural fields were mostly bare at the time of Landsat data acquisition. Accurate estimation of soil attributes is hampered if the pixels have a vegetation cover over 20% and also if the pixels are covered by crop residues (Mulder *et al*., 2011).

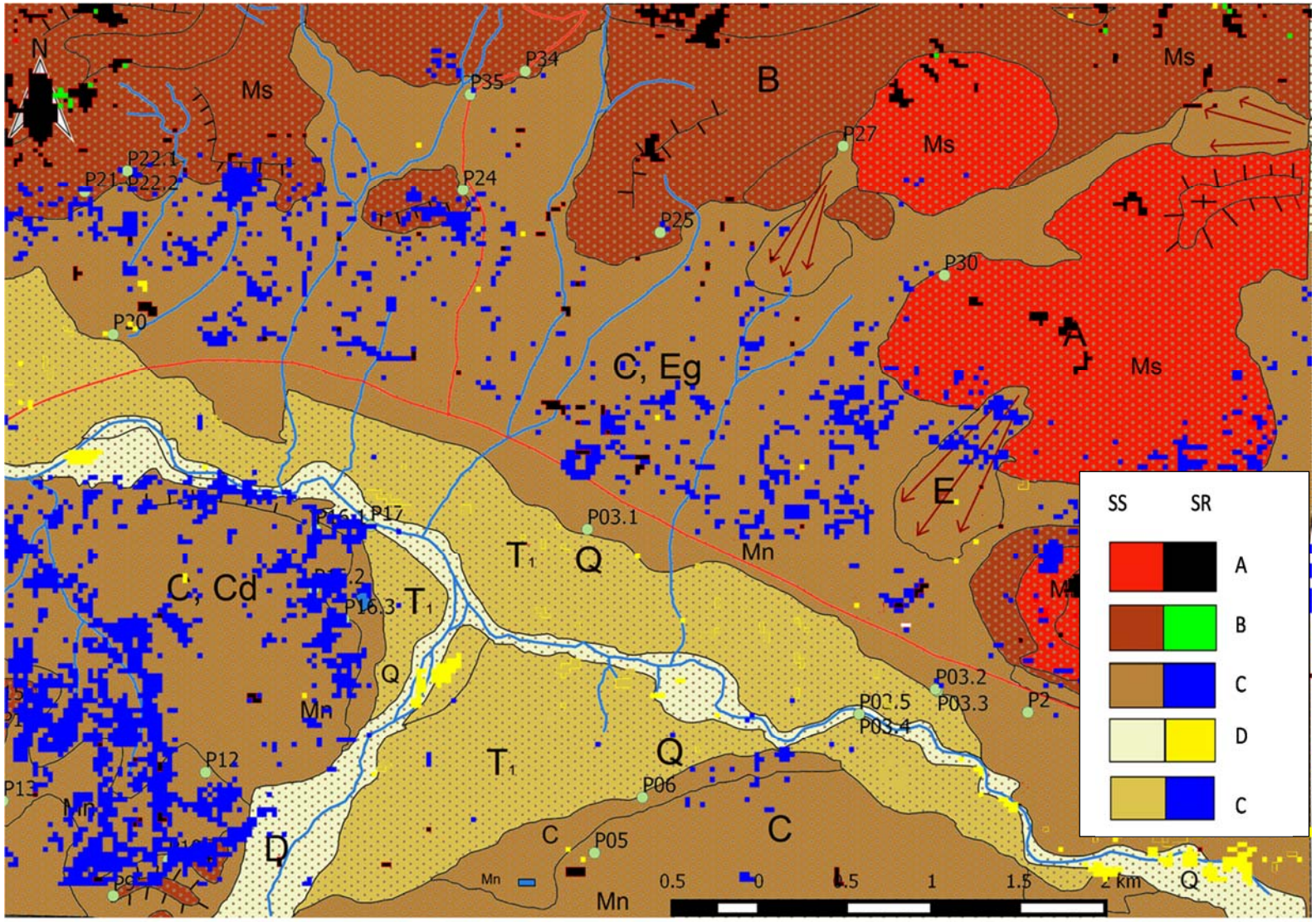

Figure 4.9: Comparison of soil map generated from Landsat 8 (SR) with soil map from field data (SS). A and B – sandy loam, C- loamy sand, and D – Sand

The black areas in Appendix L are the regions where soils were not sampled and may be due to vegetation, availability of surface materials or covered by development. Consequently there is no reflectance from the endmember collection spectra associated with them, and they therefore appear black. In order to show the correlation between the soil maps, the soil map from Landsat 8 image were overlaid.

The yellow polygon represents sand; blue represents soil, which is loamy sand; and blue and green represent soil categories A. Landsat 8 imagery creates similar soil boundaries as in the map generated from field data. The soil map generated from Landsat 8 imagery overlays perfectly with the map generated from field data. The soil reflectance of one endmember may be visible in the other selected endmember due to the processes involved in the terrain. The unclassified patches are areas that are occupied by other types of land use other than the reflectance of the endmember selected for that particular area, the soil map shows a general pattern as the soil map generated from field data.

4.4.3. Slope Accuracy

The calculated Topographic Position Index (TPI) for the DEMs showed some similarities between the global DEMs and the Reference DEM. The comparative analysis of the accuracy of the SRTM and ASTER DEMs allows the advantages and limitations of the DEMs to be assessed before future use in areas of a similar nature. The results demonstrate that automated detailed geomorphological mapping shows varying results for the different landforms. This could be attributed to the pixel size of the DEMs.

Jobin and Prasannakumar (2015) stated that slope of a pixel is calculated based on the neighbouring slopes, so the resolution has to be higher to take into account the small change in breaks of slope. The study has revealed that 3-arc SRTM DEM is suitable when compared to the reference geomorphological map than 1-arc DEMs in terms of delineating accurate geomorphological units.

An accuracy assessment for slope classes was performed using the reclassified slope maps' categories to determine how each data set performed regarding slope classes. The results are presented in Tables 4.4, 4.5 and 4.6. The field measured slope categories are the reference data while the DEM generated slopes are the predicted classification. The overall accuracy indicates out of all the reference sites what proportions were correctly classified. The bold diagonal elements indicate areas that were correctly classified.

Table 4.4 is an error matrix comparing the field surveyed slope angles (columns: truth) with 1-arc SRTM DEM predicted slopes (rows: predicted). The error matrix yielded an overall accuracy of 43.3%. Slope category 5 had four correctly classified samples and one sample incorrectly classified. Thirteen out of 30 sample points were correctly classified. The correctly classified slope categories are shown in bold. Slope category 1 had five samples classified as category 2 and no samples were correctly classified.

Slope category 2 had one sample categorised as category 1, six samples were correctly classified; three samples were classified as category 3 and one sample was classified as category 4. Slope category 3 had three samples correctly

classified and four samples incorrectly classified. Slope category 4 had zero correct classification and two samples were incorrectly classified.

Table 4.4: Error matrix (1-arc SRTM DEM) reclassified slopes

Field measured slope categories								
Slope categories as generated by GRASS GIS from 1-arc SRTM DEM		0-2 (1)	2-7 (2)	7-13 (3)	13-20 (4)	20-55 (5)	Row total	User's accuracy
	0-2 (1)	**0**	1	0	0	0	1	0
	2-7 (2)	5	**6**	2	0	0	13	46
	7-13 (3)	0	3	**3**	0	1	7	43
	13-20 (4)	0	1	1	**0**	0	2	0
	20-55 (5)	0	0	1	2	**4**	7	57
	Column total	5	11	7	2	5	30	
	Producer's accuracy	0	55	43	0	80		Overall accuracy = 43.3% K = 0.23

The 1-arc SRTM DEM poorly classified the slope classes. The error matrix shows a high producer's accuracy for slope category 5, showing that four out of five validating datasets are within category 5 on the classified image. A Kappa (K) value of less than 0.4 implies that there was poor agreement; 0.40-0.59, fair agreement; 0.60-0.74, good agreement, and greater than 0.74, excellent agreement between the reference and predicted classes.

The confusion matrix for 1-Arc ASTER yielded an overall accuracy of 33.3% (Table 4.5). Ten samples out of 30 were correctly classified. Slope category 1 had zero samples correctly classified and five samples were incorrectly classified as category 2. Slope category 2 had three samples correctly classified and eight samples incorrectly classified whereby one sample was classified as category 1,

four samples as category 3 and two samples as category 5. Slope category 3 had three samples correctly classified and four samples incorrectly classified.

Table 4.5: Error matrix (1-arc ASTER DEM) reclassified slopes

Field measured slope categories								
Slope categories as generated by GRASS GIS from 1-arc ASTER DEM		0-2 (1)	2-7 (2)	7-13 (3)	13-20 (4)	20-55 (5)	Row total	User's accuracy
	0-2 (1)	**0**	1	0	0	0	1	0
	2-7 (2)	5	**3**	1	0	0	9	33
	7-13 (3)	0	4	**3**	0	0	7	43
	13-20 (4)	0	2	2	**0**	1	5	0
	20-55 (5)	0	1	1	2	**4**	8	50
	Column total	5	11	7	2	5	30	
	Producer's accuracy	0	27	43	0	80		Overall accuracy=33.3% K =0.14

Slope category 4 had zero samples correctly classified and two samples incorrectly classified as category 5. Slope category 5 had four samples correctly classified and one sample incorrectly classified as category 4. This model performed even poorly compared to 1-Arc SRTM DEM with an overall accuracy of 43.3% and a k value of 0.14.

3-Arc SRTM DEM yielded an overall accuracy of 50% (Table 4.6). 15 samples out of 30 samples were correctly classified. Three samples were correctly classified for slope category 1 and two samples were incorrectly classified as category 2. Slope category 2 had four samples correctly classified and seven samples incorrectly classified. Slope category 3 had four samples correctly classified and three samples incorrectly classified. Slope category 4 had zero samples correctly

classified and two samples classified as category 5. Slope category 5 had four samples correctly classified and one sample classified as category 1.

Table 4.6: Error matrix (3-arc SRTM DEM) reclassified slopes)

		Field measured slope categories						
Slope categories as generated by GRASS GIS from 3-arc SRTM DEM		0-2	2-7	7-13	13-20	20-55	Row total	User's accuracy
	0-2	**3**	2	0	0	1	6	50
	2-7	2	**4**	1	0	0	7	57
	7-13	0	5	**4**	0	0	9	44
	13-20	0	0	1	**0**	0	1	0
	20-55	0	0	1	2	**4**	7	57
	Column total	5	11	7	2	5	30	
	Producer's accuracy	60	36	57	0	80		Overall accuracy =50% K=0.5

Although Sefercik *et al*. (2007) suggests that since slope of a pixel is the rate of change of elevation with respect to surrounding cells, the spatial resolution of the DEMs have significant role in the computation of slope. In this case, however, the lowest resolution DEM, the 3-Arc SRTM DEM had an overall accuracy higher than the two 1-Arc DEMs. The 3-Arc SRTM DEM performed better in comparison with the other two DEMs (1-Arc SRTM and 1-Arc ASTER).

1-arc ASTER and SRTM DEM had a K value of 0.23 and 0.14, respectively. The K value for the two DEMs shows poor agreement with the observed classes. 3-arc SRTM on the other hand had a K value of 0.5 implying a fair agreement between the classified slopes and the observed slopes. Since the 1-arc DEMs have a 30m spatial resolution and slope is measured per pixel in DEMs (Sefercik *et al*., 2007), the slope derivatives that are covered by a single pixel in the 3-arc (90m resolution) are visible in the 1-arc DEMs causing the salt-and-pepper effect. The average of

the pixel slope may also not fall within the range of the sample site selected in the field, because each pixel in the field has varying ruggedness.

The accuracy of a slope map determines many of the predictions that geomorphologists, engineers, hydrologists, and ecologists, farmers or foresters make about the behaviour of environmental variables, about natural hazards, land-use potential, and for planning. Errors on slope propagate to more sophisticated DEM-derived terrain attributes such as slope curvature, drainage networks, slope channel lengths, slope widths or topographic wetness indices. Therefore, the accuracy of DEM in deriving slope is vital.

4.4.4. Elevation Accuracy/ Statistical Analyses

The vertical accuracy assessment of the DEMs was evaluated. The results of vertical accuracy assessment of the DEMs with respect to reference elevations are given in Figure 4.10. The scatter plot of elevation of reference points and corresponding elevation obtained from the DEMs shows a significant linear positive relationship. Field data were positively correlated with the DEM data showing a strong correlation for 3-arc SRTM with the R^2 value of 0.992, 0.996 for 1-arc SRTM, and 0.992 for ASTER.

The DEMs had RMSE values of 6.79 for 1-arc ASTER; 3.88 for 1-arc SRTM and 5.65 for 3-arc SRTM (Figure 4.10). The RMSE values were less than the estimated vertical error, making them more accurate. 1-arc SRTM is claimed to have a vertical accuracy of less than 16m, ASTER DEM, 20m, while the 3-arc SRTM is reported to have a vertical error of less than 16 m (Mulder *et al*., 2011; Jobin and Prasannakumar, 2015; Pipaud *et al*., 2015).

These results show that the elevation data from the DEMs are accurate and therefore suitable for analysis. 1-arc SRTM had the highest correlation amongst the two other DEMs which had a similar correlation. The graph of elevation of reference points and corresponding elevation obtained from the DEMs shows a significant linear positive relationship.

Milledge *et al.* (2009) raised issues of data quality that DEM error affects individual point elevations as well as the geomorphological parameters determined from them. For the DEM to delineate geomorphological units that resemble geomorphological units delineated from interpretation, the elevations from both datasets need to correlate strongly. The results from the elevation accuracy indicate that the SRTM and ASTER DEMs meet their predefined vertical accuracy specifications of 16m and 20m respectively. Therefore the performance in geomorphological mapping cannot be attributed to low elevation accuracies. This is in line with the results of previous studies (Mulder *et al*., 2011; Jobin and Prasannakumar, 2015; Pipaud *et al*., 2015; Salleh *et al*., 2015).

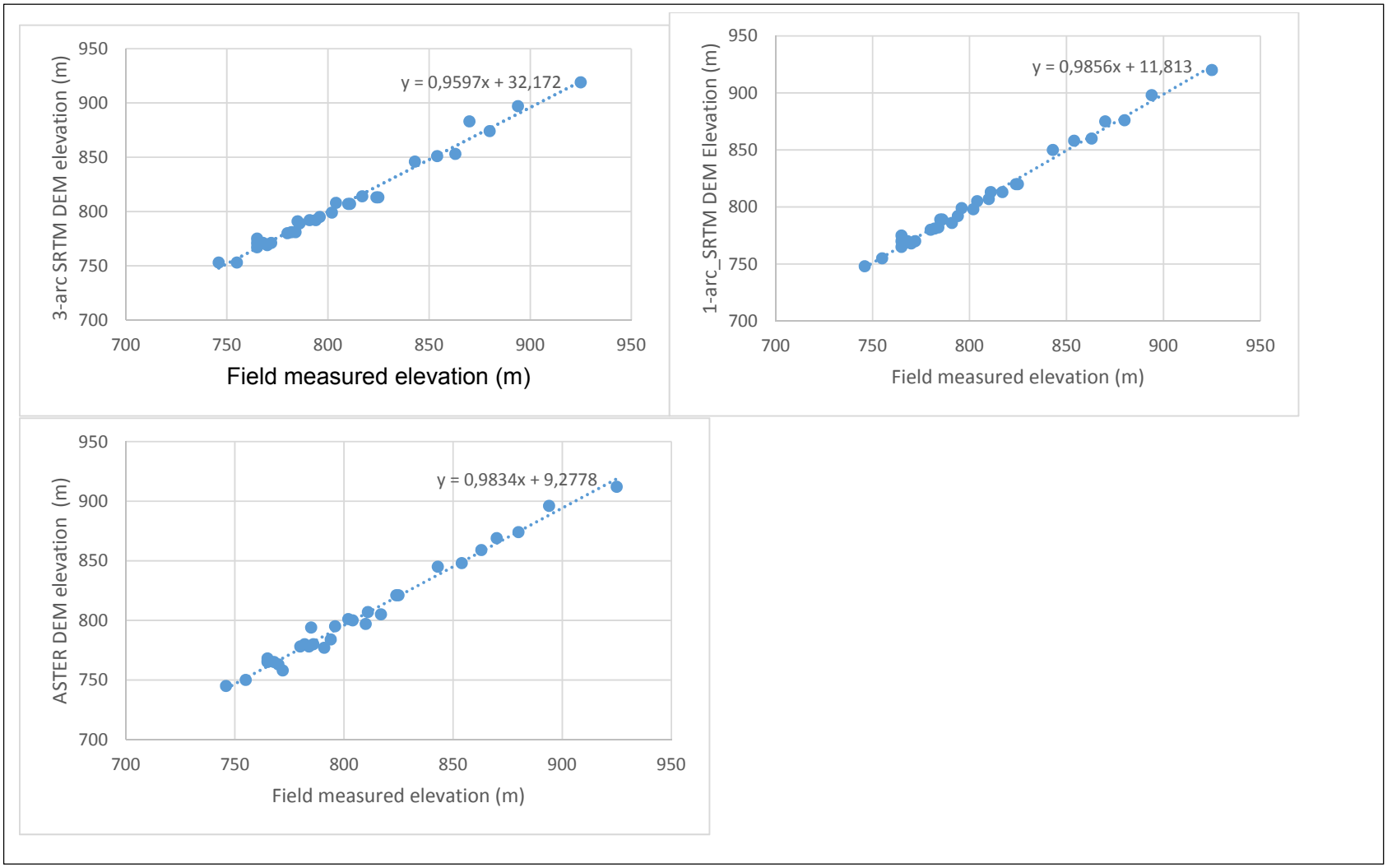

Figure 4.10: Correlation of field data with 3-arc SRTM, 1-arc SRTM and ASTER

4.5. Chapter Summary

In this chapter, the methods of assessing whether ASTER and SRTM DEMs, and satellite imagery are suitable for detailed geomorphological mapping were implemented and the results were presented. A detailed geomorphological map was produced from aerial photo interpretation and field surveys that served as a reference for accuracy assessment of the satellite data generated maps. DEM quality was evaluated in terms of elevation and slope accuracies and also to determine how spatial resolution affects the performance of DEM in delineating geomorphological units. The conclusions and recommendations based on the general and specific objectives of the study as well as the research question are presented in Chapter 5.

CHAPTER 5

CONCLUSIONS AND RECOMMENDATIONS

5.1. Introduction

This study was carried out to assess whether automated geomorphological mapping from ASTER and SRTM DEMs used in combination with Landsat 8 imagery is suitable for detailed geomorphological mapping compared to manual mapping. The results obtained were validated against the reference geomorphological map produced manually from aerial photographs and field data.

5.2. Conclusions

The resultant geomorphological units' maps from the DEMs when compared with the reference geomorphological map show that the automated classification technique has advantages in terms of its efficiency and reproducibility. Nevertheless, distinct limitations of the technique are apparent and the technique is not suitable for detailed geomorphological mapping in the proposed study area. The results demonstrate that detailed geomorphological units cannot be confidently delineated from the DEMs. Slope maps from DEMs are not able to delineate surface processes like aerial photographs can.

The derived geomorphological units from 1-arc ASTER, 1-arc SRTM and 3-arc SRTM DEMs had accuracies with k value of 0.01, 0.21, and 0.39, respectively. The poor performance of the DEMs can be attributed to the inability of the DEMs to delineate slope angles accurately and the resolution of the DEMS. The similarity index of the slope angles for 1-arc ASTER, 1-arc SRTM and 3-arc SRTM DEMs

had relatively low accuracies with overall percentage of total correct cells of 33.3%, 43.3% and 50%; and kappa coefficient (K) of 0.14, 0.23 and 0.5; respectively.

The Landsat 8 image was consistent in generating soil reflectance that had a similar pattern as the map produced from manual map. The visual inspection demonstrates that the automatic technique is capable of reconstructing geomorphological units where distinct breaks in slope occur (i.e. where the rise in elevation is apparent). The elevation data had relatively high accuracies as well; therefore, elevation did not contribute to the poor performance of the DEMs.

5.3. Recommendation for further studies

For further research, the quality of geomorphological unit classification may be improved by using high resolution DEMs. The study tested 1-arc and 3-arc DEMs, therefore DEMs of higher resolution can be used to derive more accurate morphometric attributes. Saˇvulescu and Mihai (2011) have shown that the use of multiple geomorphometric parameters may contribute to higher classification accuracy.

In this study, the *r.slope.aspect* algorithm in GRASS was used, which has embedded morphometric calculations that the user cannot manipulate. The multiresolution segmentation algorithm has been used for landform segmentation (Grohmann *et al*., 2007; Mulder *et al*., 2011); the scale at which landforms can be segmented is determined by the user. Regardless of how accurate and efficient the data and the methods of analysis are, field check is inevitable in order to provide users with valid and reliable maps (Guth, 2010). Geomorphological mapping is better performed through field survey and aerial photo interpretation.

Therefore, novice mappers should be provided with training to provide reliable maps.

5.4. Chapter Summary

It is suggested that this study has accomplished the general aim that was set out to assess the suitability of ASTER and SRTM DEMs, and satellite imagery for detailed geomorphological mapping in Dzanani area. Conclusions based on the general and specific objectives and research questions were made and recommendations for further research given thereafter.

REFERENCES

Aksoy, E., Özsoy, G. and Dirim, M.S. 2009. Soil mapping approach in GIS using Landsat satellite imagery and DEM data. *African Journal of Agricultural Research,* 4 (11): 1295-1302.

Ali, R.R. and Moghanm, F.S. 2013. Variation of soil properties over the landforms around Idku Lake, Egypt. *The Egyptian Journal of Remote Sensing and Space Sciences*, 16: 91–101.

Berhanu, K.A. 2005. *Spectral unmixing of hyperspectral and multispectral images for predictive mapping of surface soil organic matter.* Master of Science in Geioinformatics. Internation institute for geo-information sciences and earth observation enschede, the Netherlands.

Bishop, M.P., James, L.A., Shroder Jr., J.F., and Walsh, S.J. 2012. Geospatial technologies and digital geomorphological mapping: Concepts, issues and research. *Geomorphology,* 137: 5–26.

Blaschke,T., Hay, G.J., Kelly, M., Lang, S., Hofmann, P., Addink, E., Feitosa, R.Q., van der Meer, F., van der Werff, H., van Coillie, F. and Tiede, D. 2014. Geographic Object-Based Image Analysis – Towards a new paradigm. *Journal of Photogrammetry and Remote Sensing,* 87: 180-191.

Bocco, G., Mendoza, M. and Vela´zquez, A. 2001. Remote sensing and GIS-based regional geomorphological mapping—a tool for land use planning in developing countries. *Geomorphology,* 39: 211–219.

Bolch, T., Kamp, U. and Olsenholler, J. 2005. Using ASTER and SRTM DEMs for studying geomorphology and glaciation in high mountain areas. *New Strategies for European Remote Sensing.*

Carter, M.R. and Gregorich, E.G. 2008. Soil sampling and methods of analysis. 2nd edition. Tailor and Francis, USA.

Castiglioni, G.B., Biancotti, A., Bondesan, M., Ortemiglia, G.C., Elmi, C., Favero, V., Gasperi, G., Marchetti., G., Orombelli, G., Pelle-Grini, G.B. and Tellini, C. 1999. Geomorphological map of the Po Plain, Italy, at a scale of 1:250 000. *Earth Surface Processes and Landforms,* 24: 1115-1120.

Chigbu, N., Igbokwe, J.I., Bello, I., Idhoko, K. and Apeh, M. 2015. 'Comparative study of pixel-based and object-based image analysis in landcover and landuse mapping of ABA main Township for environmental sustainability', FIG working week, Sofia Bulgaria, 17-21 May 2015. Available from: https://www.fig.net/resources/proceedings/fig_proceedings/fig2015/ppt/TS02E/TS02E_chigbu_igbokwe_et_al_7622_ppt.pdf. Accessed (16 March 2018).

Chiliza, S.G. and Richardson, S. 2008. Landslide Incidence in the Limpopo Province, South Africa. Conference Paper.

Clowes, R. and Comfort, P. 1987. *Process and landform: an outline of contemporary geomorphology*. 2nd edition. Oliver and Boyd, Singapore.

Cooke, R.U., and Doornkamp, J.C. 1990. *Geomorphology in environmental management: a new introduction*. 2nd edition. Oxford university press, New York.

Diko, M.L., Banyini, S.C. and Monareng, B.F. 2014. Landslide susceptibility on selected slopes in Dzanani, Limpopo Province, South Africa', Jàmbá: *Journal of Disaster Risk Studies*, 6(1): 101-107.

Dogan, H.M. and Kılıç, O.M. 2013. Modelling and mapping some soil surface properties of Central Kelkit Basin in Turkey by using Landsat-7 ETM+ images, *International Journal of Remote Sensing*, 34(15): 5623-5640.

Drăguţ, L. and Eisank, C. 2012. Automated object-based classification of topography from SRTM data. Geomorphology, 141-142: 21–33.

Du, X., Guo, H., Fan., X., Zhu, J., Yan, Z., and Zhan, Q. N.d. Vertical accuracy assessment of srtm and aster gdem over coastal regions of China: a comparative analysis. The 33rd Asian conference on remote sensing.

Ehsani, A.H. and Quiel, F. 2008. Geomorphometric feature analysis using morphometric parameterization and artificial neural networks. *Geomorphology,* 99: 1–12.

Evans, I.S. 2012. Geomorphometry and landform mapping: What is a landform? *Geomorphology*, 137: 94–106.

Evelpidou, N., Vassilopoulos, A., Vaiopoulos D. and Komianou, A. n.d. Geomorphological cartography using Remote Sensing and GIS techniques at Milos island. Available from: https://pdfs.semanticscholar.org/4dca/eb1ae6d875961e1e647dcdebc931d8566257.pdf. Accessed (15 June 2017).

Farhan, A., Millington, A.C., and McLaren S.J. 2003. Merged remotely sensed data for geomorphological investigations in deserts: examples from central Saudi Arabia. *The Geographical Journal,* 169(2): 17–130.

Fonseca, A.F. 2011. Geomorphology of the Montejunto massif (Portugal). *Journal of Maps*, 138-147.

Forkuor, G. and Maathius, B.H.P. 2012. Comparison of SRTM and ASTER Derived Digital Elevation Models over Two Regions in Ghana – Implications for Hydrological and Environmental Modeling. *Studies on Environmental and Applied Geomorphology,* 219-240.

Gerçek. D. 2017. A Conceptual Model for Delineating Land Management Units (LMUs) Using Geographical Object-Based Image Analysis. International Journal of Geo-Information, 6: 170-187.

Gerçek, D., Toprak, V. and Strobl, J. (2011) Object-based classification of landforms based on their local geometry and geomorphometric context.

International Journal of Geographical Information Science, 25(6): 1011-1023.

Giles. P.T. 1998. Geomorphological signatures: classification of aggregated slope unit objects from digital elevation and remote sensing data. *Earth Surface Processes and Landforms,* 23: 581–594.

Gonga-Saholiariliva, N., Petit, Y.G.C. and Mering, C. 2011. Techniques for quantifying the accuracy of gridded elevation models and for mapping uncertainty in digital terrain analysis. *Progress in Physical Geography,* 35(6): 739–764.

Grohmann, C.H. 2005. Trend-surface analysis of morphometric parameters: A case study in southeastern Brazil. *Computers & Geosciences*, 31: 1007–1014.

Grohmann, C.H., Riccomini, C. and Alves, F.M. 2007. SRTM-based morphotectonic analysis of the Poc-os de Caldas Alkaline Massif, southeastern Brazil. *Computers & Geosciences,* 33: 10–19.

Grosse, G., Schirrmeister, L., Kunitsky, V.V. and Hubberten, H. 2005. The Use of CORONA Images in Remote Sensing of Periglacial Geomorphology: An Illustration from the NE Siberian Coast. Guido Grosse. *Permafrost and Periglacial Processes,* 16: 163–172.

Gustavsson, M., Kolstrup, E. and Seijmonsbergen, A.C. 2006. A new symbol-and-GIS based detailed geomorphological mapping system: Renewal of a scientific discipline for understanding landscape development. *Geomorphology,* 77: 90-111.

Gustavsson, M., Seijmonsbergen, A.C. and Kolstrup, E. 2008. Structure and contents of a new geomorphological GIS database linked to a geomorphological map - With an example from Liden, central Sweden. *Geomorphology,* 95: 335–349.

Guth, P.L. 2010. Geomorphometric comparison of ASTER GDEM and SRTM. A special joint symposium of ISPRS Technical Commission IV & AutoCarto in conjunction with ASPRS/CaGIS 2010 Fall Specialty Conference November 15-19, Orlando, Florida.

Guzzetti, F., Mondini, A.C., Cardinali, M., Fiorucci, F., Santangelo, M. and Chang, K. 2012. Landslide inventory maps: New tools for an old problem. *Earth-Science Reviews,* 112: 42–66.

Hayden, R.S. 2009. Chapter 11. NASA. Availablel from: http://disc.nasa.gov.geomorphology//GEO_11/index.shtml#Fig11.1. Accessed (17 November 2017).

He, Y. and Beighley, R.E. 2008. GIS-based regional landslide susceptibility mapping: a case study in southern California. *Earth Surface Processes and Landforms,* 33: 380 –393.

Hengl, T. and Reuter, H.I. (Eds). 2009. Developments in Soil Science. *Geomorphometry: Concepts, Software, Applications,* 33:387-410.

Holmes, P. and Meadows, M. 2012. *Southern African geomorphology: recent trends and new directions*. Sun press, Bloemfontein.

Horn, B. K. P. (1981). Hill Shading and the Reflectance Map. *Proceedings of the IEEE,* 69(1):14-47.

Kaya, S. 2000. Determination of geomorphological characteristics around of the Isiklar Mountain by using remote sensed data and DEM. *International Archives of Photogrammetry and Remote Sensing,* 33.

Jensen, J.R. 2007. *Remote sensing of the environment: an earth resource perspective*. 2nd edition. Pearson, USA.

Jobin, T.V. and Prasannakumar, P.V. 2015. Suitability of spaceborne digital elevation models of different scales in topographic analysis: an example from Kerala, India. *Environmental Earth Science*, 73: 1245–1263.

Jones, A.F., Brewer, P.A., Johnstone, E. and Macklin, M.G. 2007. High-resolution interpretative geomorphological mapping of river valley environments using airborne LiDAR data. *Earth Surface Processes and Landforms,* 32: 1574–1592.

Kamal A.S.M.M. and Midorikawa, S. 2004. GIS-based geomorphological mapping using remote sensing data and supplementary geoinformation: A case study of the Dhaka city area, Bangladesh. *International Journal of Applied Earth Observation and Geoinformation,* 6: 111–125.

Laurenta, O., Paquettea, J., Martina, H., Doucelancea, R. and Moyen, J. 2013. LA-ICP-MS dating of zircons from Meso- and Neoarchean granitoids of the Pietersburg block (South Africa): Crustal evolution at the northern margin of the Kaapvaal craton. *Precambrian Research,* 230: 209– 226.

Liao, K., Xu, S., Wu, J. and Qing Zhu, Q. 2013. Spatial estimation of surface soil texture using remote sensing data. *Soil Science and Plant Nutrition*, 59: 488–500.

Mashimbye, Z.E., de Clercq, W.P. and van Niekerk, A. 2014. An evaluation of digital elevation models (DEMs) for delineating land components. *Geoderma,* 213: 312–319.

Mergili, M., Marchesini, I., Alvioli, M., Metz, M., Schneider-Muntau, B., Rossi, M. and Guzzetti, F. 2014. A strategy for GIS-based 3-D slope stability modelling over large areas. *Geoscientific model development,* 7: 2969–2982.

Mili, N. and Acharjee, S. 2014. The Importance of Geomorphology in Understanding Natural Hazards with Special Reference to Hazards of The Dhansiri River Basin in The Golaghat District of Assam, India. *Global Perspectives on Geography,* 2.

Mitasova, H. (1985). *Cartographic aspects of computer surface modeling*. PhD thesis. Slovak Technical University, Bratislava.

Morgan, J.L., Gergel, S.E. and Coops, N.C. 2010. Aerial photography: A rapidly evolving tool for ecological management. *BioScience*, 60(1): 47-59.

Morgan, J.L. and Gergel, S.E. 2013. Automated analysis of aerial photographs and potential for historic forest mapping. *Canadian journal of forest research*, 43: 699-710.

Mukherjee, S., Joshi, P.K., Mukherjee, S., Ghosh, A., Garg, R.D. and Mukhopadhyay, A. 2013. Evaluation of vertical accuracy of open source Digital Elevation Model (DEM). *International Journal of Applied Earth Observation and Geoinformation,* 21: 205–217.

Mulder, V.L., de Bruin, S., Schaepman, M.E. and Mayr, T.R. 2011.The use of remote sensing in soil and terrain mapping — A review. *Geoderma,* 162: 1–19.

Mwaniki, M.W., Agutu, N.O., Mbaka., J.G., Ngigi, T.G. and Waithaka, E.H. 2015. Landslide scar/soil erodibility mapping using Landsat TM/ETMþ bands 7 and 3 Normalised Difference Index: A case study of central region of Kenya. *Applied Geography,* 64: 108-120.

Neeru, S. 2012. Meaning of the term- descriptive survey research method. *International Journal of Transformations in Business Management,* 1(6).

Novak, I.D. and Soulakellis, N. 2000. Identifying geomorphic features using Landsat-5/TM data processing techniques on Lesvos, Greece. *Geomorphology*, 34: 101–109.

Odhiambo, B.D.O. 2017. Stereoscopic interpretation of aerial photographs. Personal commucation.

Otto, J. and Smith, M.J. 2013. Geomorphological mapping. Geomorphological Techniques. *British Society for Geomorphology*.

Pelletier, J.D. 2008. *Quantitative modelling of earth surface processes*. Cambridge University press, New York.

Rao, D.P. 2002. Remote sensing application in geomorphology. *Tropical Ecology,* 43(1): 49-59.

Pipaud, I., Loibl, D and Lehmkuhl, F. 2015. Evaluation of TanDEM-X elevation data for geomorphological mapping and interpretation in high mountain environments — A case study from SE Tibet, China. *Geomorphology,* 246: 232–254.

Rhoads, B.L. and Thorn, C.E. 1996. *The scientific nature of geomorphology.* John Wiley and sons, New York.

Rokni, K., Anuar Ahmad, A. and Hazini, S. 2015. Comparative analysis of ASTER DEM, ASTER GDEM, and SRTM DEM based on ground-truth GPS data. *Jurnal Teknologi,* 76:(1): 97–102.

Rusli, N., Majid, M.R. and Din, A.H.M. 2014. 'Google Earth's derived digital elevation model: A comparative assessment with Aster and SRTM data', 8th International Symposium of the Digital Earth. IOP Publishing.

Salleh, M.R.M., Ismail, Z., and Rahman, M.Z.A. 2015. 'Accuracy assessment of Lidar-derived digital terrain model (DTM) with different slope and canopy cover in tropical forest region', Joint International Geoinformation Conference, Kuala Lumpur, Malaysia, 28–30 October 2015. Available from: https://www.isprs-ann-photogramm-remote-sens-spatial-inf-sci.net/II-2-W2/183/2015/isprsannals-II-2-W2-183-2015.pdf. Accessed (23 November, 2017).

Sa˘vulescu, I. and Mihai, B. 2011. Mapping forest landscape change in Iezer Mountains, Romanian Carpathians - A GIS approach based on cartographic heritage, forestry data and remote sensing imagery. *Journal of Maps,* 429-446.

Schaetzl, R.J. and Anderson, S. 2005. *Soils: Genesis and geomorphology.* Cambridge university press, New York.

Sefercik, U., Jacobsen,K., Oruc, M. and Marangoz, A. 2007. Comparison of Spot, SRTM and Aster DEMs. Comparison of Spot, SRTM and ASTER DEMs. Availavble from: https://www.researchgate.net/publication/228354471_Comparison_of_spot_SRTM_and_ASTER_DEMs. Accessed (21 January 2017).

Seif, A. 2014. Landform Classification by Slope Position classes. *Bulletin of Environment, Pharmacology and Life Sciences,* 3(11): 62-69.

Shabou, M., Mougenot, B., Chabaane, Z.L., Walter, C., Boulet, G., Aissa, N.B. and Zribi, M. 2015. Soil clay content mapping using a time series of landsat tm data in semi-arid lands. *Remote Sensing*, 7: 6059-6078.

Sharma, M.P. and Kujur, A. 2012. ASTER DEM Based Studies for Geological and Geomorphological Investigation in and around Gola block, Ramgarh District, Jharkhand, India. *International Journal of Scientific & Engineering Research*, 3(2).

Siart, C., Bubenzer, O. and Eitel, B. 2009. Combining digital elevation data (SRTM/ASTER), high resolution satellite imagery (Quickbird) and GIS for geomorphological mapping: A multi-component case study on Mediterranean karst in Central Crete. *Geomorphology,* 112: 106–121.

Smith, M.J. and Clark, C.D. 2005. Methods for the visualization of digital elevation models for landform mapping. *Earth Surface Processes and Landforms*, 30: 885–900.

Smith, M.J., Rose, J. and Booth, S. 2006. Geomorphological mapping of glacial landforms from remotely sensed data: An evaluation of the principal data sources and an assessment of their quality. *Geomorphology,* 76: 148–165.

Smith, M.J. and Pain, C.F. 2009. Applications of remote sensing in geomorphology. *Progress in Physical Geography,* 33(4): 568–582.

Smith, M.J. and Griffiths, J.S. 2017. Physical Landscapes. *Mapping across academia*.

Straumann, R. 2010. 'Extraction and characterisation of landforms from digital elevation models: Fiat Parsing the elevation field', Giebenach BL dissertation, Universität Zürich, Switzerland.

Tomar, A.S. and Singh, U.C. 2012. Geomorphological mapping using remote sensing and GIS - A tool for land use planning around Shivpuri City, M.P., India. *IOSR Journal of Computer Engineering* 5(1): 28-30.

Townsend, D. B. and Rosser, B. 2012. Canterbury Earthquakes 2010/2011 Port Hills slope stability: Geomorphology mapping for rockfall risk assessment, GNS Science Consultancy Report 2012/15. 21 p + maps (91 p).

Van Zuidam, R.A. and van Zuiddam-Cancelado, F.I. (1985). *Aerial photo-interpretation in terrain analysis and geomorphic mapping. International Institute for Aerospace Survey and Earth Science (ITC)*. Smits Publication. The Hague.

Verhagen, P. and Dragut, L. 2012. Object-based landform delineation and classification from DEMs forarchaeological predictive mapping. *Journal of archaeological science,* 39: 698-703.

Vidhya, L,S., Jijo, J., Soundariya, S., Vishalini, T. and Kasinatha P.P. 2015. A Comparison of Soil Texture Distribution and Soil Moisture Mapping of Chennai Coast using Landsat ETM+ and IKONOS Data. *Aquatic Procedia,* 4: 1452-1460.

Walstra, J., Heyvaert, V.M.A. and Verkinderen, P. 2011. Mapping Late Holocene Landscape Evolution and Human Impact - A Case Study from Lower Khuzestan (SW Iran). *Developments in Earth Surface Processes*, 15.

Warren S.D., Hohmann M.G., Auerswald K. and. Mitasova, H. 2004. An evaluation of methods to determine slope using digital elevation data. *Catena,* 58: 215–233.

Wechsler, S.P. and Kroll, C.N. 2006. Quantifying DEM Uncertainty and its Effect on Topographic Parameters. *Photogrammetric Engineering & Remote Sensing*, 72(9): 1081–1090.

Wei, Z., He, H., Hao, H. and Gao, W. 2017. Automated mapping of landforms through the application of supervised classification to lidar-derived DEMs and the identification of earthquake ruptures. *International Journal of Remote Sensing*, 38(23): 7196-7219.

Zhang, X., Drake, N.A., Wainwright, J. and Mulligan, M. 1999. Comparison of slope estimates from low resolution DEMs: scaling issues and a fractal method for their solution. *Earth surface processes and landforms,* 24: 763- 779.

APPENDICES

Appendix A

Stereopairs used for stereoscopic analysis

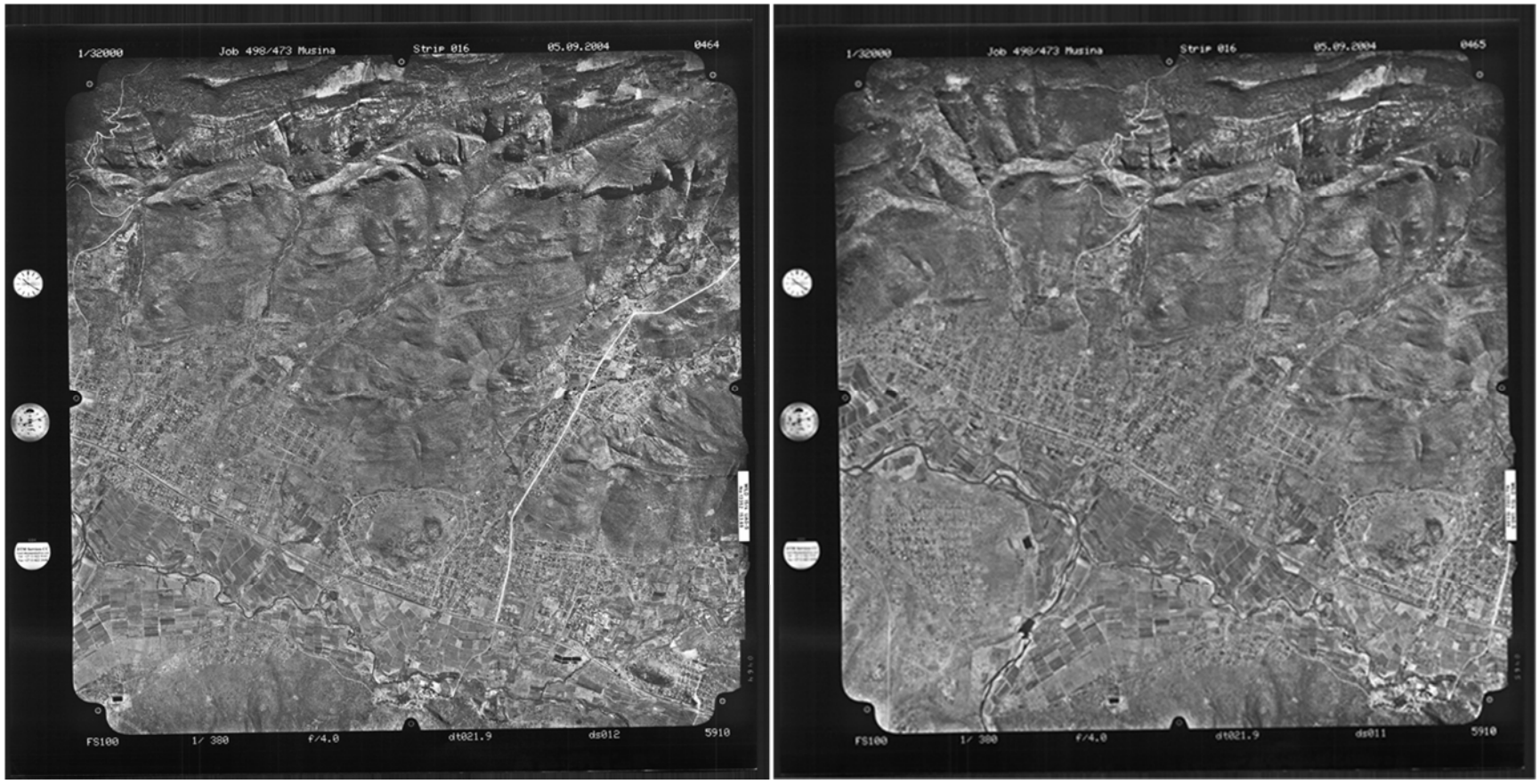

Appendix B

Originally downloaded DEM resized to study area

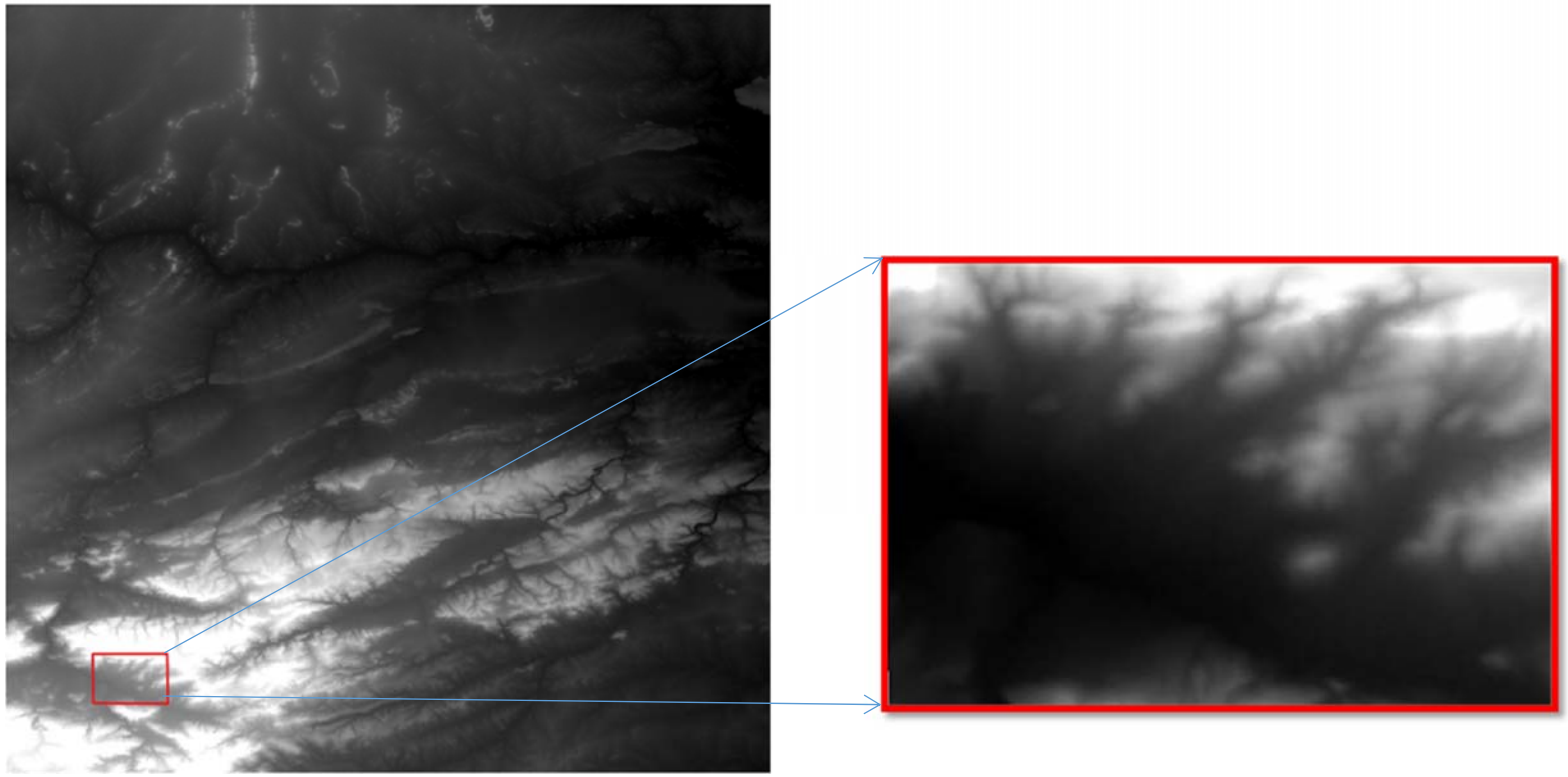

Appendix C

Landsat 8 image

Appendix D.1

Interpreted map from aerial photographs

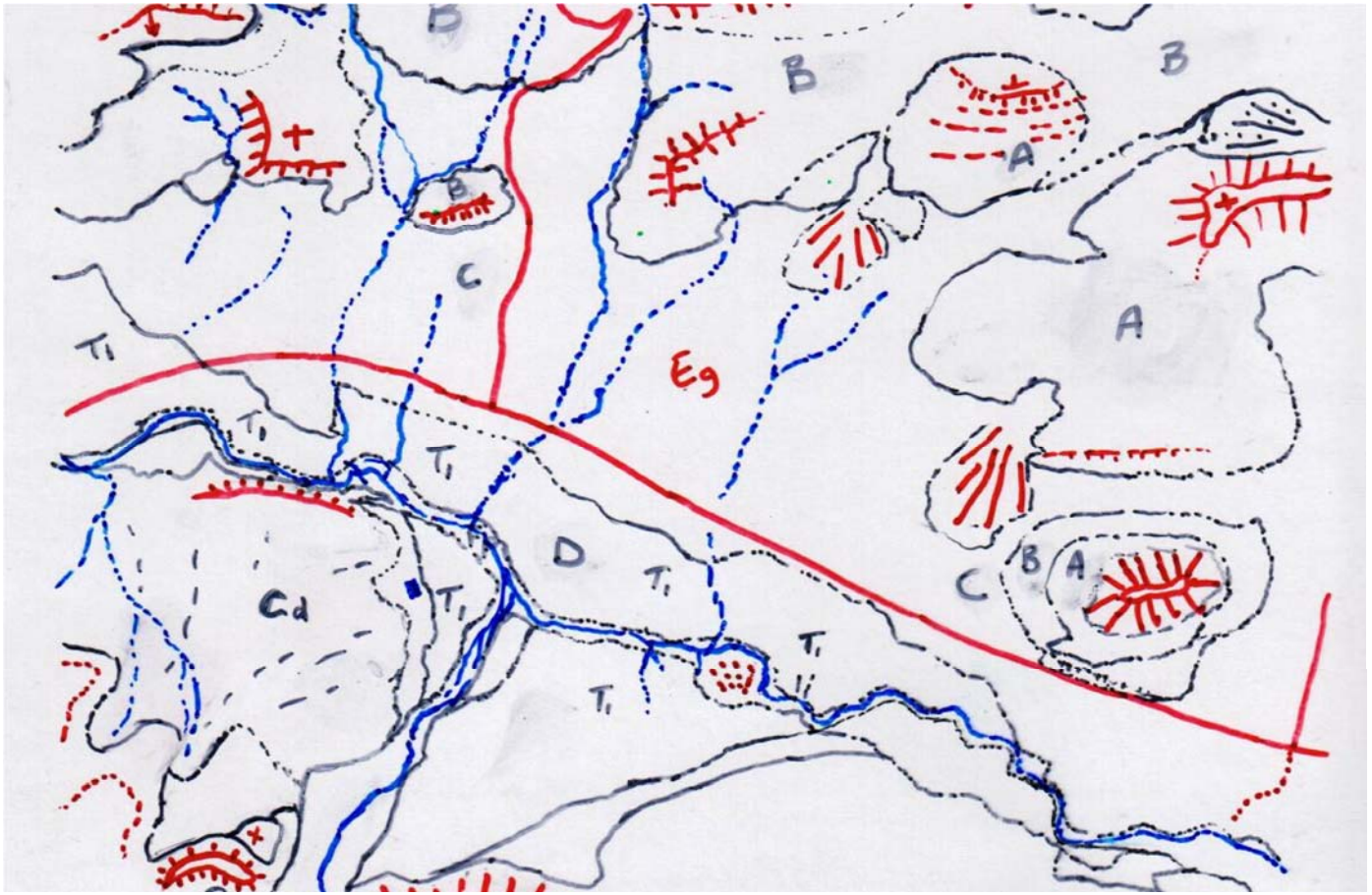

Appendix D.2

Digitized map from aerial photo interpretation showing geomorphological units

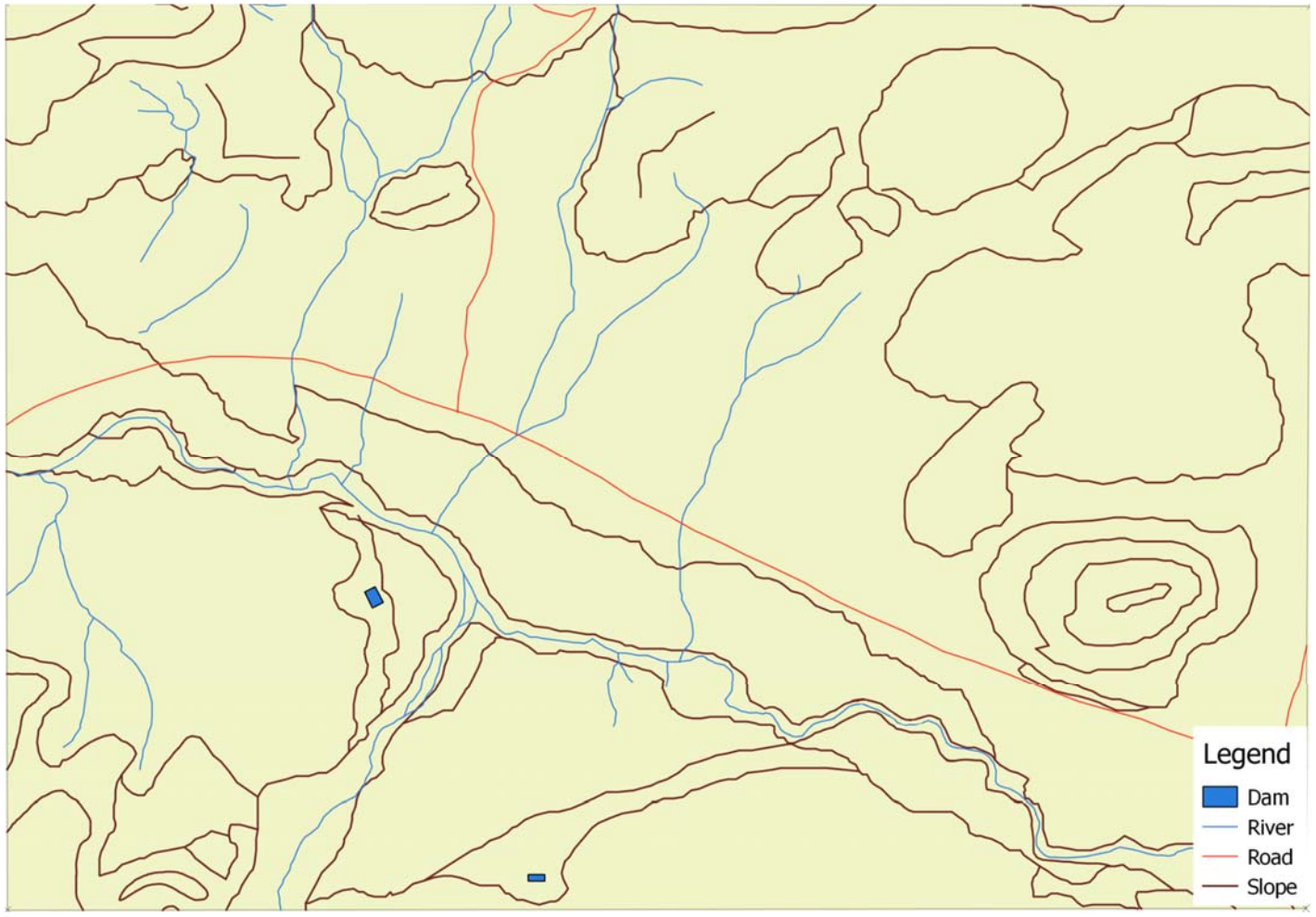

Appendix E

Table of field measured slope and elevation field data

Sample	Latitude	Longitude	Elevation (m)	Slope (%)
P13	30.113	-22.9009	796	27.77
P9	30.1192	-22.9062	817	1.44
P12	30.1244	-22.8993	780	3.85
P10	30.1223	-22.9042	802	9.34
P15	30.1123	-22.8955	791	5.95
P14	30.1129	-22.8956	794	8.75
P16.3	30.1322	-22.8907	765	4.95
P16.1	30.1305	-22.889	772	3.77
P16.2	30.1306	-22.8856	770	3.77
P17	30.1337	-22.8854	746	2.11
P21	30.1176	-22.8666	810	39.42
P22.1	30.12	-22.8654	825	19.84
P22.2	30.12	-22.8654	824	23.01
P20	30.1192	-22.8746	755	5.86
P34	30.1424	-22.8598	925	24.59
P35	30.1393	-22.8611	880	8.75
P24	30.1389	-22.8665	843	4.42
P25	30.15	-22.8689	854	9.41
P27	30.1603	-22.864	894	3.63
P30	30.166	-22.8713	870	28.32
P33	30.1749	-22.892	863	32.15
P32	30.1747	-22.8945	811	12.03
P2	30.1707	-22.8959	785	1.68
P03.2	30.1612	-22.896	765	6.43
P03.3	30.1612	-22.896	768	1.53
P03.5	30.1656	-22.8947	784	1.85
P03.4	30.1655	-22.8946	782	2.58
P03.1	30.1459	-22.8856	765	0.03
P05	30.1463	-22.9038	804	9.19
P06	30.149	-22.9007	786	7.28

Appendix F

Lab analyses for soil texture

Sieve shaker

Balance weighing 50g of soil from a sample

Treatment of soil samples for carbonates and organic matter with hydrochloric acid

Oven drying weighed soil samples for moisture content

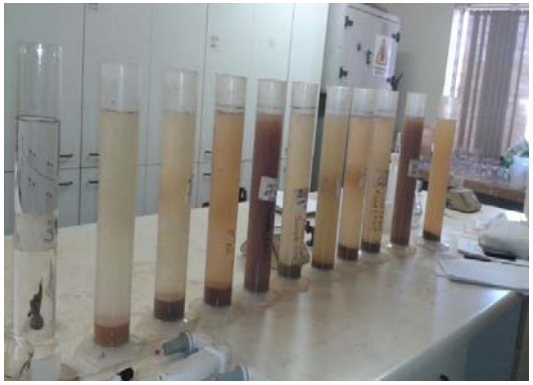

Hydrometer analysis

*Electric mix*er with sample

Measuring soil pH with pH meter

Appendix G.1

Table showing hydrometer reading

Sample	Temperature (℃)	Hydrometer reading (after 3 minutes)	Temperature (℃)	Hydrometer reading (after 2 hours)
1	22	19	22	11
2	22	18	22	9
3	22	22	22	8
4	22	18	22	8
5	22	24	22	8
6	22	24	22	9
7	22	11	22	10
8	22	24	22	11
9	22	15	22	9
10	22	20	22	13
11	22	18	22	8
12	22	16	22	8
13	22	17	22	9
14	22	15	22	10
15	22	14	22	10
16	22	14	22	8
17	22	16	22	12
18	22	11	22	4
19	22	20	22	10
Blank	22	6	22	6

The soil samples that were analysed using a hydrometer were sieved using a 2mm sieve. Therefore, the soils that were greater than 2mm were not considered for analyses which constitute coarse sand. As a result, medium and fine sands were analysed. The thermometer and the hydrometer were taken twice, first at three minutes after mixing and at two hours for each sample and the blank cylinder.

Appendix G.2
Table showing soil texture

Sample	clay %	Silt	Sand	Texture
1	10	20	70	Sandy loam
2	6	26	68	Loamy sand
3	4	34	62	Sandy loam
4	4	26	70	Loamy sand
5	4	38	58	Loamy sand
6	6	34	60	Loamy sand
7	4	16	80	Sandy loam
8	10	30	60	Sandy loam
9	6	18	76	Loamy sand
10	14	18	68	Loamy sand
11	4	26	70	Loamy sand
12	4	18	78	Loamy sand
13	6	20	74	Loamy sand
14	8	12	80	Loamy sand
15	8	8	84	Loamy sand
16	6	4	90	Sand
17	12	8	80	Loamy sand
18	12	20	68	Loamy sand
19	8	2	90	Sand

Appendix G.3

Table showing soil moisture content and pH of collected soil samples

Sample	Mass (g) of weighing and sample	Mass (g) of weighing tray and dried sample	$\%H_2O$	Soil pH
P3/1	220.10	219.20	0.4	7.37
P24/2	220.22	213.77	2.9	6.62
P17/3	220.20	201.47	8.5	8.39
P12/4	220.25	211.59	3.9	8.12
P7/5	220.14	213.68	2.9	7.17
P6/6	220.09	209.78	4.7	7.74
P30/7	220.07	215.59	2.0	7.88
P1/8	220.09	213.19	3.1	8.35
P27/9	220.08	213.25	3.1	7.94
P3/10	220.11	211.53	3.9	8.70
P32/11	220.28	204.41	7.2	8.35
P16/12	220.07	216.42	1.7	8.08
P2/13	220.18	214.38	2.3	8.14
P20/14	220.10	204.02	7.3	8.33
P34/15	220.05	195.50	11.2	8.41
P16/16	220.17	209.58	4.8	7.96
P3/17	220.12	197.90	10.1	7.60
P3/18	220.06	202.47	8.0	8.50
P5/19	220.14	209.08	5.0	7.78

Appendix H.1

1-arc ASTER DEM reclassified slope

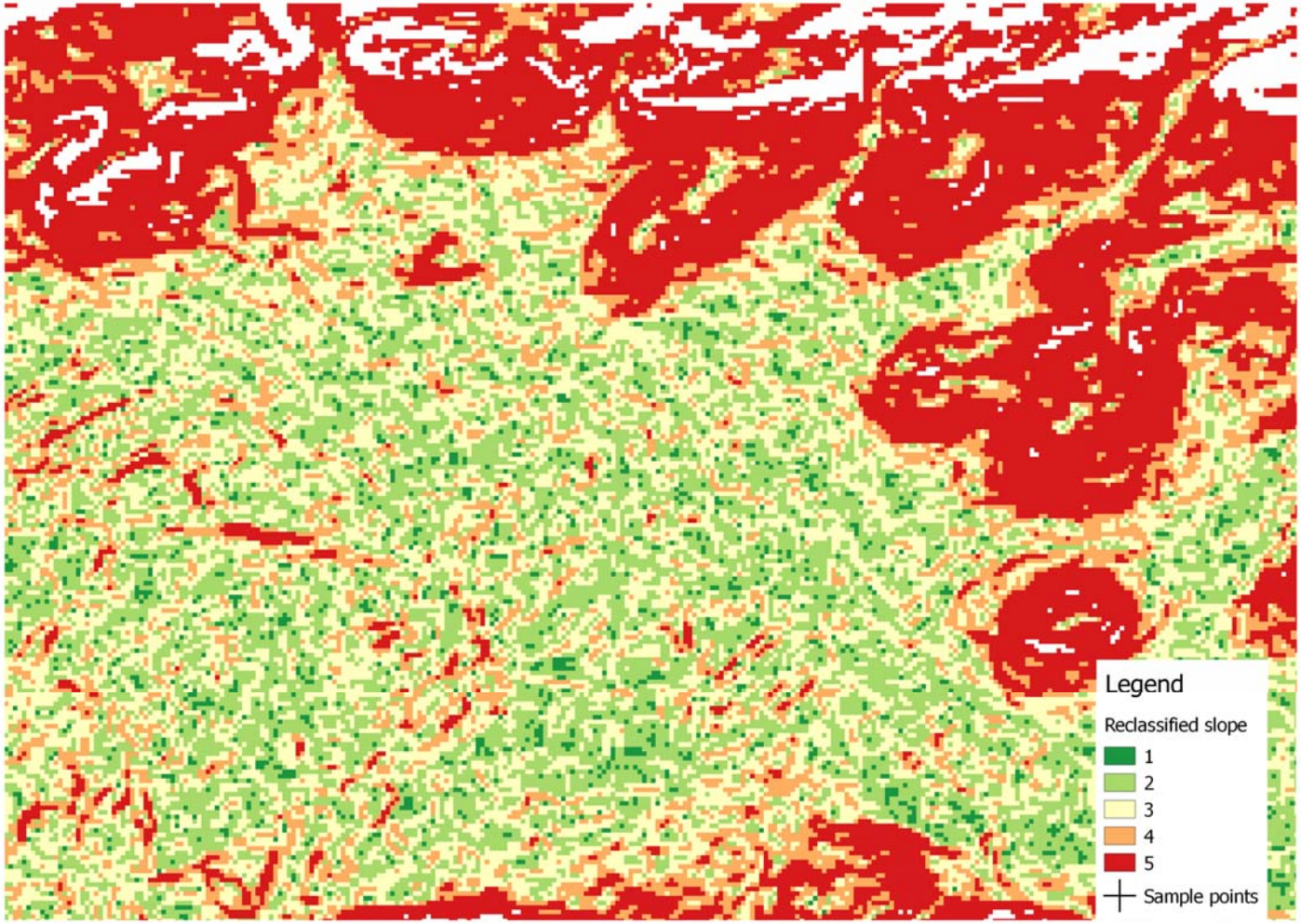

Appendix H.2

1-arc SRTM DEM reclassified slope map

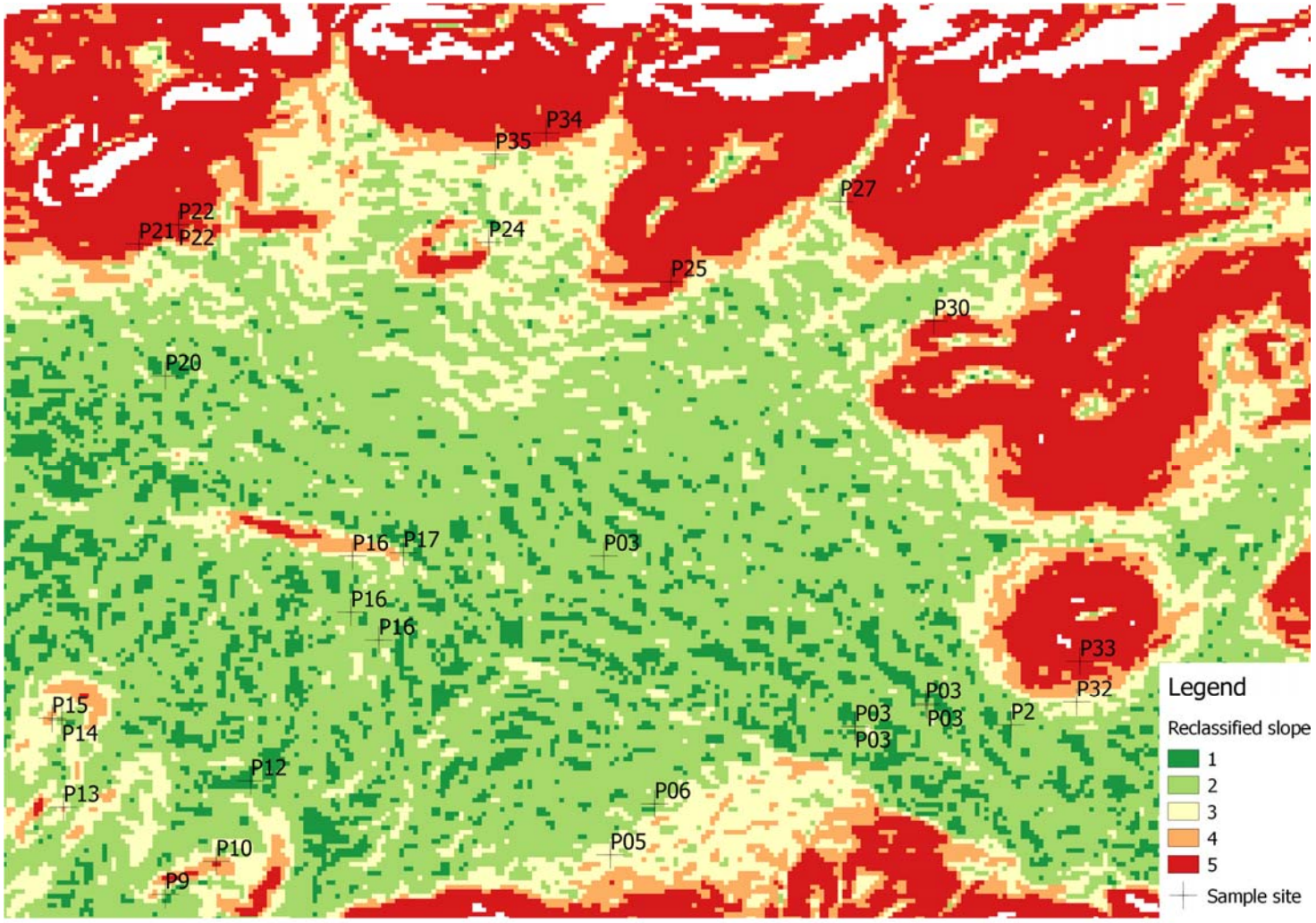

Appendix H.3

3-arc SRTM DEM reclassified slope map

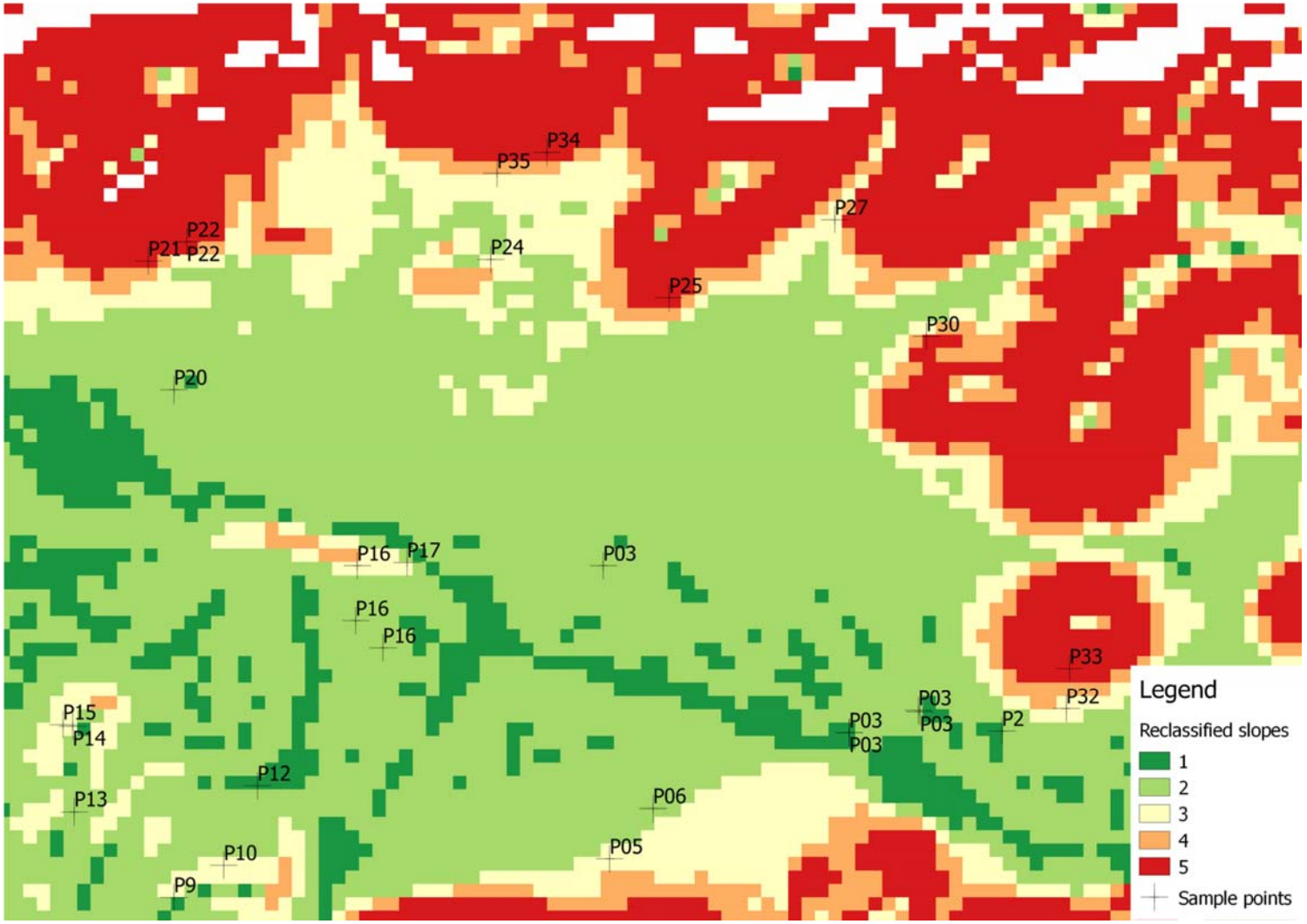

Appendix I

Comparison of reclassified slope classes between DEM derived and field measured slopes

Sample ID	1-arc SRTM DEM slope (%)	1-arc ASTER DEM slope (%)	3-arc SRTM DEM slope (%)	Field measurement (%)
P13	3	4	2	5
P9	2	2	1	1
P12	1	3	1	2
P10	4	4	3	3
P15	4	3	3	2
P14	2	3	3	3
P16.3	2	5	2	2
P16.1	2	2	2	2
P16.2	3	4	3	2
P17	2	3	3	2
P21	5	5	5	5
P22.1	5	5	5	4
P22.2	5	5	5	4
P20	2	3	2	2
P34	5	5	5	5
P35	3	3	4	3
P24	3	1	3	2
P25	5	5	5	3
P27	3	4	3	2
P30	5	5	5	5
P33	5	5	5	5
P32	3	3	3	3
P2	2	2	1	1
P03.2	2	2	1	2
P03.3	2	2	1	1
P03.5	2	2	2	1
P03.4	2	2	2	2
P03.1	2	2	2	1
P05	3	4	3	3
P06	2	2	2	3

Appendix J

Showing the elevation values of DEMs in comparison with field data

FID	Field measured elevation (m)	ASTER DEM elevation (m)	1-arc_SRTM DEM Elevation	3-arc_SRTM_DEM elevation (m)
P13	796	795	799	795
P9	817	805	813	814
P12	780	778	780	780
P10	802	801	798	799
P15	791	777	786	792
P14	794	784	792	792
P16.3	765	766	765	767
P16.1	772	758	770	771
P16.2	770	763	768	769
P17	746	745	748	753
P21	810	797	807	807
P22.1	825	821	820	813
P22.2	824	821	820	813
P20	755	750	755	753
P34	925	912	920	919
P35	880	874	876	874
P24	843	845	850	846
P25	854	848	858	851
P27	894	896	898	897
P30	870	869	875	883
P33	863	859	860	853
P32	811	807	813	807
P2	785	794	789	791
P03.2	765	765	770	771
P03.3	768	765	770	771
P03.5	784	778	782	781
P03.4	782	780	781	781
P03.1	765	768	775	775
P05	804	800	805	808
P06	786	780	789	789

Appendix K.1

1-arc SRTM TPI

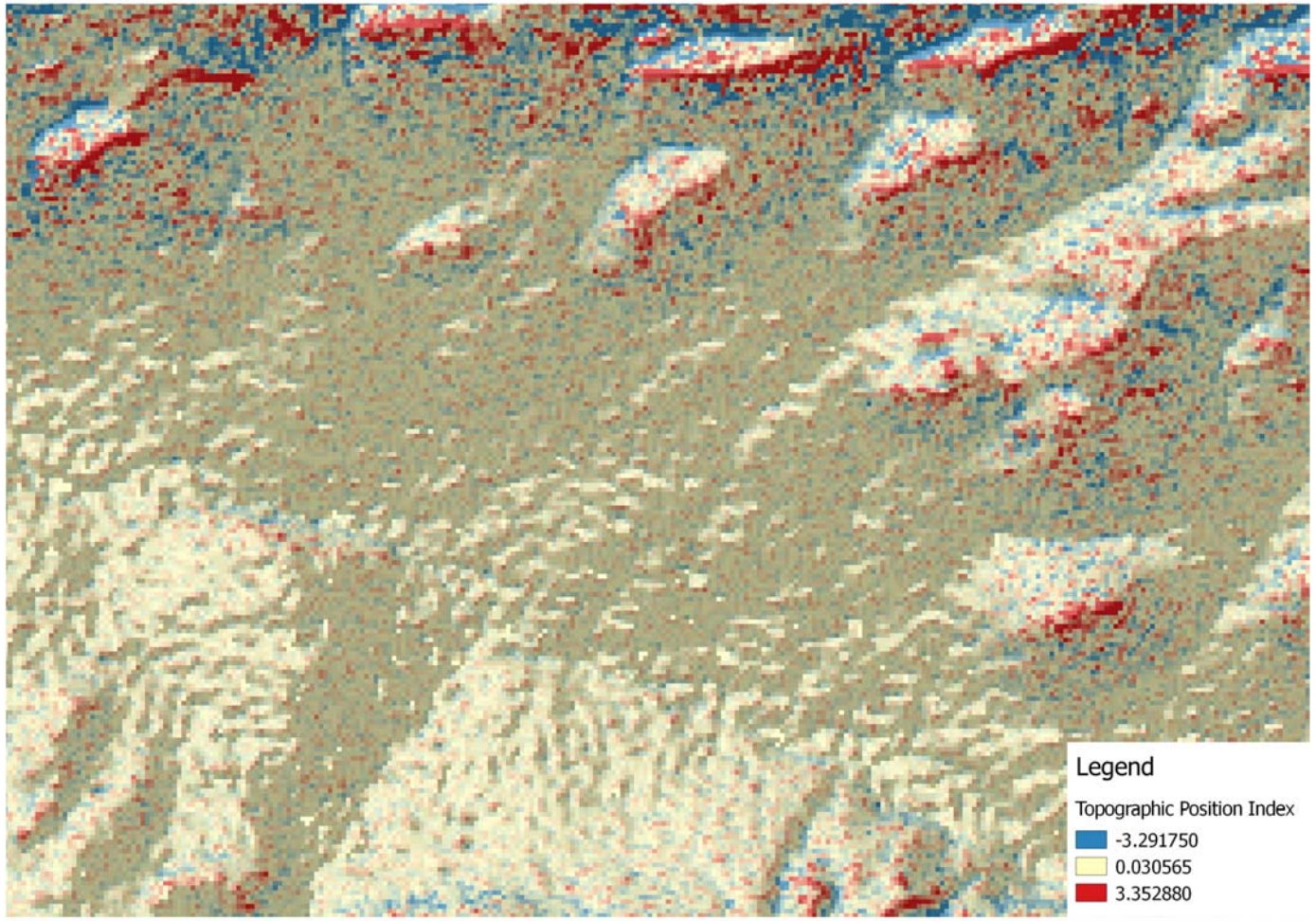

Appendix K.2

1-arc ASTER TPI

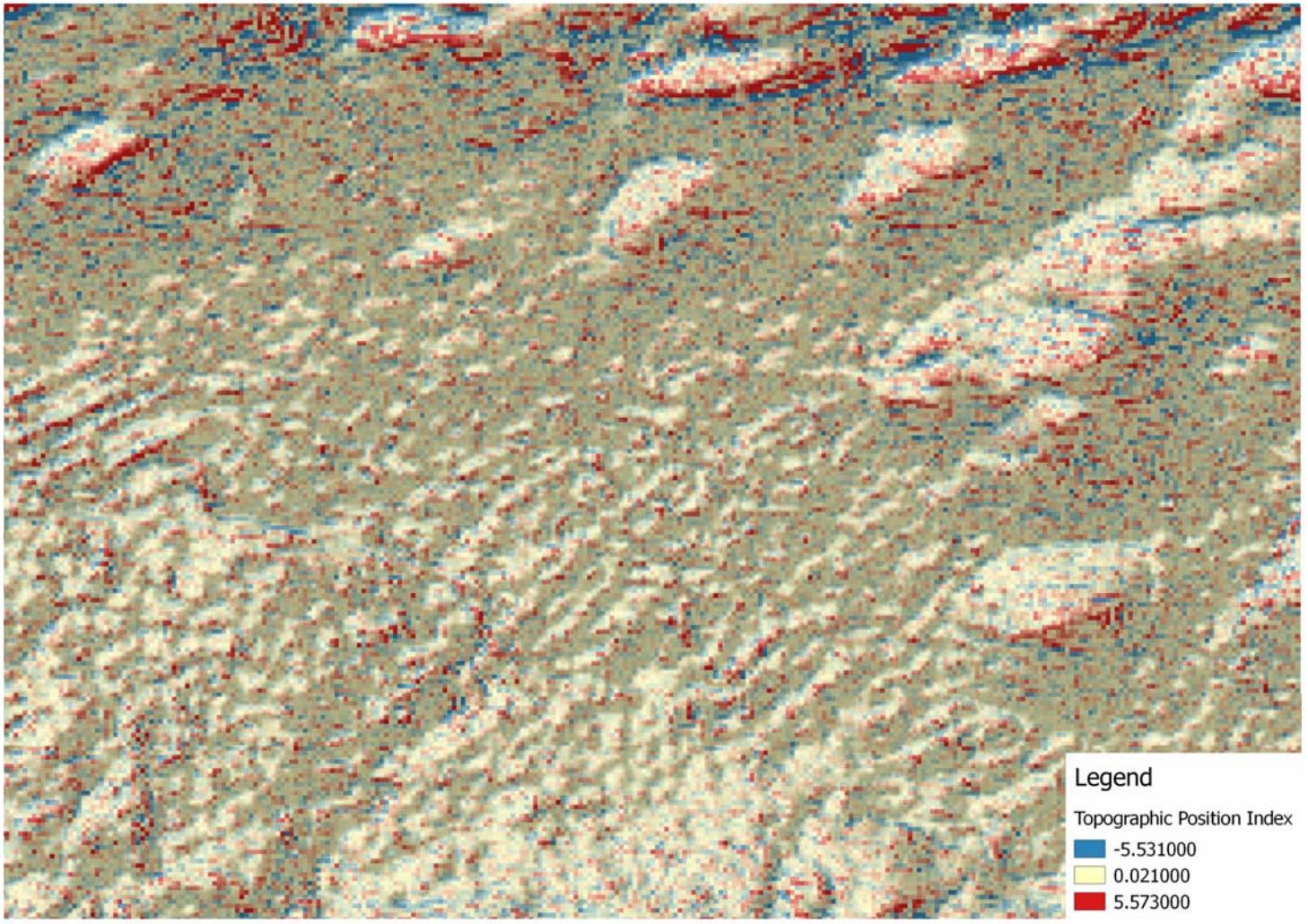

Appendix K.3

3-arc SRTM TPI

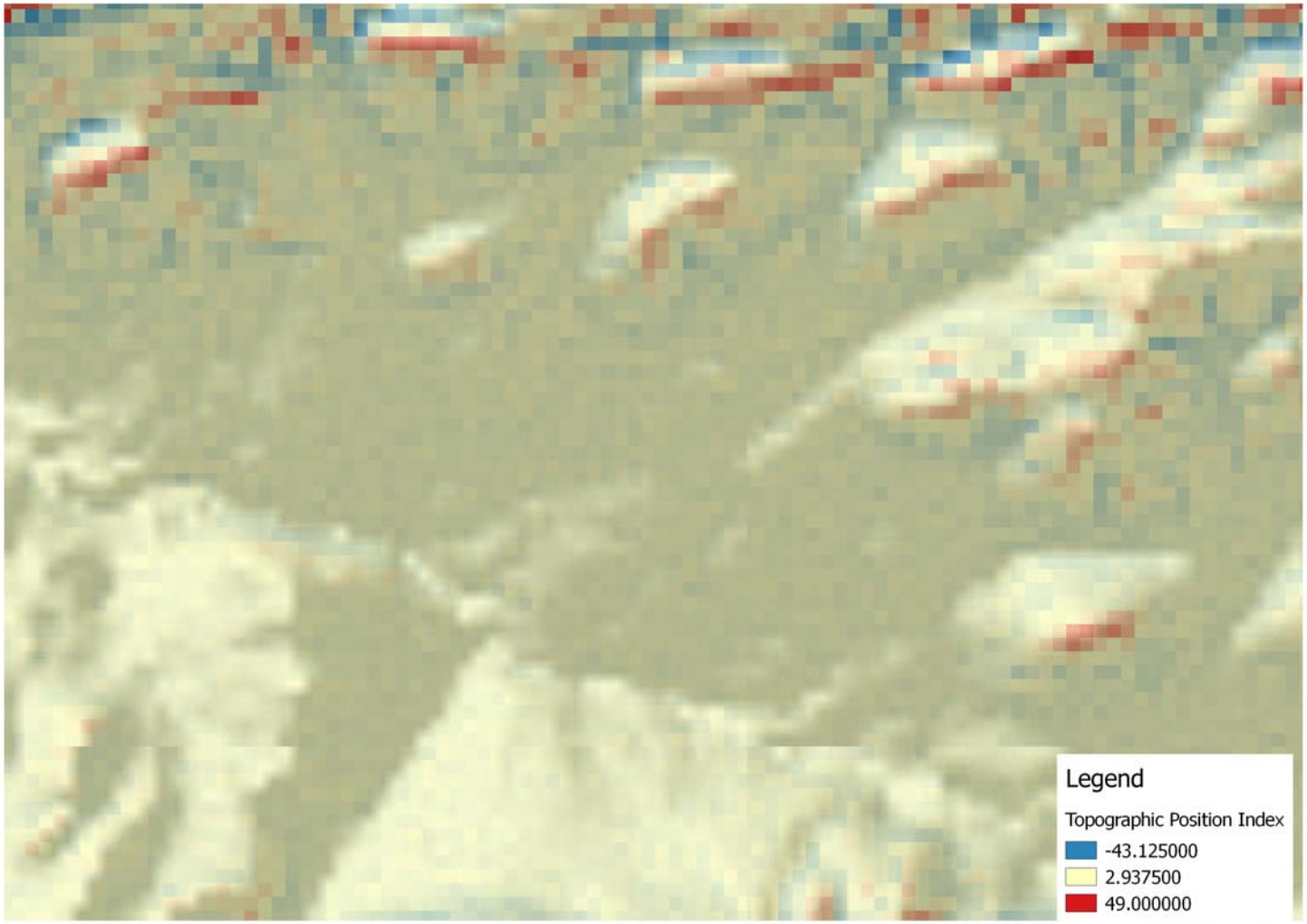

Appendix L

Soil spectra extracted from the Landsat 8 image